SAHC

3D numerical simulation of the load test on a masonry barrel arch bridge

Roberta Palermo

Spain | 2019

ADVANCED MASTERS IN STRUCTURAL ANALYSIS
OF MONUMENTS AND HISTORICAL CONSTRUCTIONS

Master's Thesis

Roberta Palermo

3D numerical simulation of the load test on a masonry barrel arch bridge

UNIVERSITAT POLITÈCNICA
DE CATALUNYA

University of Minho

Spain | 2019

ADVANCED MASTERS IN STRUCTURAL ANALYSIS
OF MONUMENTS AND HISTORICAL CONSTRUCTIONS

Master's Thesis

Roberta Palermo

3D numerical simulation of the load test on a masonry barrel arch bridge

Spain | 2019

DECLARATION

Name: Roberta Palermo

Email: roberta.palermo20@gmail.com

Title of the Msc Dissertation: 3D numerical simulation of the load test on a masonry barrel arch bridge

Supervisor(s): Climent Molins

Year: 2019

I hereby declare that all information in this document has been obtained and presented in accordance with academic rules and ethical conduct. I also declare that, as required by these rules and conduct, I have fully cited and referenced all material and results that are not original to this work.

I hereby declare that the MSc Consortium responsible for the Advanced Masters in Structural Analysis of Monuments and Historical Constructions is allowed to store and make available electronically the present MSc Dissertation.

University: Universitat Politecnica de Catalunya

Date: 16/07/2019

Signature: 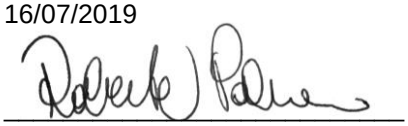

This page is left blank on purpose.

ACKNOWLEDGEMENTS

Working on this dissertation has been a big challenge and a great opportunity.

This work would have not been materialized without the observations, directions and patient guidance of my supervisor, Professor Climent Molins, to whom I owe a sincere thank you.

I would also like to extend my gratitude to the SAHC Master Consortium for giving me the chance to attend this Master by providing me a scholarship.

Finally, I wish to thank all the people who provided me their support, academic and personal.

This page is left blank on purpose.

ABSTRACT

Researches show that around half a million masonry arch bridges are currently in use around the world. Many of them are carrying roads and railways, condition that increases their social, functional and economic value. This reason, together with the unquestionable cultural and historical value that they have, makes masonry arch bridges, structures to be assessed, preserved and rehabilitated through repair and strengthening, when required.

Arch masonry bridges are ancient structures whose general behavior is well known, however, the assessment of their condition and the evaluation of their load-bearing capacity are still rather challenging. Many parameters contribute in increasing the complexity of these structures. For instance, the wide range in which the properties of the materials used in their construction may vary, as well as the contribution of all the consitutive structural elements in their overall behaviour.

Getting a better understanding of how masonry bridges work was the main scope of an experimental campaign that was carried out at the Structural Technology Laboratory of the UPC between 2002 and 2004. Real scale masonry bridges were tested to failure in order to gather information regarding their collapse mechanisms and their load bearing capacity. Object of this dissertation is to develop a numerical simulation of the load test performed on one of the two masonry bridges tested, thanks to the use of the software DIANA FEA, and therefore to provide a detailed simulation of a real phenomenon.

At first, the results obtained experimentally are analysed and a review of literature on the simulation of similar bridges is presented. Next, a research and review of literature focused on the material models and the properties to be assigned to the numerical model is performed and reported.

The numerical model is then studied, first with a simplified bi-dimensional approach and later with a tri-dimensional approach. An activity of calibration of the numerical model and its properties is presented.

Finally, the results obtained through a finite element analysis are compared to the experimental ones and a sensitivity analysis is developed to demonstrate how changing different parameters has a direct effect on the results.

This page is left blank on purpose.

RESUMEN

Actualmente, se estima que alrededor de medio millón de puentes en arco de fábrica están en servicio en todo el mundo. La mayoría de ellos soportan carreteras o líneas de ferrocarril, lo que aumenta su valor social, funcional y económico. Ésta razón, junto con el incuestinable valor histórico y cultural que poseen, hace de los puentes en arco de mampostería sean estructuras que deben ser evaluadas, conservadas y rehabilitadas a través de reparaciones o refuerzos, cuando sea necesario.

Los puentes en arcos de mampostería son estructuras milenarias cuyo comportamiento general es bien conocido, sin embargo, la valoración de su estado y la evaluación de su capacidad portante suponen todavía un desafío. Muchos parámetros contribuyen en incrementar la complejidad de estas estructuras. Por ejemplo, la variabilidad de las propiedades de los materiales empleados en su construcción, así como la contribución de todos los elememtos estructurales que lo conforman en su comportamiento global.

Intentar llegar a comprender mejor como funcionan los puentes en arco de piedra fue el objetivo principal de una campaña experimental que fue llevaba a cabo por el laboratorio tecnológico y estructural de UPC entre los años 2002 y 2004. Puentes de obra de fábrica a escala fueron testados hasta su rotura para recopilar información sobre sus mecanismos de colapso y su capacidad portante. El objetivo de ésta tesis, titulada " *Simulación numérica 3D de una carga aplicada en un puente en arco de de medio punto de mampostería*", es el desarrollo de una simulación numérica del efecto de la carga sobre el puente arco de medio punto ensayado, mediante el programa DIANA FEA y, por tanto, aportar una simulación detallada de éste fenómeno.

Al principio, los resultados obtenidos experimentalmente son analizados y se presenta una revisión sobre la simulación de otros puentes similares. Después se efectúa una investigación y una revisión de la literatura basada en los materiales empleados y en las propiedades a asignar en el modelo numérico. El modelo numérico es estudiado, primero con un enfoque simplificado bidimensional para después hacerlo ya tridimensional. Se presenta una actividad de calibración del modelo numérico y de sus propiedades.

Por último, los resultados obtenidos a través del análisis son comparados con los resultados experimentales y se desarrolla un análisis de sensibilidad para conocer el efecto de la variación de las propiedades de los materiales sobre la respuesta resistente.

This page is left blank on purpose.

ABSTRACT

Molteplici ricerche dimostrano che circa mezzo milione di ponti ad arco in muratura sono attualmente in uso nel mondo, molti dei quali ad uso infrastrutturale o ferroviario. Questa condizione ne aumenta notevolmente il valore economico e sociale, divenendo una delle ragioni, insieme all'indiscutibile valore sociale e culturale che li caratterizza, tale da renderne necessaria un'attività di studio, di conservazione e riabilitazione attraverso opere di restauro e rinforzo.

I ponti ad arco in muratura sono strutture storiche di cui si conosce il comportamento generale, tuttavia la determinazione della loro condizione e del loro fattore di sicurezza presentano tuttora delle difficoltà, dovute principalmente ai molteplici parametri che ne caratterizzano il comportamento e la risposta strutturale. In primis, i parametri che si riferiscono alle proprietà dei materiali utilizzati nella loro costruzione possono variare entro range piuttosto ampi, inoltre, i componenti strutturali che li compongono hanno un'influenza significativa sul loro comportamento globale.

Un'attività di ricerca è stata condotta al laboratorio di Strutture dell'Università Politecnica della Catalogna tra il 2002 e il 2004, per ottenere infromazioni riguardo il comportamento dei ponti ad arco in muratura. Due ponti in scala reale sono stati sottoposti ad una prova di carico per raccogliere informazioni riguardo carico limite e meccanismo di collasso. Lo scopo di questo lavoro di tesi dal titolo "*Simulazione numerica in 3D di una prova di carico su un ponte ad arco in muratura*" è di realizzare un modello tridimensionale di uno dei ponti testati in laboratorio e di eseguire su di esso un'analisi numerica mediante l'uso del software DIANA FEA.
In una prima fase, vengono analizzati i risultati sperimentali e viene condotta una revisione della letteratura relativa alle simulazioni numeriche di strutture simili. In seguito, una ricerca condotta su i possibili modelli applicabili ai materiali e i valori da assegnare ai relativi parametri è sviluppata e documentata. Infine, il modello numerico è analizzato, dapprima con un approccio bidimensionale e in seguito con un più dettagliato approccio tridimensionale. Un'attività di calibrazione del modello e dei valori assegnati ai vari parametri viene descritta in dettaglio e i risultati ottenuti dalle analisi agli elementi finiti sono confrontati con i risultati sperimentali. A conclusione, un'analisi di sensitività è sviluppata per dimostrare come cambiare diversi parametri abbia un'influenza nella risposta della struttura e dunque, nei risultati ottenuti.

This page is left blank on purpose.

TABLE OF CONTENTS

LIST OF FIGURES

LIST OF TABLES

1. INTRODUCTION AND OBJECTIVE

1.1 Introduction

Around half a million masonry arch bridges are currently in use around the world, mainly carrying roads and railways. [1] Their priceless cultural and economic value make them an important built cultural heritage that should be studied in order to be preserved and rehabilitated, if required. For this reason, it is important to have a good understanding of how these structures work and to develop tools that can be used in their analysis and assessment.

1.2 Objective

The study developed in this thesis is the simulation of the load test that was performed on a masonry barrel arch bridge. The test was part of an experimental campaign developed at the Structural Technology Laboratory of the UPC on two real scale bridges. This thesis analyses one of the arches tested experimentally; the final object is to provide a detailed numerical simulation of a real physical phenomenon.

1.3 Content of the thesis

In Chapter 2 of the dissertation the basic principles related to the structural behaviour of masonry arch bridges are recalled, along with a description of the state of the art of the assessment of these structures, based on information gathered from a literature review.
In Chapter 3 the experimental activity and the results obtained are described.
Chapter 4 presents shortly a preliminary analytical study developed on the bridge object of the study, whereas the chapters that follow describe the numerical approach that was developed. In particular some previous dissertations developed on the arches tested during the experimental campaign were studied and presented in Chapter 5 along with information regarding material models and values to be assigned to the parameters involved, which was gathered during a literature review.
The numerical analysis was first developed with a simplified bi-dimensional approach, as described in Chapter 6 and then with a more complex tri-dimensional model, described in the chapter that follows.
Chapter 7 reports the calibration activity developed on the 3D models and the comparison between the results obtained and the experimental data. Finally, a sensitivity analysis is described to show how the uncertainties related to different parameters affect the results.
Chapter 8 presents the conclusion, with a particular focus on the way forward and on the possible future development of this research.

2. STATE OF THE ART – MASONRY BRIDGES

The invention of the arch goes back to 6.000 years ago when the first arches were built in Babylon. [2] Since then, the technology has developed thanks to centuries of studies, experiments and practical applications. In particular, masonry bridges represent a very significant application of the technology of the arch that nowadays are considered as a cultural heritage to be preserved and enhanced.

Figure 1 – Ennisnag Bridge, Kilkenny, Ireland. [3]

The interest in studying arch masonry bridges is closely connected to the need of assessing their safety level, their stability and their compatibility with current use requirements. [4] In relatively recent times, masonry arch bridges have faced important changes related to their extended service life and to the changes in transport systems [5], as a consequence, since they are still in use as transport infrastructures, their maintenance, conservation and repair represent a necessary but also strategic form of investment.

Furthermore, a full understanding of the principles that lie behind their working mechanism and the longevity they have demonstrated are of extreme interest, since they might become the starting point for the development of modern efficient technologies [6], and they can orient future research activities. [7]

2.1 Elements of Masonry Bridges

Although it can be said that arch masonry bridges are ancient structures whose general behaviour is well known, the assessment of their condition and the evaluation of their load-bearing capacity are still rather challenging. The reason for this difficulty is intimately related to the nature and the complexity of the structure itself and to the many mechanical variables that affect the behaviour of the materials involved. Furthermore, the presence of many components and their mutual interaction influence the overall behaviour of masonry bridges, making the assessment of these structures extremely complex.[1] The first step in the analysis of masonry arch bridges is therefore to understand which elements are present and how they interact between each other.

The expression masonry bridge is commonly used to define a structure that can be built in bricks or in masonry blocks. [6] Although masonry bridges can differ for their specificities, linked to materials but also to shapes and building techniques, some generic common features and elements can be identified, which include:

- Arch: curved structural member that supports vertical loads across an opening and that transfers them to piers or abutments. [5]
- Barrel arch: the load-bearing part of the arch that might contain a single thickness of voussoirs or several rings. [5]
- Abutment: a masonry body that provides resistance to the vertical forces and to the thrust of the arch. [5]
- Spandrel walls: masonry walls sitting on the edge of the barrel arch that retain the infill. [5]
- Infill material: granular material located in the spandrel, the area between the barrel arch and the road surface and laterally retained by the spandrel walls.

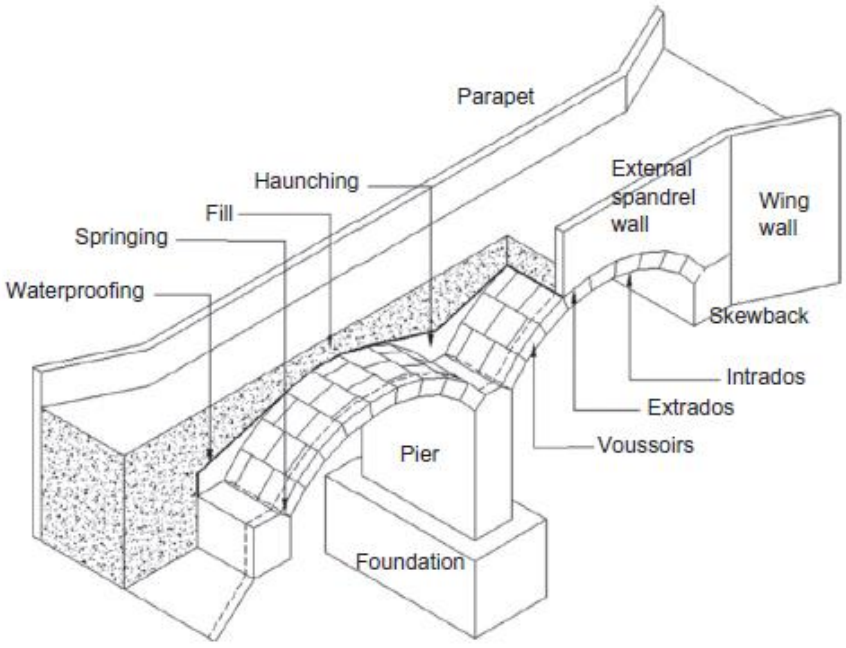

Figure 2 – Main elements of a masonry arch bridge. [7]

2.2 Behaviour of Masonry Arch Bridges

In order to understand how arch masonry bridges work; it is paramount to provide an overview of the mechanism behind the behaviour of the arch.

Arches, similarly to other curved structures such as vaults and domes, are particular structural elements in which the behaviour and the equilibrium are mainly dependent on the geometry, along

with the support conditions. When referring to a masonry structure, in particular, we are considering a heterogeneous material with almost null tension strength, whose main resistance is in compression, therefore the geometry of the structure and the position of the load are the key aspects in its equilibrium. [8]

Moreover, further aspects should be considered in the specific assessment of the behaviour of masonry arch bridges. For instance, these constructions are strongly affected by the presence of an existing crack pattern and furthermore the presence of spandrel walls and infill plays an important role.

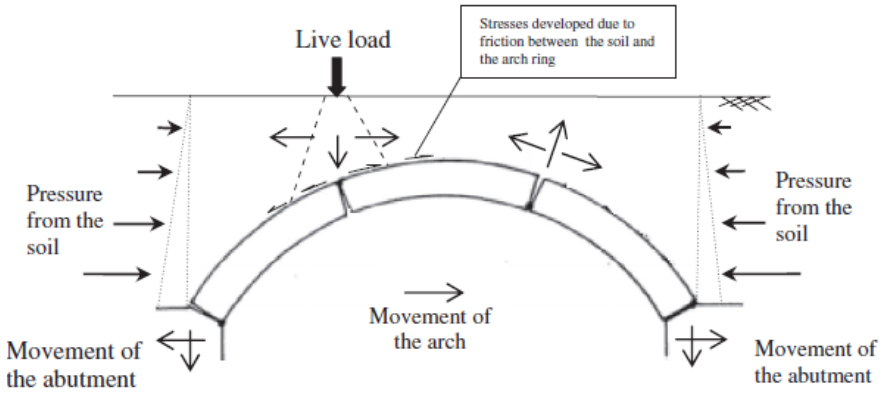

Figure 3 – Schematic structural behaviour of a masonry arch bridge. [7]

In particular, the infill has a positive influence: its weight has a stabilizing effect and contributes in increasing the overall stiffness of the structure. As for the distribution of the loads on the structure, it has to be kept in mind that distributed loads, such as the self-weight of the infill and the spandrel walls is distributed directly to the arch, whereas point loads are distributed to the arch through the infill, as shown in Figure 3 and Figure 4. The consequence is that the properties of the infill have a contribution on the transmission path to the arch.

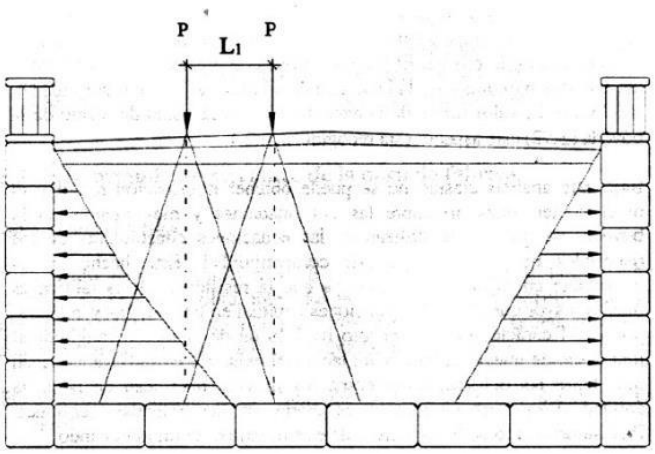

Figure 4 – Cross section of a masonry arch bridge showing the lateral force acting from the infill to the spandrel walls. [8]

A number of researches has been done to evaluate the influence of the presence of the soil on the load-carrying capacity of the arch and many of them are still ongoing. [7] For instance, the graphs in Figure 5 show some of the results of a study conducted by Nobile and Bartolomeo [9], aiming to demonstrate how some parameters of the infill such as specific weight and height, influence the ultimate load of the bridge being studied. A similar consideration can be done with reference to the spandrel walls.

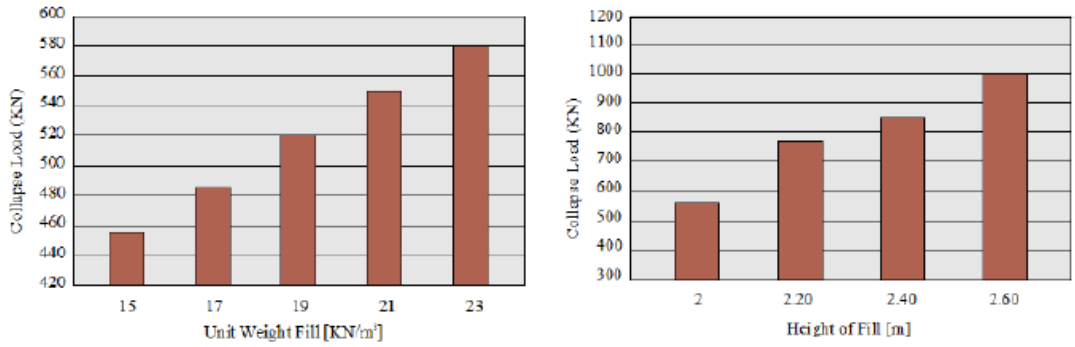

Figure 5 – Influence of the density of the infill (left) and of its height (right) on the ultimate load of a masonry bridge. [9]

Another interesting peculiarity of arch masonry bridges with spandrel walls and infill is that the latter causes a horizontal force acting on the spandrel walls, as shown in Figure 4.

Although spandrel walls give a contribution to the overall stiffness of the structure, it is to be mentioned that frequently, during experiments, a separation between these structural elements and the infill has been observed. As a consequence, the two different elements act separately; for this reason the contribution of the walls has been very frequently neglected. [8]

Early masonry arch bridges were built using materials with poor mechanical properties that were often subjected to deterioration during time, whereas in more recent times an evolution in the production of the materials has made the construction of structures with stronger and more durable materials possible. [7] Usually the stress state to which masonry bridges are subjected are lower than the compressive strength of the masonry, this is the reason why their collapse is mainly due to loss of equilibrium [7] and less frequently to crushing failure.

2.3 Assessment of Masonry Arch Bridges

Arches play a fundamental role in masonry constructions being the structural elements that, as an evolution of the lintel system and thanks to their geometry, allow spanning over a large void, using a material with almost no tensile strength. [2] As mentioned previously, this technology has been used for many centuries, during which geometrical and empirical principles linked to its construction have been developed. However, despite its long life and its widespread use, only a few geometrical rules related to the dimensions of its structural members could be found in ancient treaties, whereas no

scientific or rational explanations were provided. In fact, for a very long time, the information about construction of arches and vaults was only shared from a generation to another, led by experience and observation.

A rational theory of masonry arches was developed only in relatively recent times, when the need to predict the in-service behaviour and the load-bearing capacity of the structures led different research activities. [7]

The first rational approaches date back the mid of 17th century, when the first theories related to the stability of the arch were developed. Multiple were the contribution given to this development. One of the starting points was for instance the contributions given by Robert Hooke, who defined the *Principle of the inverted catenary* representing the solution for the equilibrium of an arch; and by David Gregory who also provided an input to the development of the same principle. An important step forward was done in the 19th century, when further researches about the catenary principles involved a graphical approach that led to the development of the concept of thrust line, such as for instance the formulation of Moseley. The thrust is defined as the resultant of the stresses acting in each joint of the voussoirs, a compressive force applied in the so-called centre of thrust. When all the centres of thrust are joined, depending on the geometry of the arch and the loads applied, the thrust line is obtained. [2] The studies on the thrust line led to the definition of a possible equilibrium solution of the arch.

Further contributions to the theory of equilibrium of the arch as well as to the formulation of the theory that explains the mechanism of collapse of the arch relating it to the development of hinges, were given by Moseley, Leonardo Da Vinci and Couplet. These and other contributions, as well as Coulomb's theory on the stability of masonry arches, led to the modern formulation of the limit analysis attributed to Heyman, which dates back to 1966.

Nowadays the assessment of masonry arches is based on three main methods:

- The Thrust Line Analysis Method;
- The Mechanism Method;
- The Finite and Discrete Element Methods.

The first two are intimately related to the theorems of the Plastic Analysis, whereas the Finite and Discrete Element Methods are numerical methods developed in more recent times. [9] The methods differ not only for the principles upon which they are based, but also on the level of complexity and the level of approximation used. As a consequence, different methods and approaches provide different levels of estimation of the results. [7]

2.3.1 Plastic Analysis

The theory of limit analysis represents a very effective tool that allows estimating the collapse load of a system. [10] It is based on three fundamental hypotheses:

- Masonry has no tensile strength;
- The compression strength of masonry is infinite;
- Sliding between stone blocks is not possible.

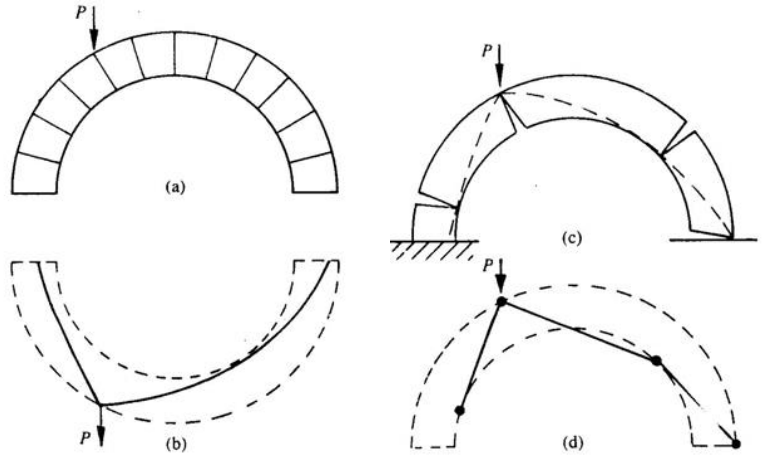

Figure 6 – Collapse of a semi-circular masonry arch under a point load [11].

Under these conditions a masonry structure can be studied as an assemblage of rigid elements and the theorems on which the limit analysis is based are applicable. According to this theory, failure occurs when a plastic mechanism is generated, due to the formation of non-dissipative hinges. [10] A hinge is formed every time the thrust line touches the boundaries of the arch; when, as a consequence of the load applied, the hinges are four, a mechanism leading to collapse of the structure is generated.[2]

Three theorems characterize the principles of limit analysis:

1) Lower-bound theorem: the structure is safe when a statically admissible state of equilibrium can be found, condition that occurs when a thrust line inside the boundaries of the arch can be determined. In this case, the external load applied is the lower bound of the actual ultimate load causing the failure. When talking about lower-bound theorem we refer to a static limit analysis.
2) Upper bound theorem: if an admissible mechanism, for which the work developed by external forces is equal or bigger than zero, can be found, the structure will collapse. In this case the load applied is an upper-bound of the ultimate load and we talk about a kinematic limit analysis.

3) Uniqueness theorem: when both a statically and kinematically admissible collapse mechanism can be found, a limit condition is reached. A thrust line causing the formation of plastic hinges required to develop a mechanism can be found and the load applied is the ultimate load. The thrust line is the only possible one.

The principles of limit analysis are used in the assessment of existing masonry arch bridges thanks to specific softwares. The arch is defined by a series of blocks that cannot slide, have infinite compressive strength and no tensile strength. Softwares are able to identify the position of hinges and a possible thrust line; a lower bound solution can therefore be obtained. [1]

Within the Plastic Analysis, two methods can be identified, namely the Thrust Line Analysis Method and the Mechanism Method. [9] The first one uses a static approach to define the limit loads for equilibrium on the bases of the lower bound theorem. The second is based on the upper bound theorem and by applying a kinematic approach, evaluates the number of plastic hinges required to develop a mechanism. [9]

Limit analysis presents advantages when compared to elastic analysis, because when studying masonry structures, elastic analysis fails due to the fact that it is not always possible to obtain a unique equilibrium state; whereas limit analysis considers the structure in relation to its ultimate state. [9] However, although it presents advantages compared to elastic analysis, limit analysis is helpful mainly as a first approach. It fact, its main limit is not being able to predict displacements and stress and strain distributions. [1]

2.3.2 Numerical approach

A numerical simulation of masonry constructions represents nowadays the most common and sophisticated approach that can be used to evaluate the behaviour of a structure. The last decades have been characterized by a significant development of methods and softwares that allow obtaining this objective [12], and make accurate analysis of complex structures feasible.

However, it is important to point out that a numerical approach is based on several approximations. First, it requires a simplification of the properties of the materials, whose behaviours are represented by a mathematical simulation defined constitutive model. Second, every numerical analysis requires an idealization of the geometry. Masonry structures are very often complex structures that, in order to be understood and analysed require an idealization, which might include for instance the use of linear elements or shell elements, instead of fully three-dimensional elements, as well as, if necessary, the reduction of decorative elements and a simplification of the volumes. [12]

A further essential kind of idealization is linked to the choice of the behaviour to be considered. A masonry structure can be studied considering an elastic behaviour, plastic behaviour or non-linear behaviour. The most complete is the non-linear behaviour which allows obtaining information

regarding the complete response of the structure, from the elastic range to the failure, passing through cracking and crushing. [12]

Despite the complexity of the reality and, as a consequence, the simplifications on which they are based, numerical techniques present the advantage to offer a more comprehensive analysis of the structure if compared to classical analytical methods. [7]

The most used methods are the Finite Element Method (FEM), which follows a macro-modelling approach and the Discrete Element Method (DEM), in which a micro-modelling is applied. The macro-modelling consists in describing the masonry as an equivalent continuum, whereas the micro-modelling approach represents the masonry as formed by discrete units. [7]

Many examples of numerical analysis of masonry bridges can be found in scientific literature, which show different ways to address this kind of study. It can be observed for instance that 2D and 3D FE numerical simplifications of the structure can be performed, that different approaches regarding the way spandrel walls and infill are modelled are possible and that the presence of interfaces between different materials has a strong impact on the results.

Frunzio, Monaco and Gesualdo presented the results of their studies on the existing roman bridge Pont Saint Martin located in Aosta, Italy, in the paper "*3D F.E.M. analysis of a Roman arch bridge*". The bridge, shown in Figure 7, was modelled taking into account the presence of masonry arch and spandrel walls, fill and foundations, in order to estimate its safety level. Thanks to the analysis that was performed, the authors of the study were able to evaluate the distribution of the maximum principal stress and, since the maximum value in the arch was lower than both the stone and the mortar strength, they could confirm that the major cause of failure was the loss of equilibrium and not a material failure. [13] They also evaluated the distribution and the intensity of the stresses in case spandrel walls and fill were not modelled but considered as dead load, obtaining similar results. In their study, only dead loads were applied on the bridge and the Drucker-Prager criterion was applied to all materials.

Figure 7 – Pont Saint Martin, Aosta, Italy. [14]

Similarly, Milani and Lourenço developed a study on two existing arches that was summarised in the paper "*3D non-linear behavior of masonry arch bridges*". In particular their interest was focused on understanding which was the three dimensional behaviour of the structures in presence of eccentric loads and on the strengthening role of the backfill. Moreover, an accent was given to the definition of the non-linear characteristics of the materials and of the interfaces, and to the difference between the response of a skew arch and a straight arch. Finally, a comparison between 2D and 3D limit analysis was performed to get a better understanding of their pros and cons, given that only a 3D discretization allows considering both the backfill and the spandrel walls.[15] The numerical model that was developed included spandrels, infill and interfaces. The definition of the properties of the material was based on experimental evidences and on information obtained from literature. The results obtained by Milani and Lourenço demonstrated that the 3D model yielded better results given by a more accurate definition of the model, in terms of geometry and structure-backfill interaction. Furthermore, a higher resistance than in the 2D model was observed, most likely due to the presence of the spandrel walls.[15] Although a benefit linked to the use of 3D models was clearly shown, this study showed that generally a 2D approach is adequate for a straight arch, whereas in case of skew arches in which the disregarded effects due to the geometry are larger, a more time consuming 3D analysis can be justified. [15]

Another interesting study was developed by Cavicchi and Gambarotta and presented in "*Collapse analysis of masonry bridges taking into account arch-fill interaction*". As the title suggests, the central focus of the study was to analyse the effect of the infill in the collapse behaviour and the load carrying capacity of both a single span bridge and a multi-span masonry bridge. The bridges under analysis were modelled in 2D, using plane beams elements to model arches and piers. The infill was included as a continuum using plane strain hypothesis, and interfaces were applied. The comparison between the results obtained assuming heavy and resistant fill and those obtained using heavy, non-resistant fill demonstrated the positive effect of the infill on the resistance of the structure. When resistant properties are assigned to the infill, the strength properties of the arch can be exploited to a higher level and as a consequence, a significant increase of load carrying capacity is experienced. [16] The influence of other parameters such as for instance the compressive strength of the masonry was also considered in the evaluation. The following graphs shown in Figure 8 represent the influence of the cohesion (graph a) and the compressive strength of the masonry (graph b) in the collapse load of the single span bridge studied.

It is to be mentioned that being the study of Cavicchi and Gambarotta based on a bi-dimensional discretization, it does not take into account the influence of the spandrel walls. Furthermore, since a plane strain assumption for the fill is made, the spandrels are supposed to be providing a smooth boundary condition, which might be a simplification not corresponding to reality. [16]

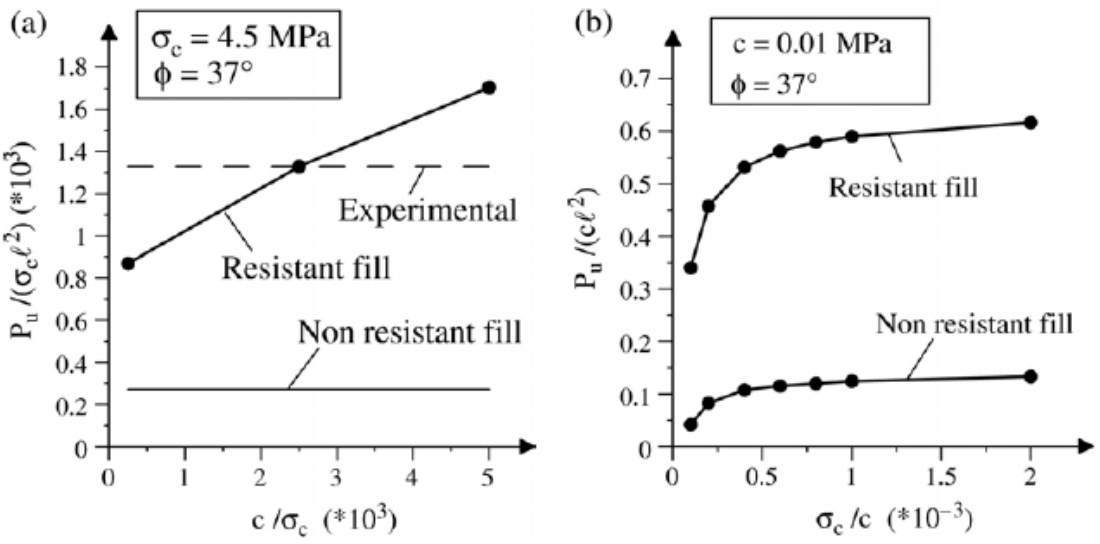

Figure 8 – Influence of cohesion (a) and compressive strenght of masonry in collapse load of a single span bridge. [16]

Gago, Alfaiate and Lamas analysed the effect of the infill in their paper "*The effect of the infill in arched structures: Analytical and numerical modelling".* In particular they performed a simplified numerical simulation of the Bargower bridge destructive experimental test, modelling only the masonry arch as a continuum and considering the presence of the infill in terms of initial state of stress and as a boundary condition by adding lateral spring supports. [17] Nodal loads corresponding to the self-weight of the fill and the lateral earth pressure were applied to the arch. In this case study the presence of spandrel walls was intentionally neglected due to the fact that during the experimental test they detached from the arch at an initial stage as a consequence of their higher stiffness. The authors of the paper carried out different simulations that offer a good insight of how large the influence of the infill can be. At first, the infill was considered as vertical load only (Model I). As a consequence of the choice to neglect its horizontal restraint, the ultimate load resulted being a much smaller value than the experimental one. In Model II, the infill contribution was taken into account through both vertical and horizontal stress state. The overall behaviour appeared to be less stiff than the experimental behaviour and the ultimate load was lower, although higher than the one characterizing the first trial. With the third model, the authors tried to overcome the reduction of stiffness faced in Model II by modelling the lateral stiffness introduced by the infill though the application of linear elastic springs. The results improved significantly, although the ultimate load was in this case higher than the experimental results. Finally, Model IV was modelled applying a bilinear law at the springs. Thanks to this assumption the stiffness of the structure decreased when stress increased, and the results got closer to the experimental results, although the ultimate load was still overestimated. [17] The load-displacement curves obtained experimentally and using the four models are shown in the following Figure 9.

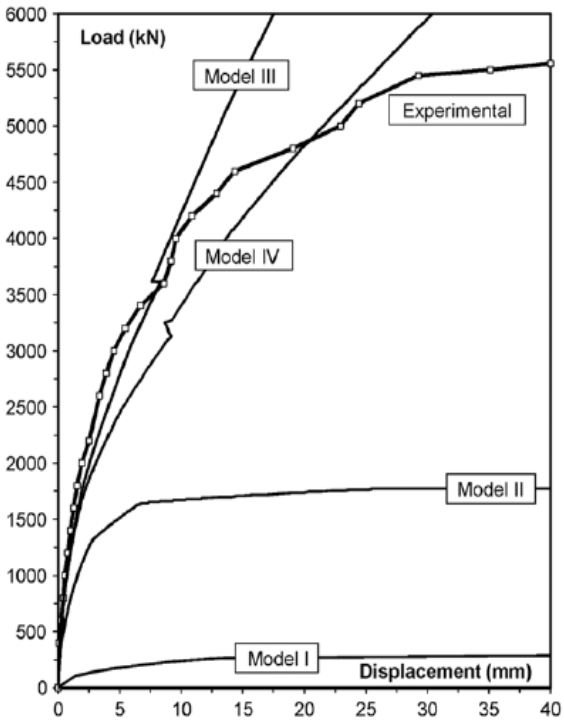

Figure 9 – Load-displacement curves from experiment and numerical models. [17]

In addition, Gago, Alfaiate and Lamas developed a more sophisticated numerical simulation by applying linear elastic and Mohr-Coulomb plasticity models to the infill, this time modelled as a two-dimensional element with a near-cohesionless frictional material. Furthermore, interfaces between masonry arch and infill were modelled. Once again, several options were studied. The results in terms of load-displacement curves are shown in Figure 10. At first, a linear-elastic behaviour of the infill was assumed. The results obtained with Model A show a good approximation in terms of stiffness but also the incapability of the model to reproduce the decrease of stiffness experienced at a later stage. This error of approximation is overcome with Model B and C in which the infill is modelled as a non-linear material. In both models, a Mohr-Coulomb yield criterion is adopted, the difference between them is due to the type of analysis performed: geometrically linear in Model B and non-linear in Model C. [17] An extremely satisfactory result is achieved with Model C, in which a good approximation is obtained also in terms of ultimate load.

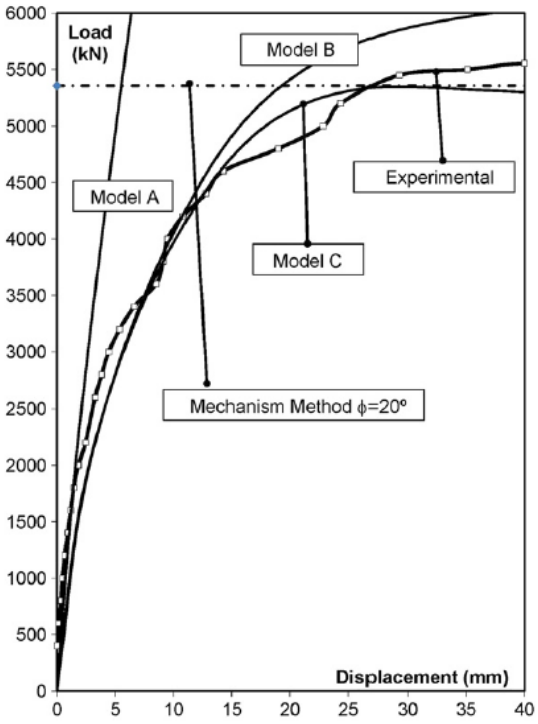

Figure 10 – Load-displacement curves from experiment and numerical models. [17]

Several further numerical analyses are available in literature. Many of them have been conducted as complementary activities to laboratory tests on masonry bridges and still represent a field under development. Useful information can be obtained for example from the dissertation theses "*3D numerical simulation of experiments on masonry arch bridges*" developed by Ignacio Brunet Coll in 2016 and "*Numerical modeling of experimental masonry arch bridge*" developed by Rafael Pereira in 2015, as it will be presented in the following sections of this Report.

3. EXPERIMENTAL DATA

Different tests on masonry bridges were done in the past in the attempt to monitor their behaviour, both in labs and as field test. The arch studied in this dissertation is a short-span, true-scale brick masonry arch bridge that was tested to failure as part of an experimental research conducted by Prof. P. Roca and Prof. C. Molins. The research was developed between 2001 and 2003 and was aimed to provide experimental evidences that could represent a useful additional tool to validate the results of structural analysis of similar structures, developed numerically. Although many studies regarding the behaviour of arches have been developed already, as described in the previous sections of this report, a complete overall understanding of the process and the behaviour of this typology of structures has not been achieved yet, especially when taking into consideration how the different members involved, influence their strength capacity. It will be shown that in the bridges studied the masonry spandrel walls have a large influence in the behaviour of the arch, especially because their thickness is relatively high compared to the overall thickness of the arches themselves.

The research was based on the study of two arches, namely a segmental arch and a semi-circular one. Both of them where built and tested to failure at the Laboratory of Technology of structures of the Technical University of Catalonia. In the scope of the work of this dissertation, the semi-circular arch will be described and studied.

3.1 Description of the experimental arch

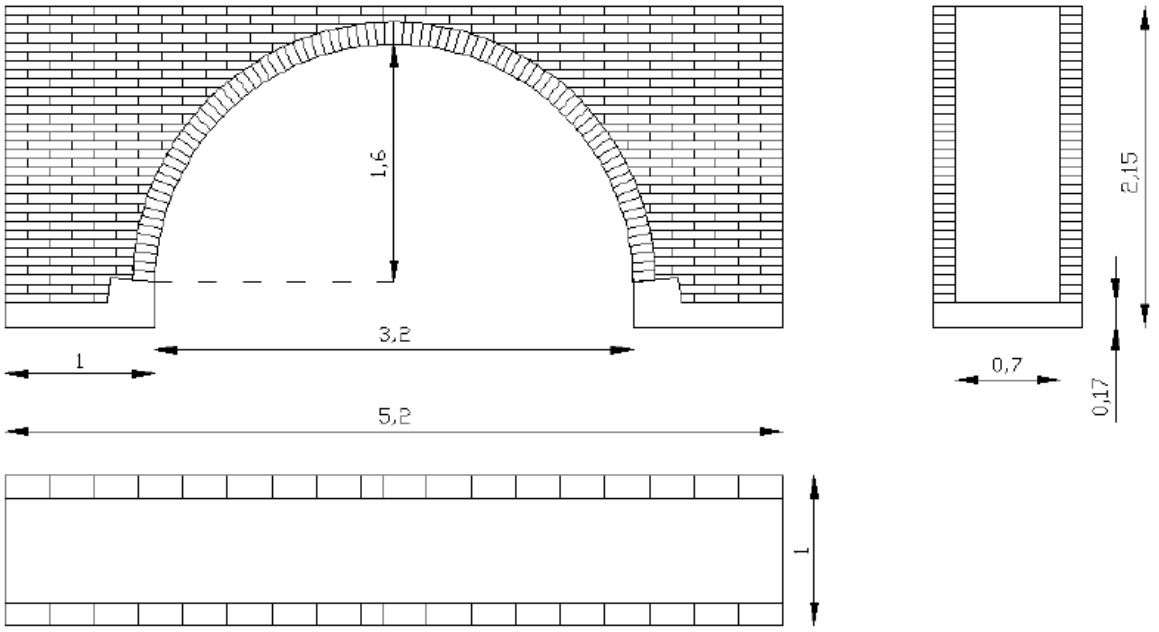

Figure 11 – Geometry and dimensions of the masonry arch bridge. [18]

The experimental masonry arch bridge was built during April 2002 and tested in July 2003. It was built with a span of 3.2 m and a rise of 1.6 m. It was 1 m wide and was built over a reinforced concrete footing, 25 cm thick. The barrel arch and the spandrel walls were built using masonry bricks and were 14 cm thick. The abutments were filled with cohesive rubble masonry made of irregular stone and Portland cement, up to a high of 1 m. The rest of the space between the arch and the walls was filled with sand.

The infill was retained laterally thanks to the use of two steel plates for each side, 1x1 m^2 and 5 mm thick. Vertical profiles with a hollow section SHS 50, 4 mm thick were welded to the plates to provide stiffness. Moreover, horizontal profiles with a hollow section RHS 140x80x6mm were welded to the vertical profiles. The horizontal elements on the two sides were then linked thanks to 8 steel rods, Φ25 mm of diameter, located four at each side of the arch. The ties were therefore simulating the effect of confinement possibly due to an extension of masonry walls beyond the abutments, as well as the presence of natural soil, as visible in Figure 12.

The brick units used in the masonry were 13.5x28.5x4.5 cm, whereas the bed joints were 1-1.5 cm thick and were made of M8 Portland cement, the same mortar was used in the rubble backing.

The infill was made of compacted sand with 6% moisture content and specific weight of 18 kN/m^3; its dry specific weight was 15.55 kN/m^3. A normal Proctor test was used during the compacting process.

Finally, two laminated profiles UPN220 were connected to the footing of the abutments through prestressed transverse bars in order to avoid possible rotations or translations of the bases and therefore simulating the presence of a stiff foundation, condition that usually characterizes real bridges.

Figure 12 – Masonry arch bridge built and tested at the laboratory. [18]

It is to be mentioned that some tests were performed on the materials used to build the bridge in order to characterize their mechanical properties. In particular, masonry bricks and mortar and masonry specimens were tested. The properties of the mortar-units interfaces were determined by testing couplets with a biaxial testing equipment. Significant information regarding the materials' properties can be found in the PhD Thesis **"***Estudio experimental del comportamiento de paredes de obra de fábrica de ladrillo ante la acción de cargas laterals***"** developed by Javier Charry, which describes experimental activities on the determination of property of masonry elements similar to those used in the bridges. [19] Some of the results of the tests are shown in Table 1.

Table 1 – Information on material properties and testing procedures.. [18]

Component	**Property**	**Average (N/mm^2)**	**Type of specimen**
Brick (lengthwise)	*Compressive strength* *Young modulus*	*56.8* *12.750*	*40x40x120 mm prisms*
Brick (flatwise)	*Compressive strength* *Young modulus*	*51.0* *10.450*	*3 stacked 40 mm cubes*
Mortar	*Compressive strength* *Flexural strength* *Young modulus*	*8.34* *2.68* *810*	*Prismatic 40x40x80 mm* *Prismatic 40x40x160 mm*
Joint interface	*Cohesion* *Cohesion* *Initial friction angle* *Residual friction angle*	*0.36* *0.33* *45°* *37.2°*	*Triplet* *Couplet (biaxial equipment)* *Couplet (biaxial equipment)* *Couplet (biaxial equipment)*
Masonry	*Compressive strength*	*14.0*	*4 flat brick prism*
Infill	*Specific weight*	*18 kN/m^3*	

3.2 Experimental Procedure and Results

The load test was performed by applying the load at ¼ of the span, as it can be seen in Figure 12. More specifically, the load was applied through a steel profile HEB200, 60 cm long, acting as a loading beam, to avoid possible local soil bearing failures under the point of application of the load. The beam was sitting exclusively on the infill, in this way no load was applied directly to the spandrel walls. Thanks to a load cell and a spherical hinge placed between the actuator and the loading beam, the load applied and its centrality was monitored throughout the whole experiment.

Three displacement sensors were located under the arch to measure its deflections, as shown in Figure 13. Moreover, two computers were used during the process. One of them was used for the acquisition and monitoring of the data, the second one allowed controlling the intensity and the velocity of the load applied through the hydraulic jack.

Figure 13 – Photo showing the sensors located under the arch. [20]

According to the plan, the load was supposed to be applied in two different cycles, in order to evaluate the development of a four hinges mechanism first and then the ultimate load of the structure. In both phases the load was supposed to be applied at a constant speed of 0.05 bar/s, corresponding to 0.25 ton/min. Unexpectedly, during the first loading cycle, due to of a malfunctioning of the system, the load was not applied for the first 20 min and the load increased all of a sudden, reaching 4 ton in few seconds, corresponding to a load speed of 40 ton/min. When the loading system was stopped, a total load of approximately 9.2 ton was already acting on the bridge and the mechanism of collapse had already started. Because of this, it was not possible to define the order at which the hinges developed, as well as to identify a relation between the level of damage and the load applied. Nevertheless, the points at which the hinges formed reflected the predictions. [20] In the second phase no more hinges appeared and the geometry was not affected by any significant change.

Further to the formation of the four hinges leading to the collapse mechanism, cracks between the spandrel walls and the arch and other longitudinal cracks were observed, as shown in Figure 14.

Figure 14 – Photos of the bridge after the test, showing cracks and hinges. [18]

It is to be specified that due to the unexpected peak of speed at which the load was applied during the first cycle, represented in Figure 15, it is possible that the recorded ultimate value does not represent the ultimate strength of the structure, although it is a reasonable good approximation of it. [20]

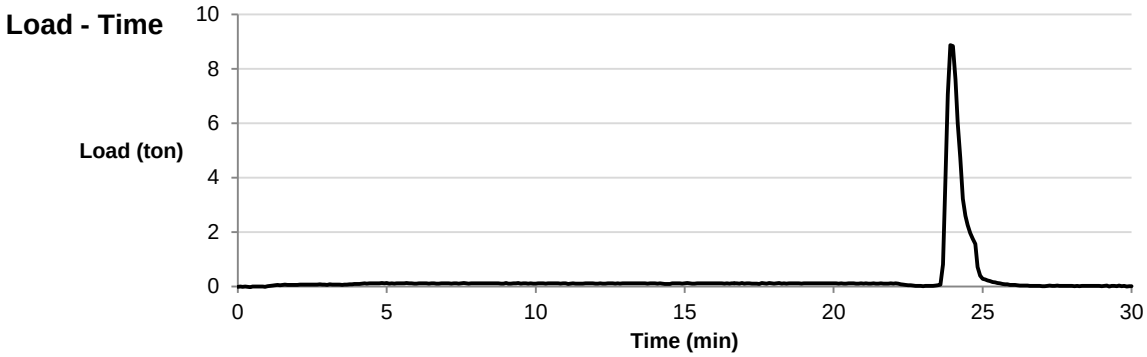

Figure 15 – Diagram relating load and time during the first phase of the experiment. [20]

The load-deflection diagram in Figure 16 shows a significant reduction of the stiffness of the structure. The failure was reached with the formation of a 4th hinge near the springing close to the loaded point.

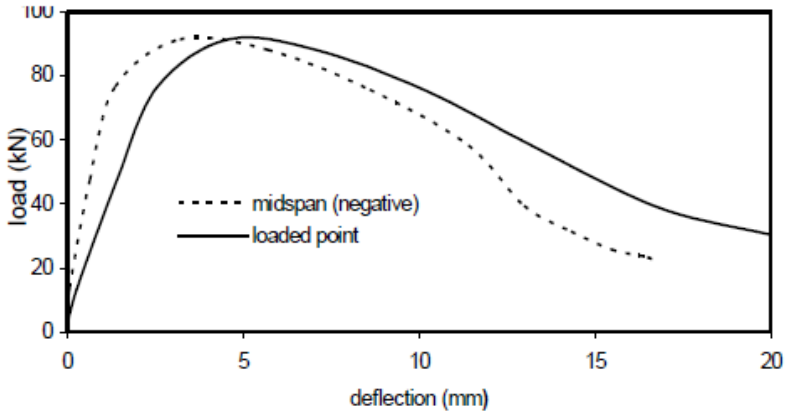

Figure 16 – Load-deflection diagram. [18]

Finally, Figure 17 shows a schematic distribution of cracking in the arch after the completion of the experiment.

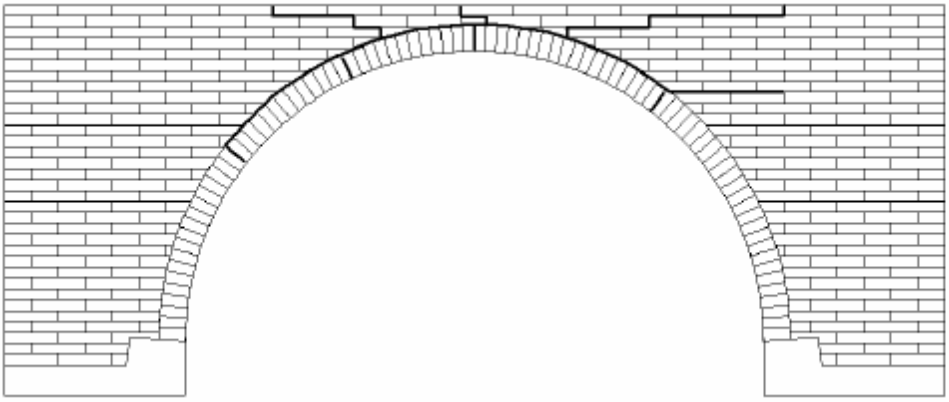

Figure 17 – Distribution of cracking in the arch after the experiment. [18]

4. ANALITICAL PREDICTION

Before proceeding with the numerical study of the load test on the arch, an analytical study of the behaviour of the structure was developed, in order to get a prediction of its ultimate capacity.

The analysis was executed using the Software *LimitState RING 3.0*. A simplified approach is applied, therefore the contributions of spandrel walls, as well as of the steel elements of the structure, were not taken into account.

The structure modelled in RING is shown in Figure 18. The software allows modelling the two materials of the infill, soil and concrete, and applying the load at ¼ of the span. The properties of the materials like masonry and infill were assigned as indicated in Table 1, however, many assumptions were done for example with reference to the coefficients of frictions assigned to the materials.

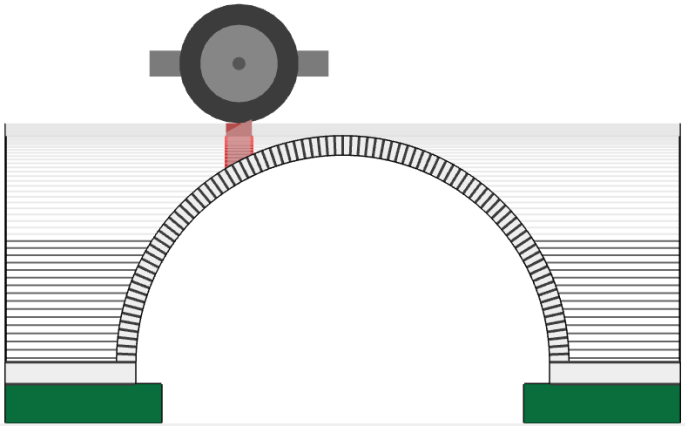

Figure 18 – Structure modelled in RING 3.0.

After running the analysis, the software provides information regarding the load at which the collapse occurs, along with a graphical representation of the collapse mechanism, which includes the hinges that develop and the thrust line, as shown in Figure 19.

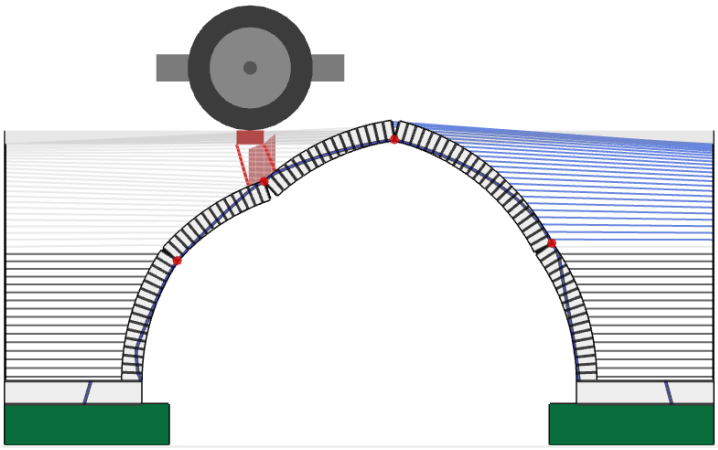

Figure 19 – Output provided by RING 3.0.

According to the limit analysis that was performed, the structure reaches the collapse when a load of 16.4 kN is applied at ¼ of the span. The result is significantly lower than the experimental result. This difference is due to several factors, which include for example the simplifications on which the model is based. As it was demonstrated by Roca and Molins, a limit analysis on the structure which takes into account the contribution of both spandrel walls and steel elements, yields a result much closer to the real one. [18]

5. NUMERICAL MODEL

The development of a numerical study of the arch was done using the finite element software DIANA FEA. The starting point of the study was based on gathering information from previous studies conducted on the two arches being part of the experimental activity.

As mentioned before, the study of an arch masonry bridge using a numerical approach is a complex task. The complexity of the problem, linked to its geometrical and material nonlinear properties, required the implementation of a simplified approach. For this reason, at first it was decided to analyse a bi-dimensional version of the model and to apply increasing levels of complexity in order to evaluate the effects on the behaviour of the structure. This approach allowed getting a better understanding of how the results were affected by the parameters and to have a prediction and a larger control on the results to be obtained through a more complex 3D model.

The following and more significant part of the study was focused on the development of the 3D model. Once again, the approach followed consisted in increasing the complexity of the model gradually.

Finally, a sensitivity analysis was performed by changing certain parameters related to the nonlinearities of the structure, in order to evaluate how the behaviour of the structure was affected.

5.1 Previous dissertations

As mentioned previously, significant information was obtained from the dissertations of Rafael Pereira "*Numerical modeling of experimental masonry arch bridge*" and Brunet Coll "*3D numerical simulation of experiments on masonry arch bridges*". The two theses are part of a study on the segmental arch tested at the UPC laboratory, which involved the participation of several Master's students.

Moreover, further information was obtained from the thesis "*Detailed numerical simulation of experiments on masonry arch bridges by using 3D FE*" developed by Iris Koltsida Spyridoula in 2011, which offered interesting information related to the semi-circular bridge, although mostly limited to a 2D approach.

5.1.1 Pereira (2015)

The analysis of Rafael Pereira was limited to a 2D approach. Pereira worked on a model that had already been studied, making some changes and improvements. Some of the changes that were made are related to the use of a displacement control in the application of the load and therefore, on the implementation of a phased analysis in DIANA FEA. Furthermore, Pereira tried to overcome the excessive rigidity of the model by substituting the rigid supports at the base of the bridge with the use of non-linear springs with infinite stiffness in compression and zero stiffness in tension. [8] However, the results obtained did not differ significantly from the previous, except for a slight decay on the ultimate load.

Figure 20 – Scheme of the implemented support conditions. [8]

Pereira developed a study on the influence of the infill on the results. He showed how an increase in the cohesion had a strong influence on the ultimate load of the structure, how the graph in Figure 21 shows.

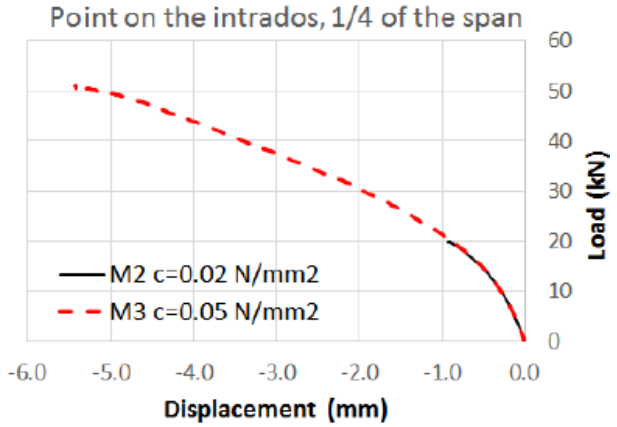

Figure 21 – Comparison between different values of cohesion of the infill. [8]

Pereira interpreted the results stating that the soil was plasticizing due to vertical compression. Therefore, to guarantee the load to reach the arch, he changed the material under the loading beam, which was modelled as being made of masonry.

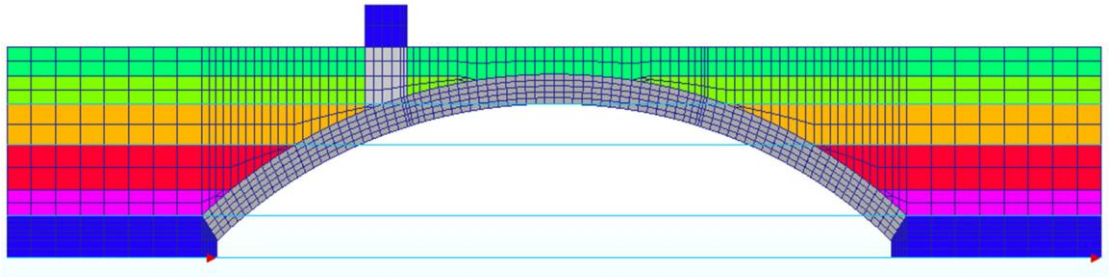

Figure 22 – Scheme of the mesh of the bridge studied by Pereira. [8]

The simplification implemented by Pereira resulted in a not very realistic solution, since the way the load reaches the arch was altered; nevertheless it yielded a good result in terms of deformed shape.

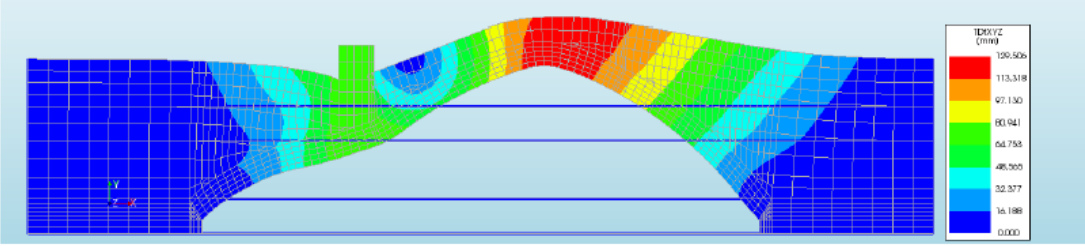

Figure 23 – Deformed shape of the model with infill under the loading block modelled as masonry. [8]

Further analysis developed by Pereira involved some changes in the constitutive model of the masonry: fixed crack was changed to rotating crack, whereas an exponential softening substituted the linear softening behaviour. The results achieved showed a more brittle behaviour. Also, Pereira tested the contribution of the infill and of the interface between arch and infill, demonstrating a beneficial effect due to the presence of the infill. On the other hand, the presence of the interface did not cause a major difference in the results in terms of ultimate load reached by the structure, as shown in Figure 24.

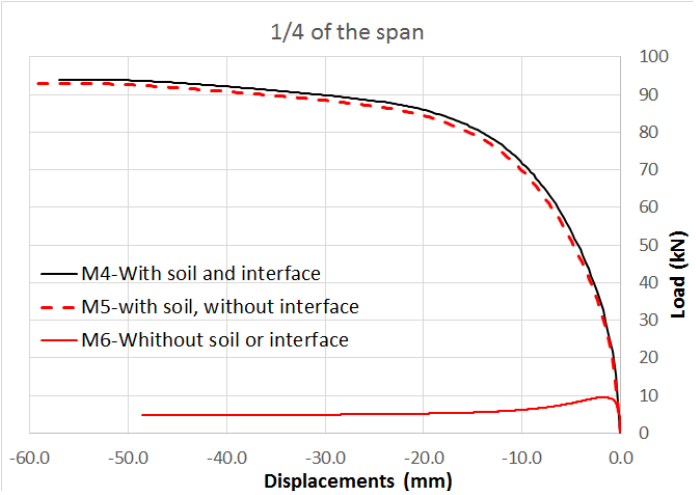

Figure 24 – Comparison of models with and without interface and infill. [8]

Finally, a sensitivity analysis was performed by Pereira, who evaluated the effects due to several parameters such as boundary conditions, cohesion of soil, fracture energy of masonry, cohesion and stiffness of the interfaces, load steps.

The results of the model which best fits the experimental output are shown in Figure 25 in terms of load-displacement diagram. The model shows an overall behaviour similar to the real bridge as well as a similar ultimate load. [8] However, it is important to stress that the model is based on important simplifications that might have affected the reliability of the results.

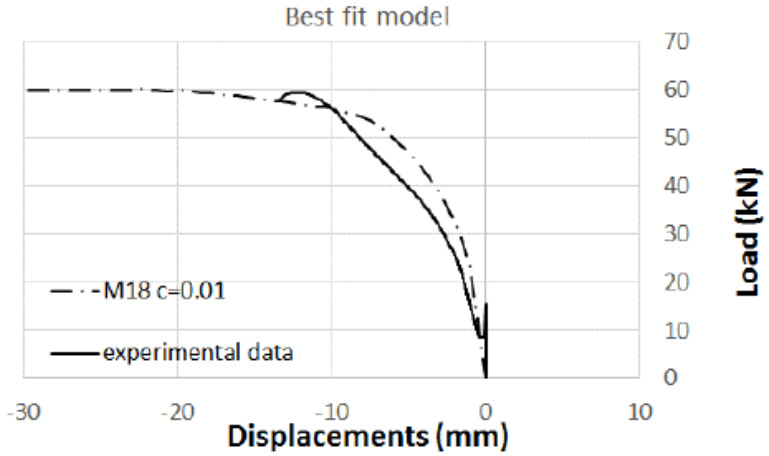

Figure 25 – Load-displacement diagram obtained by Pereira. [8]

5.1.2 Brunet (2016)

Ignacio Brunet developed his analysis on the segmental arch starting from the results obtained by Pereira. This time, the main objective was to analyse the behaviour of the bridge applying a 3D approach.

Similarly to what was done by Pereira, Brunet modelled the structure applying springs as supports and interfaces between elements of different materials. A total strain crack model was applied to the masonry, whereas a Mohr-Coulomb plasticity model was used to model the properties of the infill. The table in Figure 27 shows the material properties applied to the model.

As it was already done by Pereira, the analysis was developed in two phases using the software DIANA FEA, in such a way that the implementation of a displacement control analysis was possible. The symmetry of the load and the geometry was taken into account studying half of the structure, strategy that allowed reducing the time of the analyses. An interesting detail in the model 3D developed by Brunet consists in the slight reduction of the width of the loading beam, in order to ensure the application of the load on the infill and not on the spandrel wall, as it can be observed in Figure 26.

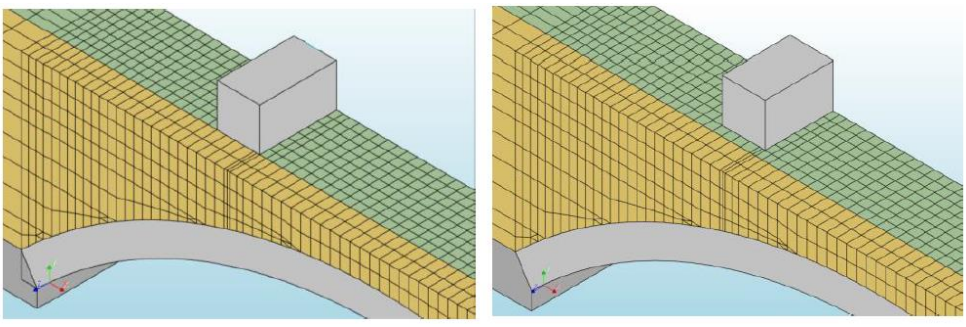

Figure 26 – Detail of the loading beam. [21]

Furthermore, Brunet modelled the soil infill in different layers assigning values of Young's modulus increasing with the depth; the same strategy had been already implemented by Pereira in his 2D model.

Concrete	Young's modulus	E=34000N/mm^2
	Density	2.2E-09 T/mm^3
	Poisson's ratio	0.15
Steel	Young's modulus	200000 N/mm^2
	Density	7.85E-09T/mm^3
	Poisson's ratio	0.27
Masonry	Young's modulus	5120 N/mm^2
	Density	1.8E-09 T/mm^3
	Poisson's ratio	0.18
	Tensile strength	ft=0.1 N/mm^2
	Mode-I tensile fracture energy	GfI=0.03 N/mm
	Compressive strength	fc=21 N/mm^2
	Compressive fracture energy	Gc=50 N/mm
Soil	Reference Young's modulus	15 N/mm^2
	Density	1.84E-09T/mm^3
	Poisson's ratio	0.2
	Mohr-Coulomb plasticity	
	Cohesion	0.003 N/mm^3
	Friction angle	38°
	Dilatancy angle	0°
	Tension cut-off	0 N/mm^2

Figure 27 – Material properties used in concrete, steel, masonry and soil by Brunet. [21]

The results obtained by Brunet are satisfactory. The behaviour of the arch follows the experimental results, both in terms of deformed shape as shown in Figure 28, and also with regards to the separation which occurs between the arch and the spandrel walls, as observed experimentally (Figure 29).

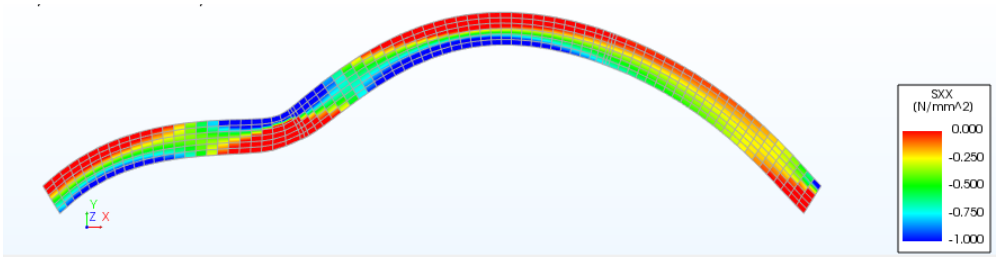

Figure 28 – Deformed mesh of the arch ring. [21]

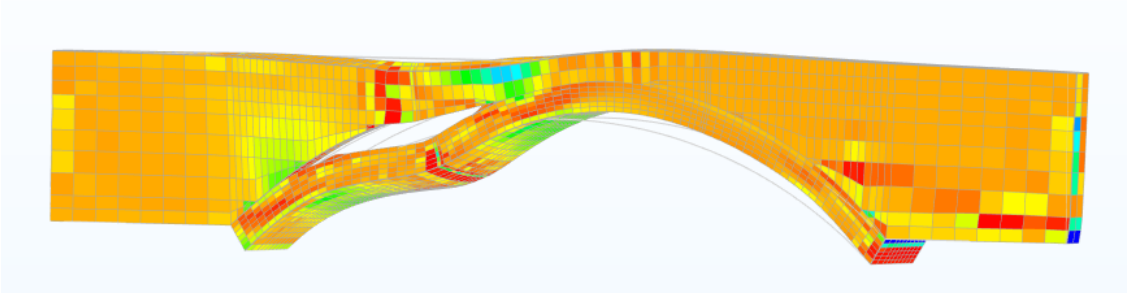

Figure 29 – Principal stress and deformed shape of the arch and spandrel wall. [21]

Similarly to what was done by Pereira, Brunet evaluated the behaviour of the bridge considering the influence of several parameters, such as masonry tensile strength, cohesion and friction angle of the infill. He demonstrated that the increase of masonry tensile strength results in an increase of stiffness of the structure in the elastic domain, as shown in Figure 30 a, whereas, the results showed that the higher the cohesion and the friction angle of the infill, the higher the overall bearing capacity and stiffness (Figure 30 b, c).

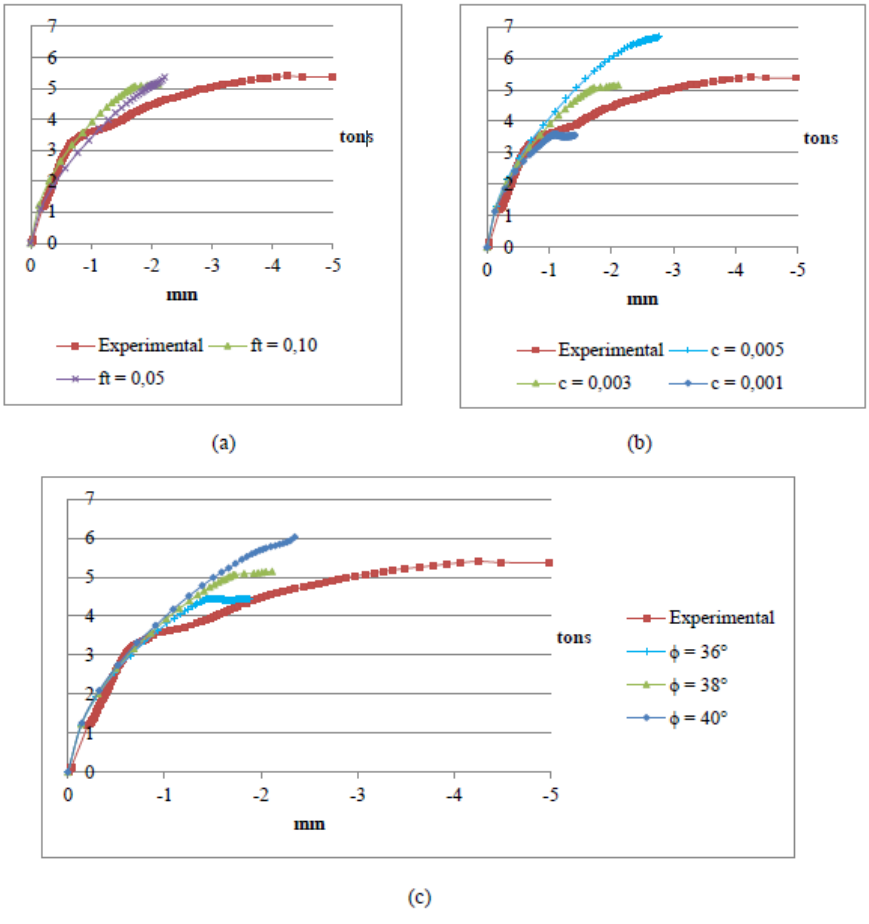

Figure 30 – Load-displacement plots. Sensitive analysis of masonry tensile strength (a), cohesion of sand (b) and friction angle of sand (c). [21]

5.1.3 Koltsida (2011)

Iris Koltsida Spyridoula studied the load test on the barrel arch bridge in 2011 and presented the results in the dissertation "*Detailed numerical simulation of experiments on masonry arch bridges by using 3D FE*". However, despite the title, the study was mainly focused on a bi-dimensional approach.

In fact, she focused on the development of a plane stress model, which therefore neglected the contribution of the spandrel walls. Different configurations of boundary conditions were evaluated; in particular the response of the structure was analysed applying lateral constraint to simulate the presence of the steel plates and the ties, as well as modelling the steel elements. Furthermore, a comparison was developed modelling the infill as a layer or as multiple layers with the value of Young modulus increasing with the depth.

Both a linear and a nonlinear analysis were developed. The Mohr-Coulomb plasticity model was applied to the soil, with the following properties:

- Young's modulus: 37.76 N/mm^2;
- Poisson's ratio: 0.2;
- Mass density: 1.8e-06 kg/mm^3;
- Cohesion: 0.018 N/mm^2;
- Friction angle: 38°;
- Dilatancy angle: 38°.

The masonry was studied considering the energy based total strain fixed crack model with the following properties:

- Young's modulus: 5500 N/mm^2;
- Poisson's ratio: 0.18;
- Mass density: 1.8e-06 kg/mm^3;
- Tensile strength: 0.05 N/mm^2;
- Compressive strength: 14 N/mm^2;
- Tensile fracture energy: 0.03 Nmm^{-1};
- Compressive fracture energy: 5 Nmm^{-1};
- Shear retention factor: 0.01.

Finally, a frictional contact surface for the interface between soil and arch with no hardening was implemented, with:

- Linear normal and tangent stiffnesses: 1e+06 N/mm;
- Cohesion: N/mm^2;
- Friction angle: 38°;
- Dilatancy angle: 38°.

The results achieved in the different models and configurations correspond to ultimate loads much lower than the experimental value. The reason of the discrepancy might be the lack of the contribution of the spandrel walls.

5.2 Constitutive models and material properties

One of the most complicated aspects related to numerical modelling is connected to the choice of the parameters that define the mechanical properties of a material. The complexity is related both to the uncertainties regarding such parameters in the real structure and to the difficulty of translating them in actual numbers. DIANA FEA offers several material models that can be applied, such as for example concrete, masonry, concrete, steel and soil. It is very important to properly select the material model since its parameters have a strong effect on the results obtained.

Moreover, DIANA FEA allows assigning specific properties to the interface of two different materials, for a better simulation of their real behaviour, as it will be presented shortly.

The following paragraphs describe the models that were applied to each material and the values assigned to each parameter. It is important to stress that these values, mostly taken from literature, are the results of experimental activities and can vary within a range that is very often quite large. As a consequence, it is not possible to identify a unique correct value, but several attempts are required to calibrate the model and to identify the combination of values given to all the parameters that provide the best description of the behaviour of a structure.

5.2.1 Concrete and steel

Concrete and steel are materials that have a limited application in this model. Concrete is used in the bases of the arch and as fill of the abutments up to a high of 1 m; whereas steel is the material of the plates and profiles used to retain the infill laterally, of the ties that link them and of the beams at the base.

For both concrete and steel, a linear elastic isotropic material is used. This simplification is justified by the fact that these materials will not reach their ultimate strength. The properties used in the model are indicated in Table 2.

Table 2 – Properties of Concrete and Steel.

Concrete	*Young's modulus*	*34000 N/mm^2*
	Density	*2.5 10^{-9} T/mm^3*
	Poisson's ratio	*0.15*
Steel	*Young's modulus*	*200000 N/mm^2*
	Density	*7.85 10^{-9} T/mm^3*
	Poisson's ratio	*0.27*

5.2.2 Masonry

DIANA FEA offers several models to simulate the behaviour of this complex orthotropic material. First of all it was decided to follow a macro-model approach, which yields a good efficiency despite its higher simplicity compared to a micro-model approach. Masonry was therefore modelled as a continuum.

At a macro level, several material models are available in DIANA FEA; in this case the *Total Strain Crack Model* is used, as it was done in the previous dissertations analysed. [21] The model is based on the use of a smeared approach for the fracture energy, which simulates cracked materials as continuous with anisotropic characteristics.[22] Within this model, different approaches can be used, namely *Fixed Crack Model*, *Rotating Crack Model* and *Rotating to Fixed Crack Model*. A Total Strain Crack Model evaluates the stress as function of the strain, in the direction given by the cracks. However, when using a rotating approach, the stress-strain relations are evaluated in the principal directions of the strain vector [22], whereas in a fixed crack model, stress-strain relations are evaluated in a fixed coordinate system. For the sake of simplicity, it can be said that the crack directions are considered fixed or rotating with the principal direction of the strain vector. [22] In this study, a *Rotating Crack Model* was applied.

The behaviour of masonry materials can be described by the typical stress-displacement plots represented in Figure 31. When studying masonry in compression, we can observe an almost elastic behaviour up to 80-90% of the strength, with nonlinearity due to early micro-cracking and damage. In the post peak, a plastic behaviour can be observed, due to the formation of irreversible deformation, as shown in Figure 31, graph (a).[23] In the case of tension, the behaviour up to the maximum strength can be reasonably defined as linear, with tensile strength always much lower than the compressive strength.[23] A phenomenon of softening, defined as a gradual decrease of mechanical resistance under a continuous increase of deformation [23], is common to both compression and tension after reaching the maximum value of strength. The area under the curves shown in Figure 31 represents the compressive fracture energy (G_c) and the tensile fracture energy (G_f).

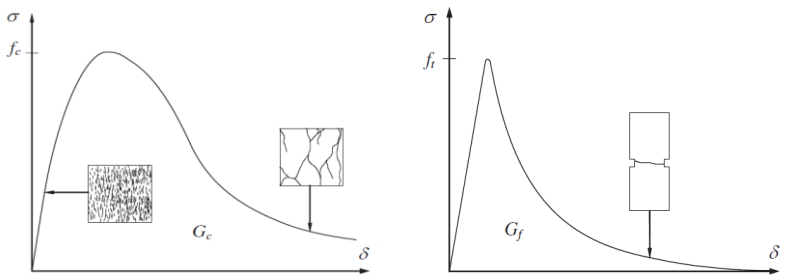

(a) (b)

Figure 31 – Typical stress-displacement plot for masonry in compression (a) and tension (b). [23]

Many functions can be applied in DIANA FEA to describe the tension and compression behaviour of masonry. The model of this work is based on the use of a parabolic function in case of compression and a linear softening function based on fracture energy to describe the tension softening, as shown in Figure 32. The parameters required by the software are compressive strength and fracture energy, along with tension strength and fracture energy.

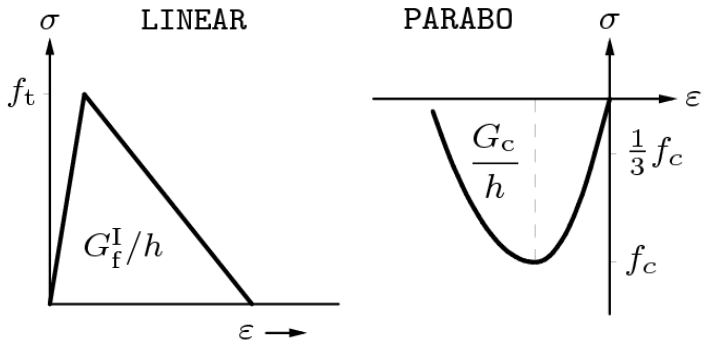

Figure 32 – Linear tension softening behaviour (left) and parabolic compression function (right). [22]

The compressive strength of the masonry is based on the tests on the materials conducted during the experimental activity, it is therefore assumed equal to 14 N/mm^2, as indicated in Table 1. The value of tensile strength can be estimated considering that the ratio between tensile and compressive strength varies usually between 0.1 and 0.01[23], the value of 0.15 N/mm^2 is applied. The estimate of the tensile fracture energy is based on information that can be found in literature. According to data gathered during experimental activities, the recommended ductility index for bricks is 0.029 mm, being the ductility the ratio between the fracture energy and the tensile strength [24]; however, since the value that can be obtained applying this formulation is extremely low, the recommended value of 0.012 N/mm is applied. [23] As for the compressive fracture energy, the formulation proposed for concrete in the Model Code 90 can be applied [24] which states that:

$$G_{f,c} = 15 + 0.43\, f_c - 0.0036\, f_c^2$$

The Young's modulus E can be calculated according to references that can be found in literature. According to Eurocode 6 and in absence of experimental determination $E = 1000\, f_k$, being f_k the characteristic compressive strength of the masonry; according to Tomazevic it can be calculated as $200\, f_k \le E \le 2000\, f_k$ [25], finally the following relation can also be found in literature: $E=750\, f_m$ [26]. The values that can be obtained with these formulations are quite high if compared to the usual values of Young's Modulus for brick masonry that can be found in literature. The reason is probably due to the fact that when large walls are built, E modulus is considerably different than in small specimens, due to a smaller control in the uniformity of the assemblage. [27] For this reason it was decided to assume a value of Young's modulus varying between 4000 and 6000 N/mm^2.

The values of the mechanical properties of the masonry used in the model are based on the considerations presented in the previous paragraphs and are summarised in the following Table 3.

Table 3 – Properties of Masonry.

Masonry	*Young's modulus*	*5000 N/mm^2*
	Density	*1.8 kN/m^3*
	Poisson's ratio	*0.18*
	Tensile strength f_t	*0.15 N/mm^2*
	Mode-I tensile fracture energy GfI	*0.012 N/mm*
	Compressive strength f_c	*14 N/mm^2*
	Compressive fracture energy Gc	*20 N/mm*

5.2.3 Soil

Since the available information regarding the sandy material that was used during the experimental activity is limited to its density, the model was based on the use of general parameters related to sand that can be found in literature. The models offered by DIANA FEA to describe the behaviour of soil and rock are several, to allow the user to take into considerations a wide range of conditions, related for example to soil type, failure mechanisms and characteristics of loads. The *Mohr-Coulomb and Drucker-Pager Yield Condition Model* was adopted. Furthermore, given the uncertainty related to them, the properties of the soil were one of the main aspects that were studied during the sensitivity analysis performed on the structure, as it will be presented in the following sections of this Report.

The Mohr-Coulomb model is an approximation of the soil behaviour which is based on a linear elastic perfectly plastic model. [28] According to the model of Mohr-Coulomb, the behaviour is linear in the elastic range and refers to Hooke's law and therefore to mechanical properties such as Young's modulus and Poisson's ratio. The failure criteria of the material is described by two parameters, friction angle and cohesion; finally, the flow rule is described by the dilatancy angle.[29] In case of sandy materials, a non-associated rule is used to model a more realistic irreversible change in volume due to shearing.[29]

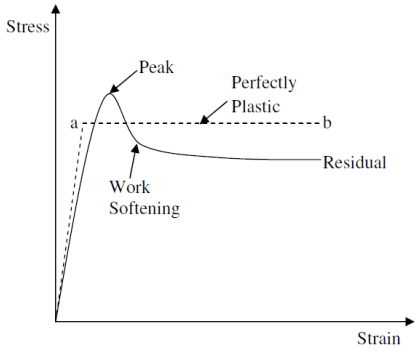

Figure 33 – Elastic-perfectly plastic assumption of Mohr-Coulomb model. [29]

The Young's Modulus E can vary significantly in case of sandy soil within a large range of values, as indicated in **Error! Not a valid bookmark self-reference.**. Similarly, the Poisson's ratio presents a variability related to its density and granulometry, as shown in Table 5.

Table 4 – Typical values of Modulus of Elasticity E. [30]

Type of soil		*E (N/mm^2)*
Sand	*Silty*	*7-21*
	Loose	*10-24*
	Dense	*48-81*
Sand and gravel	*Loose*	*48-148*
	Dense	*96-192*

Table 5 – Typical values of Poisson's ratio. [30]

Type of soil	*v*
Sand (dense)	*0.2-0.4*
Course (void ratio 0.4-0.7)	*0.15*
Fine grained (void ratio 0.4-0.7)	*0.25*

With reference to the modulus of elasticity, several studies have demonstrated that the Young's Modulus increases with the stress levels, and therefore with the depth of the soil. Different relations between E and depth of the soil can be found in literature, an example is the following:

$$E(z) = E_0 + (z - z_0)\frac{\partial E}{\partial z} \quad [31]$$

In which E_0 is the modulus of elasticity at the surface and z_0 is its coordinate, z is the vertical coordinate referring to the depth under analysis and $\frac{\partial E}{\partial z}$ is the gradient of the Young's modulus in the vertical direction.[31] The reference values for a sandy soil are:

$$E_0 = 25 \text{ N/mm}^2$$

$$\frac{\partial E}{\partial z} = -4.5\ 10^{-2} \text{ N/mm}^3 \text{ [31]}$$

The model offered by DIANA FEA does not allow taking into account the increase of E due to the depth, therefore it has to be implemented manually. In the case object of study however, given the limited depth, it was decided not to vary the value of E, with a beneficial effect on both the complexity of the model and the time spent for the analysis.

The cohesion for sandy soil is usually null, however, in order to allow convergence in the model, a value of cohesion small but still bigger than zero was applied.

The friction angle φ is influenced by soil density, shape of particles and soil gradation. [32] The values that can be found in literature for sandy soils vary within a large range, examples of experimental results are shown in Table 6.

Table 6 – Typical values of Angle of friction. [32]

Type of soil	*φ*	
	Loose	*Dense*
Uniform sand, round grains	*27*	*34*
Well-graded sand, angular grains	*33*	*45*
Sandy gravels	*35*	*50*
Silty sand	*27-33*	*30-34*
Inorganic silt	*27-30*	*30-35*

The dilatancy angle ψ was observed to be about 1/3 of the peak friction angle in case of very dense sand, whereas its value reduces to a few degrees in loose sand. [32] However, according to literature, an easy way to approximate its value is to apply the following expression:

$$\Psi = \varphi - 30° \text{ [32]}$$

Materials like soils and rocks are characterized by phenomena of hardening and softening of properties such as cohesion and friction angle when the plastic deformations increase [29]. Within the Mohr-Coulomb model, DIANA FEA offers the possibility to take into consideration the change of these parameters and of the dilatancy angle. Moreover, a tension cut-off can be included to account for the case in which tensile stresses may develop and failure of the soil may be due to tension instead of shear. This option can be selected and a value of tensile strength can be defined. [28]

The User's manual of DIANA FEA provides some guidelines to calculate and implement a cohesion hardening curve in the Software, the example presented in the documentation is shown in Figure 34.

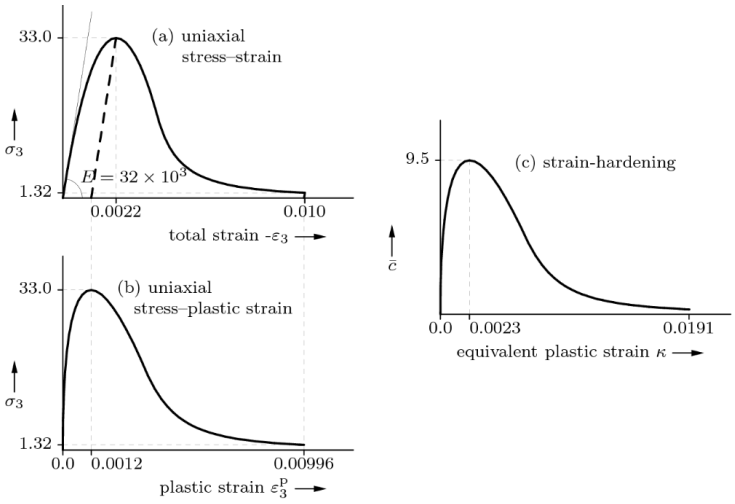

Figure 34 – Example of derivation of hardening diagram for cohesion in DIANA FEA. [22]

In the case object of the study the hardening of the cohesion was taken in account by defining the trilinear simplified diagram shown in Figure 35, in which the cohesion is calculated as:

$$c = f_c \frac{1 - \sin\varphi_0}{2\cos\varphi_0}$$

The internal state variable for a strain hardening hypothesis k, is defined as:

$$\dot{k} = -\frac{\sqrt{1 + sin^2\psi_0 - \frac{2}{3}\sin\psi_0}}{1 - \sin\psi_0}\ \dot{\varepsilon}_3^P$$

And the plastic strain ε_3^P defined as ε_3 - ε_3^e is calculated as:

$$\dot{\varepsilon}^P = \begin{Bmatrix} \dot{\varepsilon}_1^P \\ \dot{\varepsilon}_2^P \\ \dot{\varepsilon}_3^P \end{Bmatrix} = \dot{\lambda} \begin{Bmatrix} \frac{1}{4}(1 + sin\,\psi_0) \\ \frac{1}{4}(1 + sin\,\psi_0) \\ -\frac{1}{2}(1 - sin\,\psi_0) \end{Bmatrix}$$

Some assumptions were made. The compressive strength of the soil was assumed equal to f_c = 40 kPa and the value of λ is assumed equal to 0.03. [33]

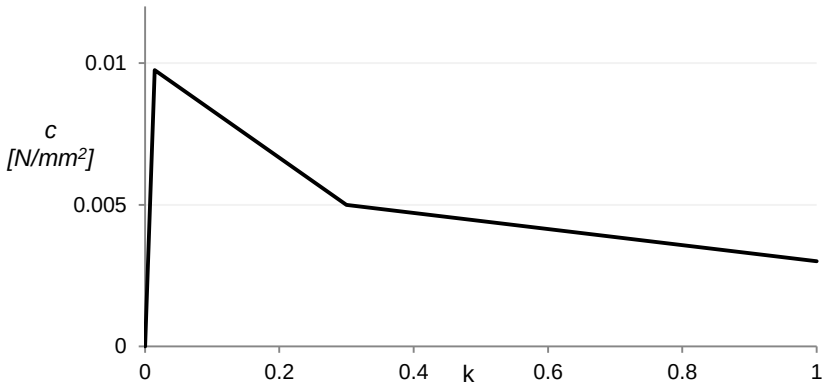

Figure 35 – Trilinear simplified diagram of cohesion based on the hypothesis of strain hardening.

All the values applied to the soil are indicated in the following table.

Table 7 – Properties of Soil.

Soil	*Young's modulus*	*35 N/mm²*
	Density	*1.84 10⁻⁹ T/mm³*
	Poisson's ratio	*0.25*
	Cohesion	*0.003 N/mm²*
	Friction angle	*38°*
	Dilatancy angle	*8°*
	Tension cut-off	*0 N/mm²*

5.2.4 Interfaces

The interface elements are structural elements which can be modelled in DIANA FEA to describe the interface behaviour in terms of normal and shear traction and relative displacements between two different elements. [22] The type of interface in terms of shape and connectivity varies according to the type of elements that are used in the model; nodal interface, two-dimensional and plane interfaces can be chosen. In the case of bi-dimensional models, linear interface elements are used, whereas in the solid model, the interface elements are plane elements.

Once again, one of the biggest challenges when using these elements is the correct choice of the parameters. For example, the interface stiffness should be selected in such a way that the load-displacement curve resemble the one obtained without interfaces, so that the influence of interfaces is taken in consideration when a true plastic slip develops. [22]

In the structure being analysed, three different typologies of interface are used. The first one is the contact surface between soil and masonry elements, namely the arch and the spandrel walls. The second is the interface between the arch and the spandrel walls; the need to model this last interface is due to the fact that during the load test a separation between spandrels and barrel arch was experienced. Finally, the third is the interface between steel plates and soil or masonry.

5.2.4.1 Soil – Masonry Interface

In a structure characterized by a combination of soil and masonry, a relative movement of the soil with respect to the main structure and *vice-versa* can occur. DIANA FEA allows taking into account the presence of an interface between the two materials to overcome the constraint characterizing the finite element method that imposes adjacent element to move together. [34]

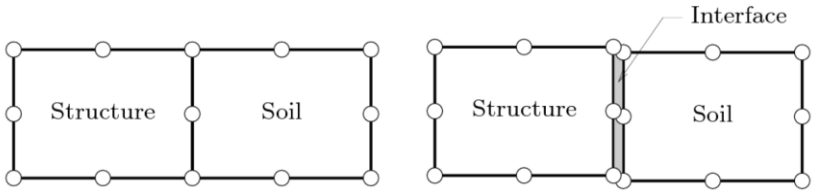

(1) (2)

Figure 36 – Finite element modelling of soil-structure interaction: Continuum elements (a), interface elements (2). [34]

Slip and gap opening might occur between soil and structure elements; therefore DIANA FEA recommends applying a Mohr-Coulomb criterion in combination with a no-tension condition. [34]

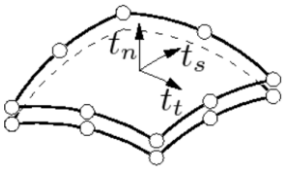

Figure 37 – Stress generated in a three-dimensional interface. [34]

To calculate the stresses developed in the interfaces represented in Figure 37, the Software requires some input that include the normal interface stiffness D_{nn}, the two shear interface stiffnesses D_{tt} and D_{ss}, cohesion, friction and dilatancy angles. According to the Guidelines provided by the Software, the stiffnesses can be calculated applying the following expression:

$$D_{tt} = D_{ss} = \frac{A^2}{t} \frac{E_{soil}}{2\,(1+\nu_{soil})}$$

$$D_{nn} = f\ x\ D_{tt}$$

In which E_{soil} and v_{soil} are the Young's Modulus and the Poisson ratio of sand respectively. A is a reduction factor that ranges from 0.5 to 1, t is a length that represents the virtual thickness of the interface and f is a factor that can vary from 10 to 100. These figures show clearly how large the range in which the values vary is.

The Coulomb friction properties such as cohesion and friction angle can be set as:

$$c = A\ c_{soil}$$

$$\tan\varphi = A \tan\varphi_{soil}$$

Dilatancy in interfaces is usually assumed equal to zero, to avoid volumetric strains that would be unrealistic; moreover, it is assumed that tensile stress cannot develop, which implies that when stress in an interface becomes positive, a gap arises. To model this situation, a tension cut-off with zero tensile strength is applied. [34] According to information based on experimental and numerical studies that can be found in literature, the thickness of the interface can be estimates ad five-to-ten times the mean effective diameter of the soil. [35] According to scientific evidences, a reasonable value of 0.2 mm is assumed as mean effective diameter of the soil. [36][37]

The values used in the calculations are indicated in the following Table 8.

Table 8 – Properties of Soil-Masonry interfaces.

Soil-Masonry Interfaces	*Reduction factor A*	*1*
	Thickness t	*2 mm*
	Normal stiffness D_{nn}	*70 N/mm^2*
	Shear stiffnesses D_{tt}, D_{ss}	*7 N/mm^2*
	Cohesion c	*0.003*
	Friction angle φ	*38°*

5.2.4.2 Masonry – Masonry Interface

The implementation of an interface between barrel arch and masonry spandrel walls follows different guidelines than the soil-masonry interface, since different materials and mechanisms are involved. In this case it was decided to apply the *Combined cracking-shearing-crushing* model that is commonly used in micro-modelling to take into account the unit-mortar interface that characterizes masonry elements and that allows the simulation of fracture, frictional slip and crushing along joints.[22]

DIANA FEA requires several parameters which include linear material properties such as Normal and Shear Stiffness, along with parameters that affect cracking, shearing and crushing phenomena.

Reasonable values of stiffnesses can be calculated following the Guidelines provided by the "*DIANA FEA frequently asked questions*" page of the Software's website. According to the information given by the Technical support, normal stiffness K_n and shear stiffness K_t can be calculated respectively as:

$$K_n = \frac{E}{l_e}$$

$$K_t = \frac{K_n}{\alpha}$$

In which l_e is the everage element size in the mesh, equal to 50 mm, E is the average elastic modulus between the elements and α is a parameter that varies between 10 and 100. [38]

According to another source available in literature, normal stiffness and shear stiffness can also be calculated as:

$$K_n = \frac{E_u E_j}{h_j(E_u - E_j)}$$

$$K_{nt} = \frac{G_u G_j}{h_j(G_u - G_j)}$$

In this case, the formulations take in consideration the values of the thickness of the joints, the Young's moduli of unit and mortar and their shear moduli. [39] The values applied to the model were calibrated evaluating the response that was obtained.

The parameters required to model the cracking behaviour are the tensile strength f_t and the fracture energy G_f. These factors are highly dependent on the units and the mortar, however the tensile bond strenght varies usually in the range of 0.1 to 0.4 N/mm^2 [23], whereas fracture energy has been observed varying within the range of 0.0005 to 0.035 mm for different combinations of mortar and units, recommended values corresponding to 0.2 N/mm^2 and 0.012 N/mm respectively were applied. [23][39]

To model the non-linear shear behaviour of the interface in DIANA FEA, a wide range of parameters is required:

- Cohesion;
- Friction angle;
- Dilatancy angle;
- Residual friction angle;
- Confining normal stress;
- Exponential degradation coefficient;
- Mode II fraction energy – Parameter a;
- Mode II fraction energy – Parameter b.

According to Eurocode 6, the bond shear strength, or cohesion c, varies between 0.1 to 0.4 N/mm^2.

The recommended values for friction angle and dilatancy angle are 0.75 and 0 respectively. [23] DIANA FEA allows the users to apply a residual friction angle and a exponential degradation coefficient because experimental results have shown a typical exponential shear softening diagram with a residual dry friction level [23], however in the absence of more information these fields were left blank.

The Fracture Energy for mode II is calculated by DIANA FEA applying the following expression:

$$G_f^{II} = a^{\sigma} + b \text{ [40]}$$

The factor a can be set as zero and as a consequence the Fracture Energy assumed constant. The recommended value of fracture energy for mode II equal to 0.028 N/mm is assumed. [23] Usually, an average value of fracture energy equal to 1/10 c is adopted. [39]

Some parameters have to be set to consider the cap mode; they include the masonry uniaxial compressive strength f_m and the shape of the elliptical cap given by $C_{s.}$ [39] The values applied are 10.5 N/mm^2 and 9, as found in literature. [41]

Finally, DIANA FEA requires the compressive fracture energy G_{fc} and the equivalent plastic relative displacement K_p corresponding to the uniaxial compressive strength. [39] According to literature, a satisfactory estimate of the compressive fracture energy can be done using the values proposed for concrete in Mode Code 90:

$$G_{fc} = 15 + 0.43\, f_m - 0.0036\, f_m^2 \quad \text{[39]}$$

Finally the equivalent relative displacement k_p can be calculated so that the total masonry strains equals 0.2%, by applying the following:

$$K_p = \left\{0.002 - f_m \left[\frac{1}{E_u} + \frac{1}{k_n\,(h_u + h_j)}\right]\right\} f_m$$

Being E_u the Young's Modulus for the unit, equal to 10.450 N/mm^2 according to the experimental results, k_n the normal stiffness at the interface and h_u and h_j the thicknesses of the units and of the joints, assumed equal to 45 mm and 15 mm respectively. According to the Guidelines provided by DIANA FEA the input of K_p has to be positive, since by applying the above mentioned formula a negative value is obtained, a very small value is applied.

Table 9 – Properties of Masonry-Masonry interfaces.

Masonry-masonry interface	***Linear material properties***	*Normal stiffness modulus*	*110 N/mm^3*
		Shear stiffness modulus	*11 N/mm^3*
	Cracking	*Tensile strength*	*0.2 N/mm^2*
		Fracture energy	*0.012 N/mm*
	Shearing	*Cohesion*	*0.3 N/mm^2*
		Friction angle	*37°*
		Dilatancy angle	*0°*
		Residual friction angle	*-*
		Confining normal stress	*-*
		Exponential degradation coefficient	*-*
	Mode II fracture energy	*Parameter a*	*0*
		Parameter b	*0.028 N/mm*
	Crushing	*Compressive strength*	*10.5 N/mm^2*
		Factor Cs	*9*
	Compressive inelastic law	*Compressive fracture energy*	*19.12 N/mm*
		Equivalent plastic relative displacement K_p	*0.001 mm*

5.2.4.3 Steel – Soil/Masonry Interface

The third typology of interface that was implemented in the model is applied between the steel plates and the soil or the masonry, at the extremities of the arch. In this case the material applied is defined as having a linear elastic behaviour. Therefore, only parameters such as normal and shear stiffness, K_n and $_{Kt}$ are required. Reference values are calculated as described previously, as:

$$K_n = \frac{E}{l_e}$$

$$K_t = \frac{K_n}{\alpha}$$

In which l_e is the everage element size in the mesh, equal to 50 mm, E is the average elastic modulus between the elements and α is a parameter that varies between 10 and 100. [38] When using the values obtained applying this formulation, problems of convergence in the model arose. It was

therefore decided to apply values closer to those used by Brunet in his study [21], which presented good results, that are shown in the following table.

Table 10 – Properties of interfaces between steel plates and the bridge.

Steel - Masonry/Soil Interfaces	*Normal stiffness*	*1700 N/mm^3*
	Shear stiffness	*170 N/mm^3*

5.2.5 Springs

Spring elements were applied at the bases of the model to simulate the fact that the real structure was simply sitting on the concrete slab of the Lab. The element applied is defined in DIANA FEA as a translational spring, for which the stiffness is to be defined by the user. The model that was chosen to describe its behaviour is defined as ultimate forces. The values applied to the parameters are shown in the following table.

Table 11 – Properties of springs.

Springs	*Spring stiffness*	*1e+15 N/mm*
	Ultimate forces	
	Minimum	*-1e+50 N*
	Maximum	*0 N*

6. MODEL 2D

The first approximation to be done when working with a bi-dimensional configuration is the selection of the section to study. In this case of study, it is possible to choose a section along the longitudinal axis of the bridge, considering only the presence of the infill, or to study a section where the contribution of the spandrel walls can be taken into account. It was decided to consider the section along the infill, disregarding the presence of the spandrel walls. The implication of this choice is evident: the presence of the spandrel wall is neglected and therefore its beneficial influence in the overall capacity of the arch is not taken into account. As mentioned previously, in the experimental arch, the influence of the walls is high, due to the fact that their thickness is high in relation to the overall thickness of the structure. However, when studying a real structure of larger size, the approximation with a bi-dimensional element results in a mistake of smaller entity, as the contribution of the spandrel walls decreases when increasing the width of the arch.

The geometrical definition of the model was done by importing a section previously drawn in Autocad. DIANA FEA transformed automatically its parts in polygon sheets, one of the 2D primitive shapes available in the software.

The geometry shapes were then assigned properties such as

- Element class;
- Material;
- Geometry.

Two different element classes were studied at an early stage, namely *Plane stress* and *Plane strain*.

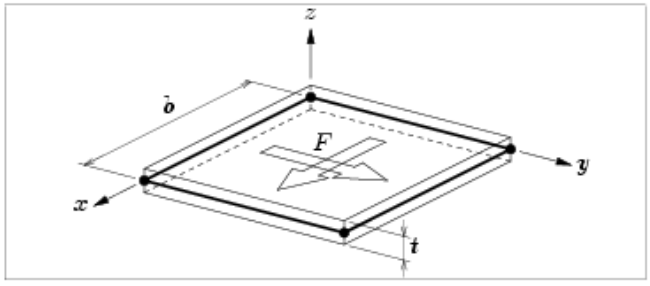

Figure 38 – Plane stress element in DIANA FEA. [22]

A *Plane stress* element can be assigned to any flat surface in which the thickness is small in relation to the dimension in the plan of the element. The thickness is in this case equal to 1 m and is assigned to the elements by defining its geometry. Plane stress elements are characterized by loads applied in the plane of the element and stresses in the plane of the surface, out-of-plane strains are considered results of the Poisson's effect. [22]

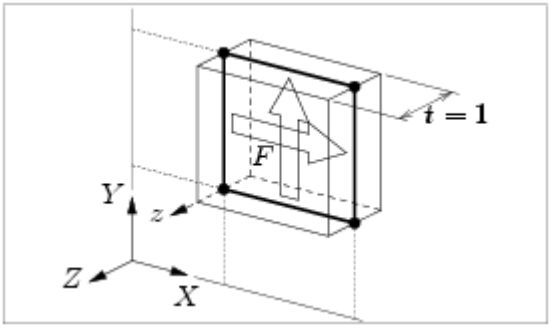

Figure 39 – Plane strain element in DIANA FEA. [22]

The element class assigned to the 2D models is *Plane strain*. These elements are usually used to model the cross-section of a long structure; the load acts on the plane of the section, the thickness is equal to 1 and the strain components perpendicular to the face are equal to zero. [22] Since DIANA FEA only allows assigning the non-linear material properties to the soil in a plane strain model and not to the plane stress, this model was used in the bi-dimensional analysis.

After choosing the element type used in the analysis, the definition of the mesh size follows. In this case the mesh was defined applying a more defined scheme in the arch, in order to capture the nonlinearity that might occur in that area, and a more coarse subdivision in meshes in the other area of the structure, as it can be seen in the following Figure 40.

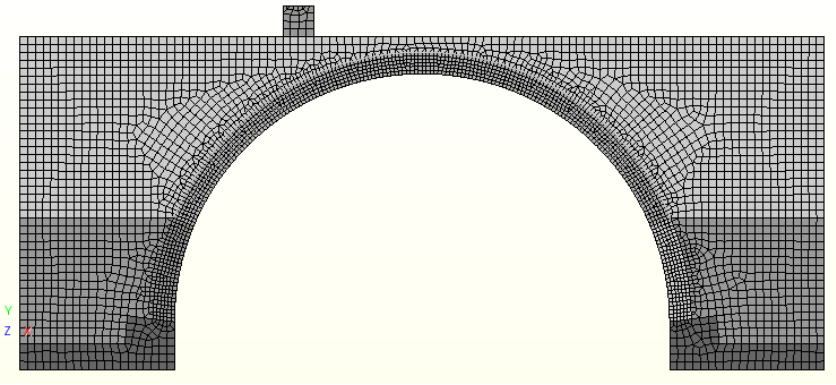

Figure 40 – 2D representation of the structure with mesh.

6.1 Boundary conditions

One of the most important aspects to be carefully evaluated in a finite element model is the definition of the boundary conditions. Their importance is related to the fact that they define the restrictions on the degrees of freedom in the nodes. [22] The masonry bridge that was tested in the lab during the experimental campaign was built on concrete bases to avoid lateral sliding, with steel profiles at the two longitudinal sides to avoid any possible lifting of the bases. Furthermore, steel plates linked by steel cables were applied at the two sides to contain laterally the infill.

The presence of the elements described above is taken into account in three different configurations of boundary conditions:

- Model A: fixed supports are applied at the bases of the bridge and horizontal translation is restrained at the sides to simulate the presence of the steel plates;
- Model B: fixed supports are applied at the bases of the bridge and steel plates and ties are modelled;
- Model C: springs are applied at the bases along with a steel beam and steel elements are modelled.

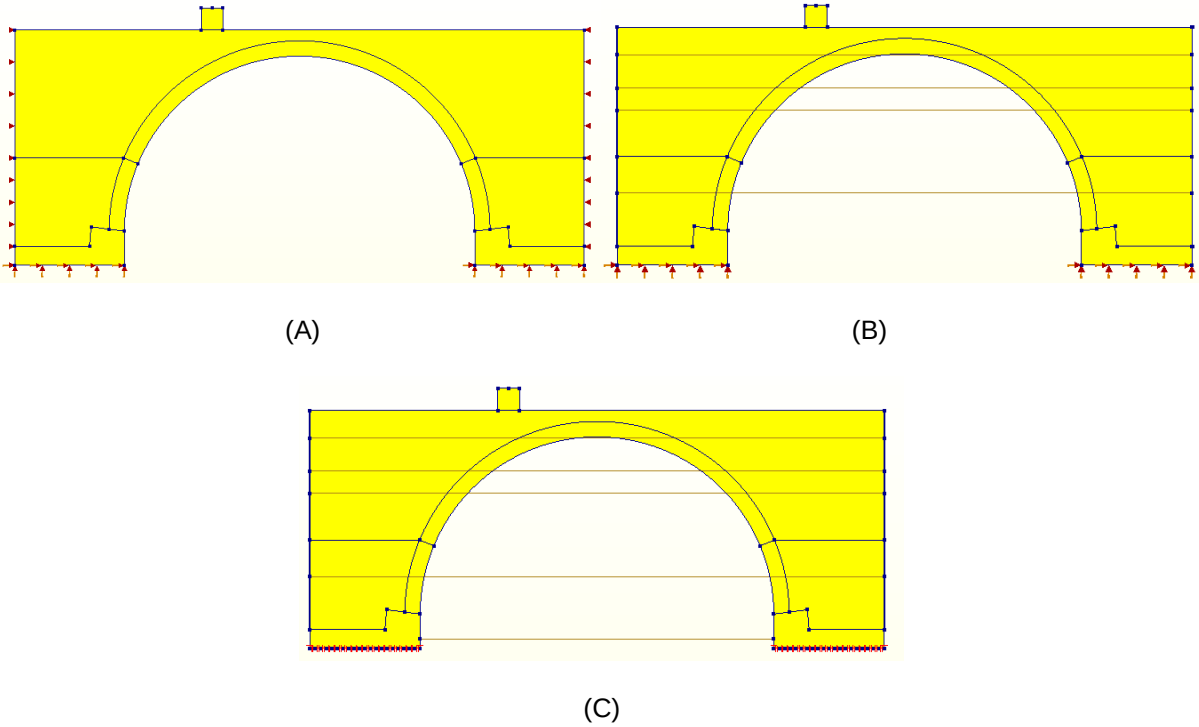

Figure 41 – Schematic representation of boundary conditions in Model A, Model B and Model C.

6.2 Load input

Another key aspect in the simulation of the load test on the structure is the proper definition of the load to be applied to the numerical model. For this purpose, a concrete loading block was modelled on top of the infill at a point corresponding to ¼ of the span of the arch. Although during the experiment the load appears to be applied on a point, it was decided to distribute the load along the side of the loading block in order to avoid stress singularities that in surface models are frequent in case of application of point loads and that might cause local failures and, as a consequence, led to divergence.

Within a nonlinear analysis it is possible to evaluate the behaviour of the structure using three different load increment procedures: load-control, displacement-control and arch-length control.

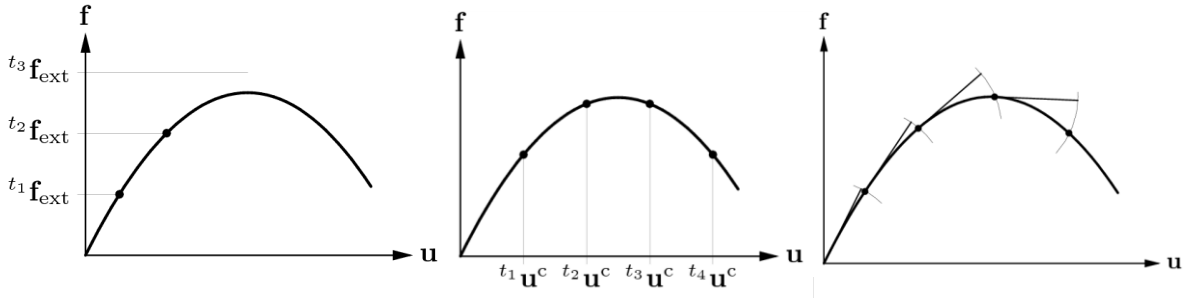

(a) (b) (c)

Figure 42 – Load control (a), displacement control (b) and arch-length. [22]

The first, load control, consists in increasing the external load applied to the structure, whereas the displacement control is based on the prescription of an imposed displacement. The choice of the displacement control is beneficial in particular when the structure presents a snap-through behaviour, as thanks to this method, limit points can be passed. [42] Arch-length control is the most complete load increment procedure as it covers all equilibrium paths, including possible snap-backs. It can be used with both external force and prescribed displacement. [42]

The arch-length control with prescribed displacements was used in all the nonlinear analysis. Since DIANA FEA allows applying an imposed displacement only where a support is provided, the analysis was defined in two phases: the first considers only the self-weight of the structure and does not take into consideration the presence of the support; the displacement, and therefore the support, are considered only in the second phase of the analysis.

6.3 Linear analysis

As a first approach, a linear analysis was performed in order to verify the accuracy of the results and the reliability of the geometrical model. To this scope it was decided to ignore the contribution of the vertical steel plates and the steel rods, to simulate their presence the boundary conditions were set as described in the previous paragraph.

The properties assigned to the materials were linear. An imposed load equal to 91 kN, corresponding to the ultimate load obtained experimentally, was applied to the structure. Figure 43, shows the deformation of the structure due to self-weight only, Figure 44 shows the deformation obtained when applying the external load too.

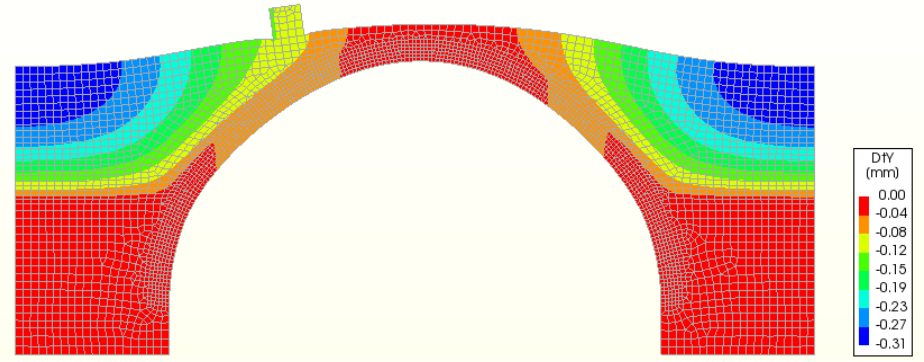

Figure 43 – Linear analysis. Deflections due to self-weight of the structure. (Model A)

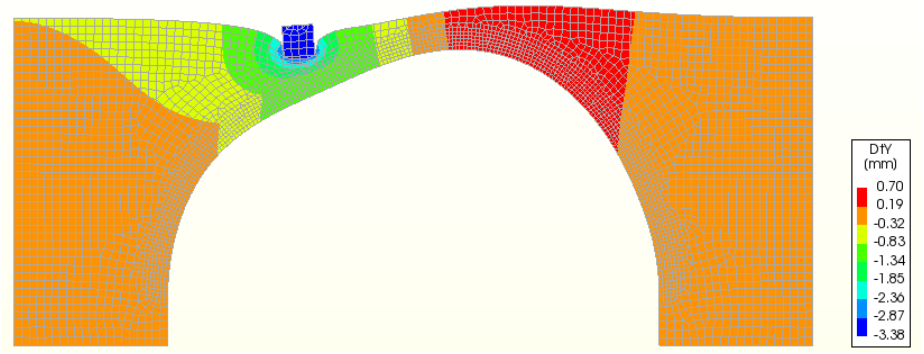

Figure 44 – Linear analysis. Deflections due to self-weight of the structure and applied load. (Model A)

6.4 Nonlinear analysis

As it was said, one of the most complex aspects in the study of the masonry bridge structure is linked to its nonlinearity. More specifically, the nonlinearity characterizes the behaviour of the materials along with the behaviour of the structure itself. When setting a nonlinear analysis in DIANA FEA, it is required to set multiple parameters, due to the fact that on the opposite of a linear elastic analysis, there is not a unique procedure that can be used to obtain the solution. Problems related to convergence might arise when solving nonlinear problems, related to either a not proper definition of the model, or to the choice of the wrong iterative solution method. For this reason, several set-ups of the model with increasing levels of complexity were studied and different iterative procedures were adopted. For the sake of simplicity, only the results referring to the model in which the nonlinearity of all the materials is applied are shown as it is described in the following sections of this report.

The parameters related to the properties of the materials were set as presented in the previous parts of this report. However, some of the values required calibration in order to achieve convergence; the values for which the results are presented are summarized in Table 12. Furthermore, being the section taken in the middle span of the bridge, the only interfaces that were applied are the one between soil and masonry arch in all the models and the interface between steel plates and soil in Model B and Model C.

Table 12 – Materials' properties in the 2D model.

Masonry	*Young's modulus*	*6000 N/mm^2*
	Density	*1.8 10^{-9} T/mm^3*
	Poisson's ratio	*0.18*
	Tensile strength f_t	*0.2 N/mm^2*
	Mode-I tensile fracture energy GfI	*0.03 N/mm*
	Compressive strength f_c	*14 N/mm^2*
	Compressive fracture energy Gc	*20 N/mm*
Soil	*Young's modulus*	*35 N/mm^2*
	Density	*1.84 10^{-9} T/mm^3*
	Poisson's ratio	*0.25*
	Cohesion	*0.003 N/mm^2*
	Friction angle	*38°*
	Dilatancy angle	*8°*
	Tension cut-off	*0 N/mm^2*
Interface soil/masonry	*Normal stiffness D_{nn}*	*70 N/mm^2*
	Shear stiffnesses D_{tt}, D_{ss}	*7 N/mm^2*
	Cohesion c	*0.003*
	Friction angle φ	*38°*

The results that follow are presented in terms of load-displacement diagrams. As it can be observed, all the models, A, B and C show similar and unsatisfactory results. As it was expected, the ultimate load of the structure is lower than the one obtained experimentally. Most probably this difference is due to the simplification of the model that does not consider the beneficial contribution given by the spandrel walls.

It is worth noting that the stiffness of the experiment, which included the spandrel walls, is almost identical to the one achieved in these 2D models with only the infill. Probably, this is due to the damage produced during the first uncontrolled load cycle, described in section 4, which already cracked significant parts of the spandrel walls and arch ring.

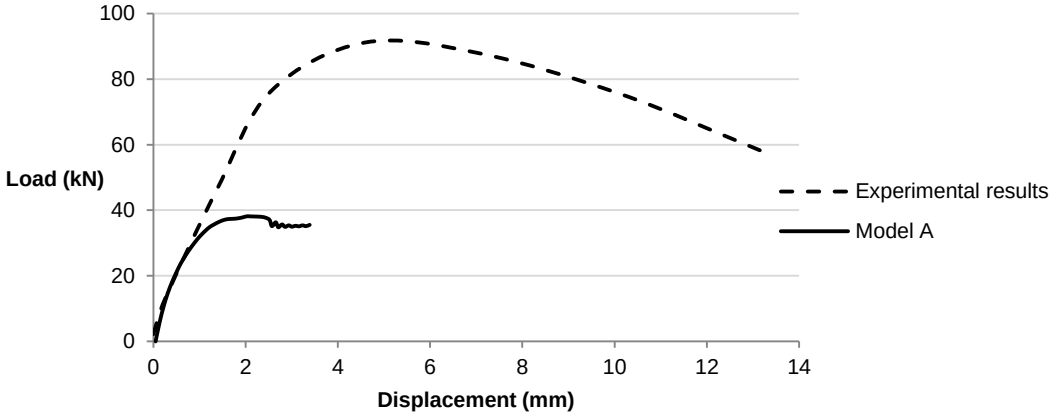

Figure 45 – Load-Displacement diagram for Model A.

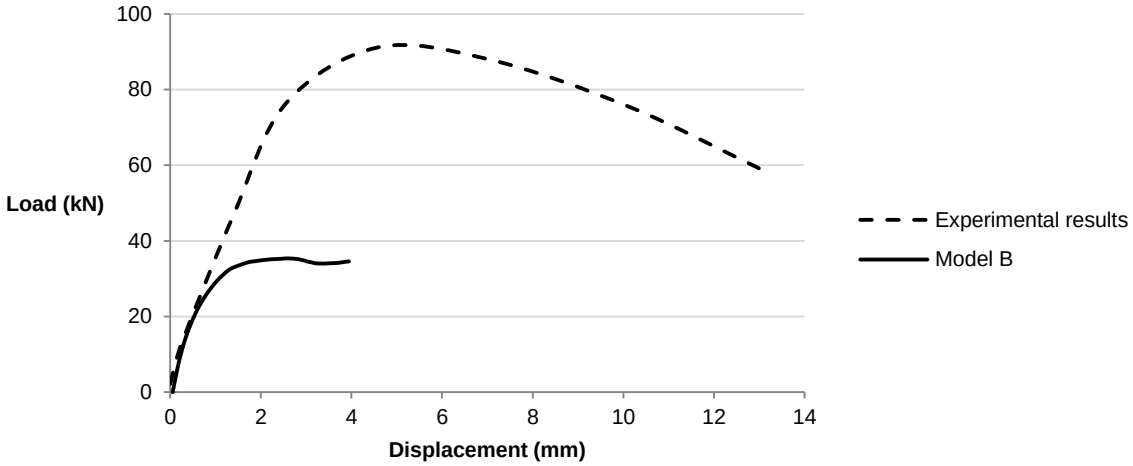

Figure 46 – Load-Displacement diagram for Model B.

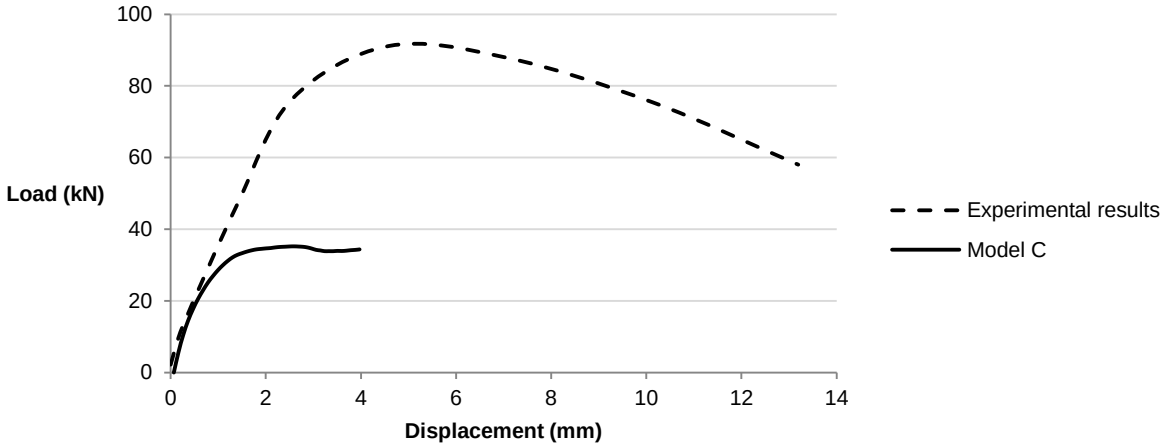

Figure 47 – Load-Displacement diagram for Model C.

The following Figure 48 shows the load-displacement diagrams for the three models. As it can be observed, model B and C present diagrams almost perfectly superimposable, which means that the implementation of the springs and the steel beam at the bases of the structure to substitute the fixed bases does not yield any significant change in this model.

On the opposite, the results obtained in Model A differ from the ones of the other two models, both in terms of ultimate load that is higher, and in terms of stiffness of the structure.

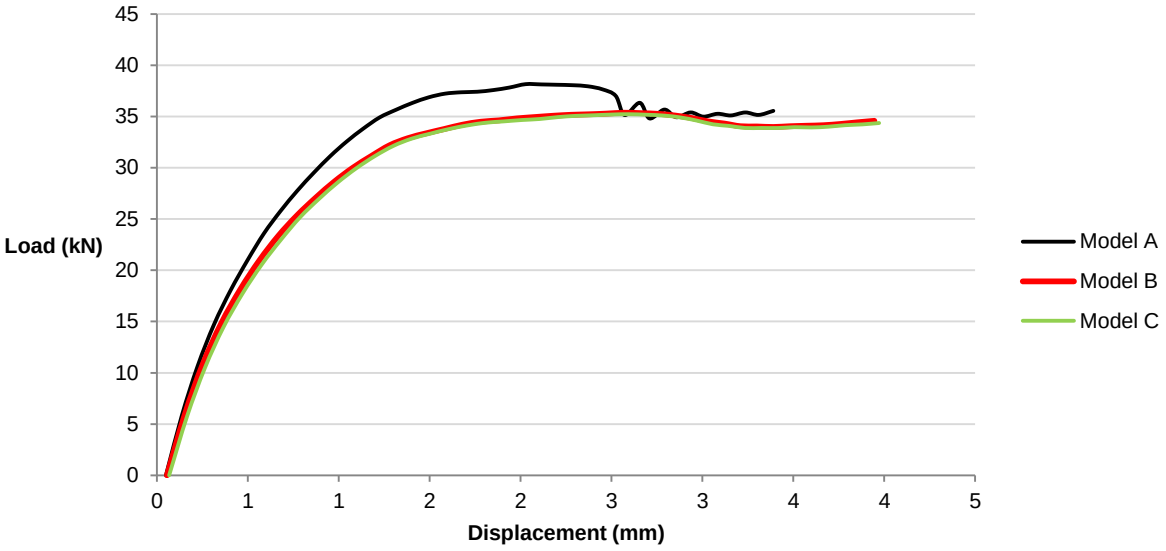

Figure 48 – Load-Displacement diagrams for Models A, B and C.

Although the load-displacement diagrams do not provide realistic results, the deformed shape, that can be observed in Figure 49 and Figure 50, is in good agreement with the expectations.

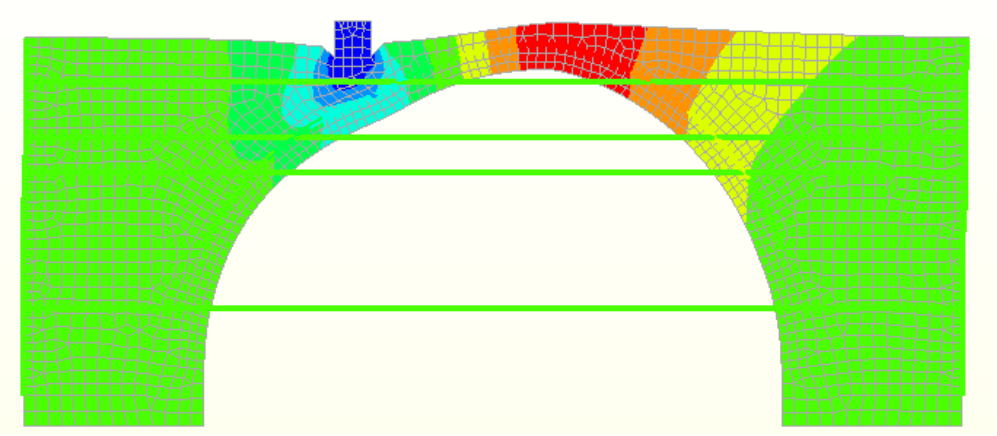

Figure 49 – Contour plot of the deformed shape of Model B.

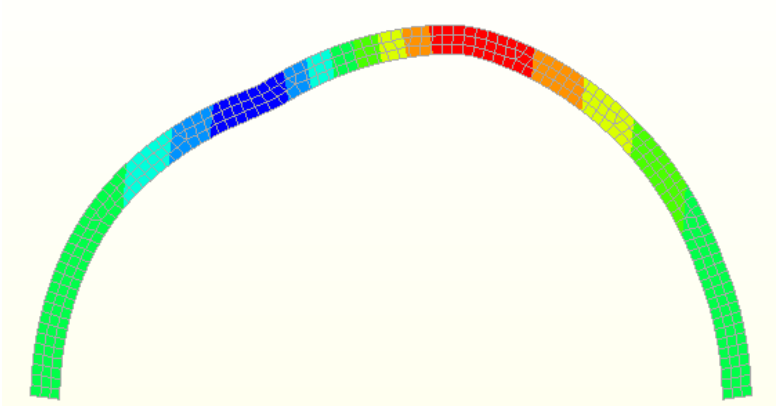

Figure 50 – Contour plot of the deformed shape of the arch in Model B.

7. 3D MODEL

Although many researches and studies have demonstrated that very often a 2D representation of a structure might be a good approximation of reality, yielding good results, sometimes a more complex 3D approach is preferable.

The unsatisfactory results obtained with the 2D models of the masonry arch bridge object of the study presented in this dissertation have demonstrated that given the complexity of the structure and the presence of several elements that should be taken into account, as for instance the spandrel walls, a 3D approach is absolutely preferable.

7.1 Modelling strategies

As it was said previously, the barrel arch bridge tested at the UPC laboratory has not been object of study in the past as much as the segmental arch bridge; therefore no models of it were available. Although the 3D model developed by Brunet for the segmental arch bridge represented an important reference and basis of comparison, a new 3D model was built from scratch.

To facilitate the process, the 3D model was built in Autocad and imported in DIANA FEA. The structural elements, divided according to the different materials, were automatically converted in solid elements by the software. Some elements such as steel ties, beam and plates were modelled directly in DIANA, along with interfaces and springs applied at the bases of the bridge.

The symmetry of the geometry and the loading was taken into account modelling only half of the bridge, with a benefit in terms of computational costs.

A 200x200 mm concrete block was modelled as loading beam, furthermore the strategy adopted by Brunet consisting in reducing its width in order to avoid that direct load could be applied directly to the spandrel wall, was reproduced.

7.2 Implementation of the load and boundary conditions

Similarly to what was done in the 2D model, the analysis was developed in two phases using a prescribed displacement approach. The first phase consisted in considering the self-weight of the structure only. The external load, applied in the form of displacement, was added in the second phase, in which an initial stress state due to the self-weight was considered.

Different boundary condition configurations were studied. As seen previously, increasing levels of complexity were added to the model gradually, in order to ensure the control of the structure and its response. As first, simplified approach, fixed bases were applied along with lateral restraints, to simulate the presence of the steel elements. The results obtained showed that the structure was too stiff compared to the real, experimental results, for this reason it was decided to include the steel elements and to model a more realistic version of the structure.

In the more accurate models, for which an activity of calibration of parameters and a sensitivity analysis were developed, the restraints applied consist of:

- Vertical constraint applied at the top of the loading block as required by the software to apply imposed displacements;
- Symmetry constraints applied to all the elements in the plane of symmetry to avoid displacements in the direction of the width of the bridge and to the vertical side of the steel plates in the plane of symmetry to avoid rotation;
- Spring boundaries applied at the bases of the structure along with a lateral horizontal restraint at one side;
- Steel elements such as steel plates at the sides, steel ties, steel beam at the base and steel profiles at the sides of the plates acting as stiffeners.

The model including steel plates and ties is shown in Figure 51, whereas Figure 52 shows the interfaces and the springs.

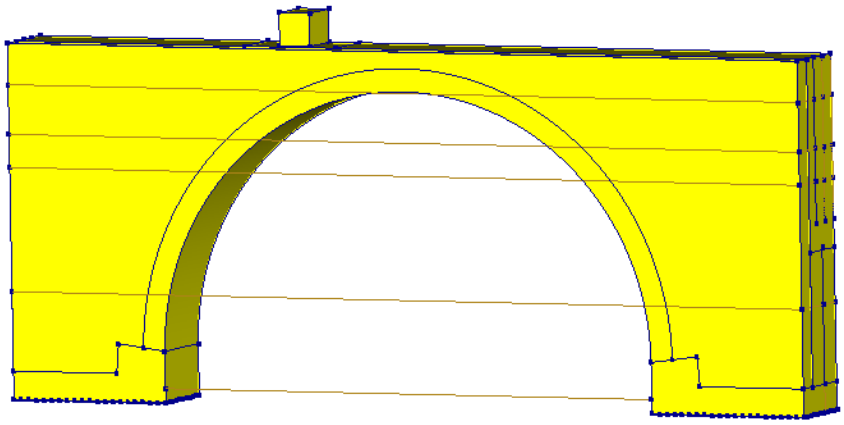

Figure 51 – Geometrical model.

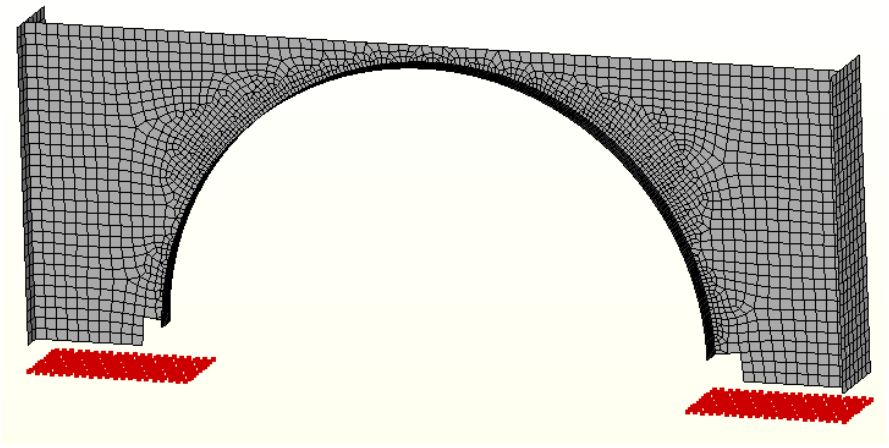

Figure 52 – Interfaces and springs applied to the model.

7.3 Calibration of the model

In section 5.2 of this Report the constitutive models used in the structure were discussed, along with the reference values applied to the several parameters according to indications found in literature. However, every model requires a process of calibration of the parameters, due to its complexity and uniqueness, aiming to achieve a result as close as possible to the experimental answer of the structure itself.

It is not only necessary to vary a single parameter and to evaluate how the change affects the response, but also to consider how several parameters interact together and how combinations of values affect the overall behaviour of the model.

For this reason, once the geometrical configuration of the structure was defined, a calibration activity was developed. The main objectives were the following:

- Ensure convergence of the results;
- Obtain a load-displacement curve close to the experimental one in terms of ultimate load and overall stiffness of the structure;
- Verify that the collapse mechanism corresponded to the real one by verifying the presence of hinges and the distribution of stress and strains;
- Obtain the separation between arch and spandrel walls as it was observed experimentally.

As it was previously mentioned, the first simplification of the model that was analysed consisted in applying fixed supports at the bases and constraints that prevent horizontal displacements at the sides of the bridge. At a second stage, the steel beam was modelled along with springs applied at the bases of the structure; in this case the lateral restraints simulating the steel elements were kept. The results, evaluated mainly in terms of load-diagram curves, showed that the models were significantly stiffer than the real structure. As a consequence, the results were disregarded and a more accurate and detailed structure was modelled; in fact, as a last step, all the steel elements were modelled.

The following paragraphs show the results obtained for different models, to describe the activity of calibration that was performed on them.

7.3.1 Model B

Model B was modelled with steel beam, steel plates and ties. The properties assigned to the parameters of the materials are the ones presented previously and defined according to the experimental tests along with the guidelines that were found in literature.

At first the results are shown in terms of load-displacement diagrams at ¼ of the span and in mid-span. As the curves in Figure 53 and Figure 54 show, the behaviour of the model differs greatly from the experimental results, both in terms of maximum load reached and of stiffness.

It can be observed that the load increases up to the load step corresponding to a load of 109 kN and then it decreases and a phenomenon of unloading occurs.

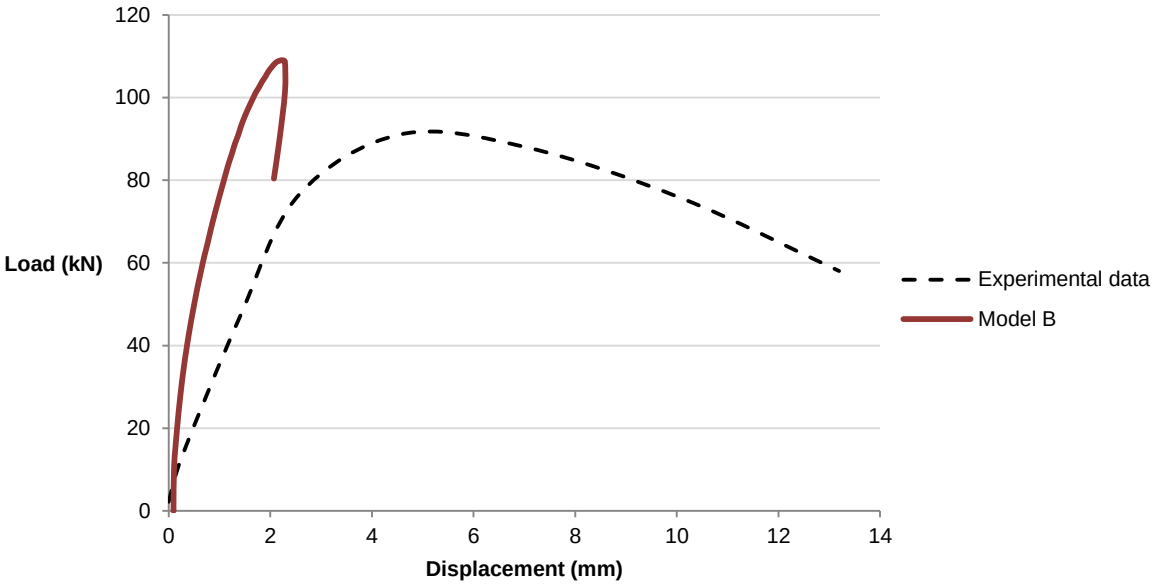

Figure 53 – Load – Displacement diagram of Model B at ¼ of the span.

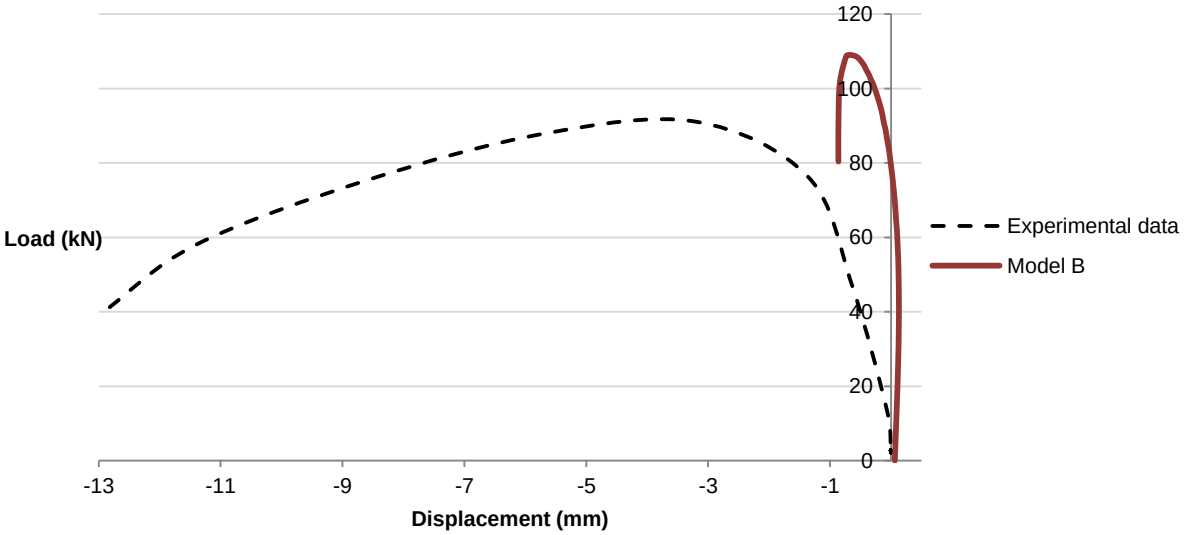

Figure 54 – Load – Displacement diagram of Model B in mid-span.

When looking more into detail at the response of the structure thanks to the output available in the software DIANA FEA, several observations can be done. First, with regards to the masonry, the

results show that the behaviour of the arch is not the one expected. In fact, both the contour plot of the deformations and the diagram of the cracks demonstrate that part of the arch behaves as if it was actually part of the spandrel wall and therefore hanging from it, as shown in Figure 56 and Figure 57, this condition is due to the fact that the gap between arch and wall is not present.

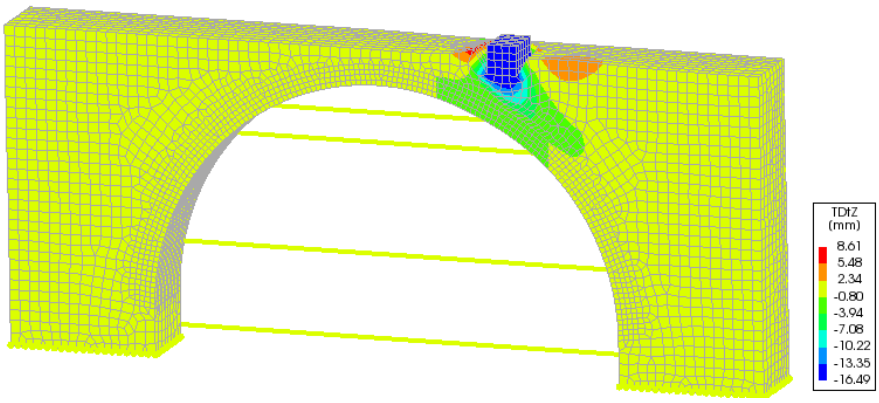

Figure 55 – Contour plot of vertical deformations at a load of 109 kN in Model B.

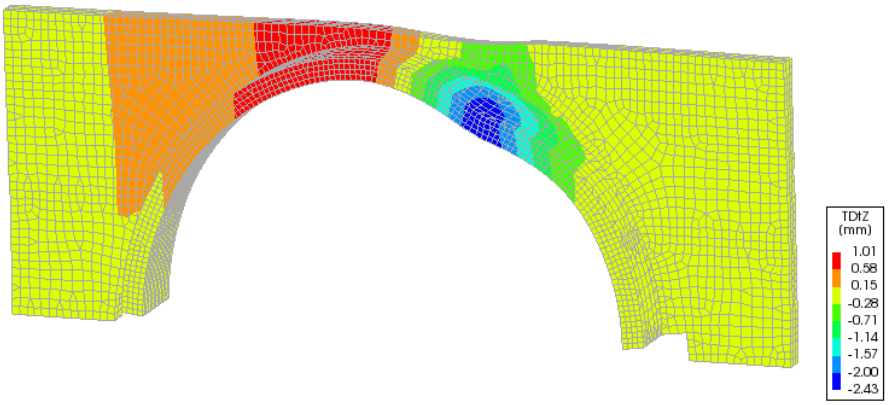

Figure 56 – Contour plot of vertical deformations in arch and spandrel wall at a load of 109 kN in Model B.

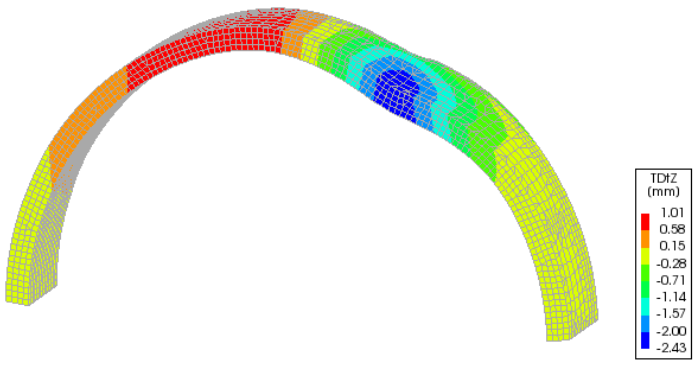

Figure 57 – Contour plot of vertical deformations in the arch at a load of 109 kN in Model B.

Furthermore, the diagram of the cracks and the contour plots of the principal stress SXX and SZZ evaluated at the load step corresponding to the maximum load, shown in Figure 58, Figure 59 and Figure 60, demonstrate that a collapse mechanism due to the formation of four hinges is not fully developed.

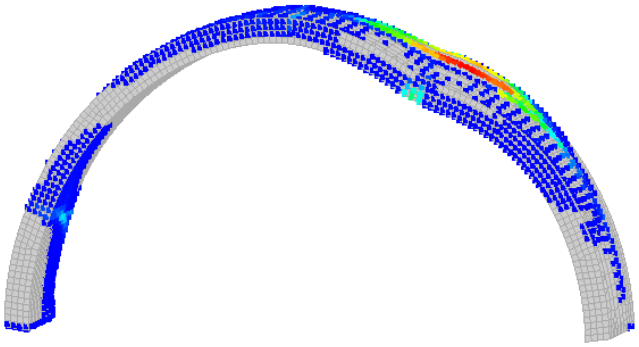

Figure 58 – Distribution of the cracks in the arch at a load of 109 kN in Model B.

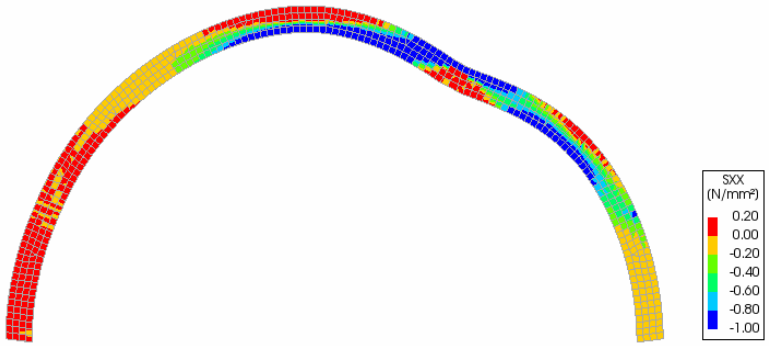

Figure 59 – Contour plot of the stress SXX in a section of the arch in Model B.

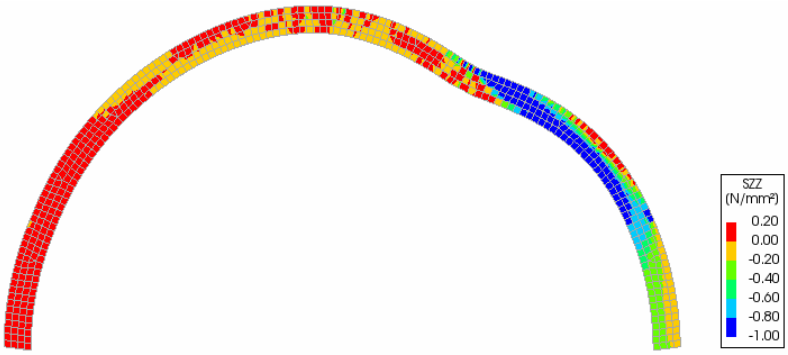

Figure 60 – Contour plot of the stress SZZ in a section of the arch in Model B.

Another critical aspect can be noticed in the contour plot of the principal stress in the masonry, which shows a concentration in the spandrel wall in the points of application of the steel ties, as shown in Figure 61.

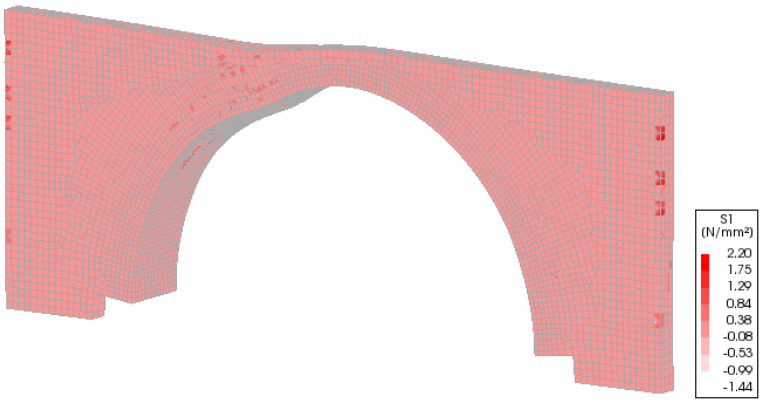

Figure 61 – Principal stresses in the arch and the spandrel wall at a load of 109 kN in Model B.

Finally, an observation regarding the behaviour of the soil is to be done: as shown in Figure 62, a concentration of plastic strains can be observed in the area of the soil under the loading beam, which might be the cause of a local failure.

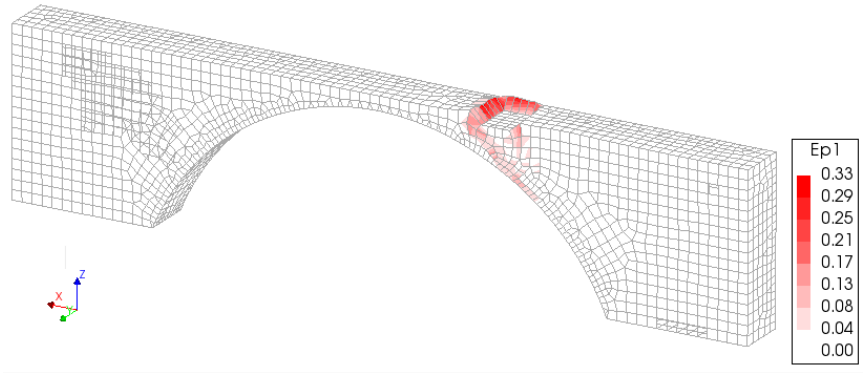

Figure 62 – Plastic strains in the soil at a load of 109 kN in Model B.

The analysis of the results have shown the need to calibrate some of the parameters assigned to the materials and possibly to change some modelling features in order to avoid irregularities which might prevent the analysis to carry on and the development of a full mechanism in the arch to be completed. In particular, it was decided to develop the following strategies:

- Improve the interaction between arch and spandrel wall, reducing the values of tensile strength and cohesion at the interface, to obtain the formation of the gap;
- Change the parameters of the soil, for instance modelling the part of the soil under the loading beam as a linear elastic material.

7.3.2 Model E

Model E included some modifications, as the application of linear elastic properties to a portion of soil located right under the loading beam. The objective is to overcome the concentration of plastic strains in the area under the loading beam and to avoid the possible local failure of the soil that might be the reason why the failure of the model occurs before the formation of the hinges in the masonry arch is completed. Furthermore, the structure was modelled with both tensile strength and cohesion of the interface equal to 0.1 N/mm^2 to ensure the formation of the gap between spandrel wall and arch.

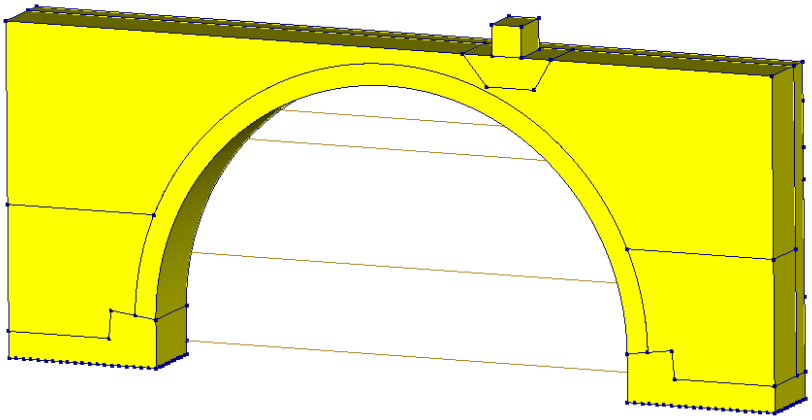

Figure 63 – Model E with part of the soil modelled with a linear-elastic behaviour.

The load-displacement curves obtained, in the mid-span and at ¼ of the span, show that the maximum load reached by the structure is 98.4 kN and that the model is stiffer than the real structure.

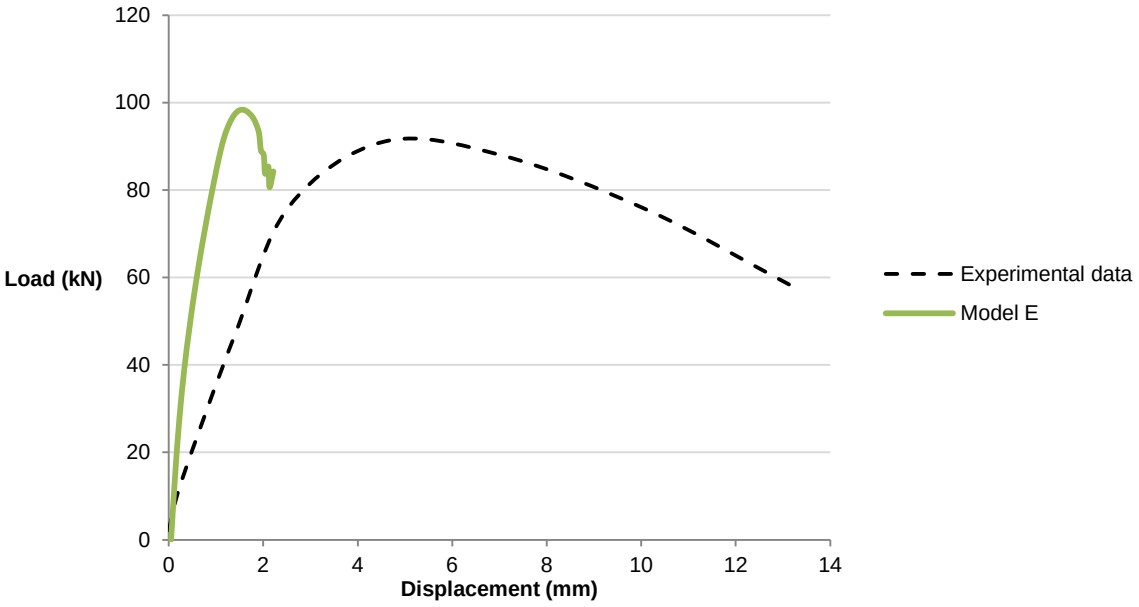

Figure 64 – Load – Displacement curve for Model E at ¼ of the span.

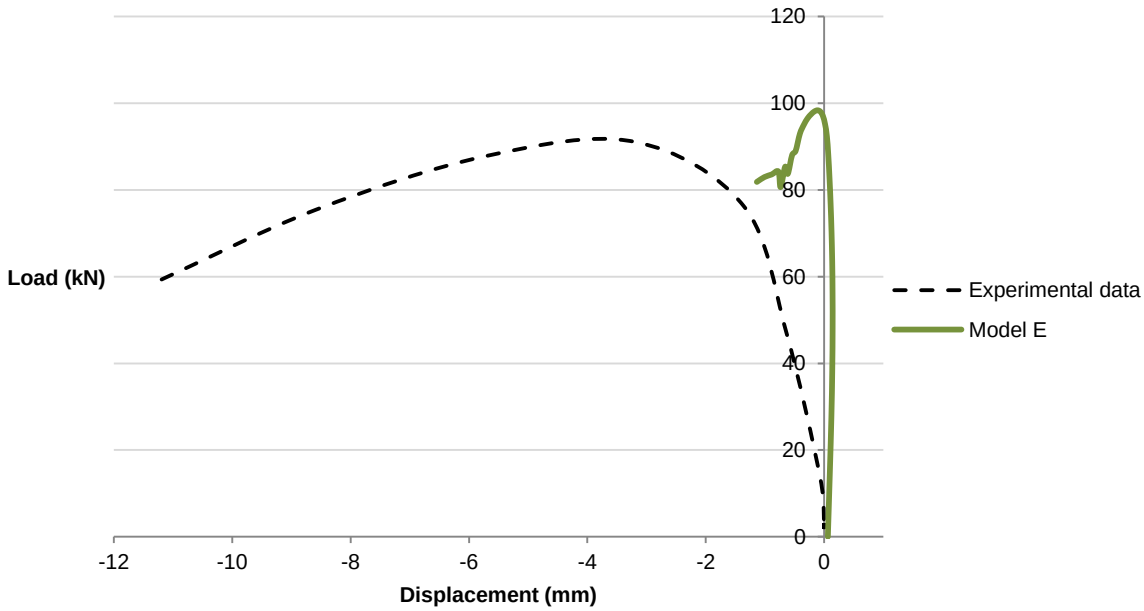

Figure 65 – Load – Displacement curve for Model E in mid-span.

Despite this unsatisfactory result in terms of ductility of the structure, the model presents some positive outcomes. The strategy of modelling part of the soil as a linear elastic material, for instance, has an interesting consequence. As it can be observed in the following Figure 66 showing the contour plot of the vertical displacements, a sliding occurs between the soil and the spandrel wall, which confirms that the interface modelled between the two materials, is working properly. This outcome could not be observed in Model B.

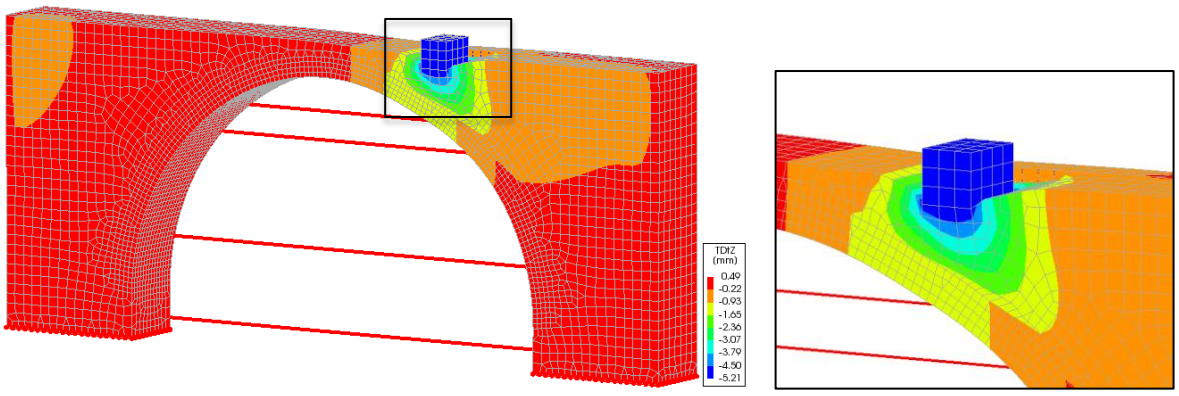

Figure 66 – Contour plot of vertical deformations at a load of 98.4 kN in Model E.

Furthermore, the concentration of plastic strains in the soil under the loading beam is reduced, both in extension and intensity, as shown in Figure 67.

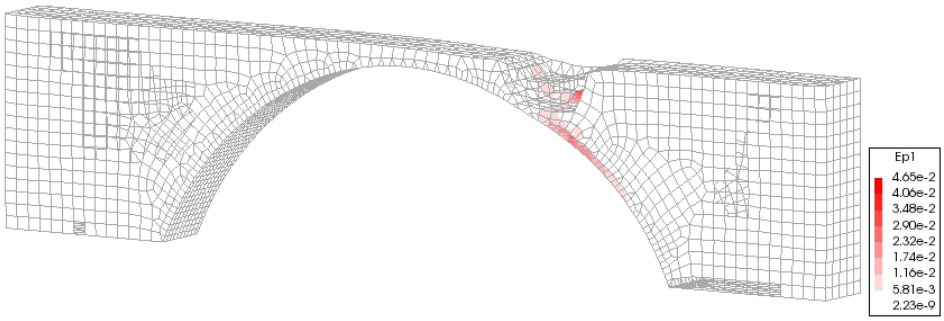

Figure 67 – Plastic strains in the soil at a load of 98.4 kN in Model E.

The analysis of the distribution of the stress for the masonry elements reveals again, as seen previously, a concentration of stresses in the spandrel wall in the points in which the steel ties are applied. However, differently than Model B, a separation between spandrel wall and arch can be observed now, as proof that changing the properties of the interface yielded a good result.

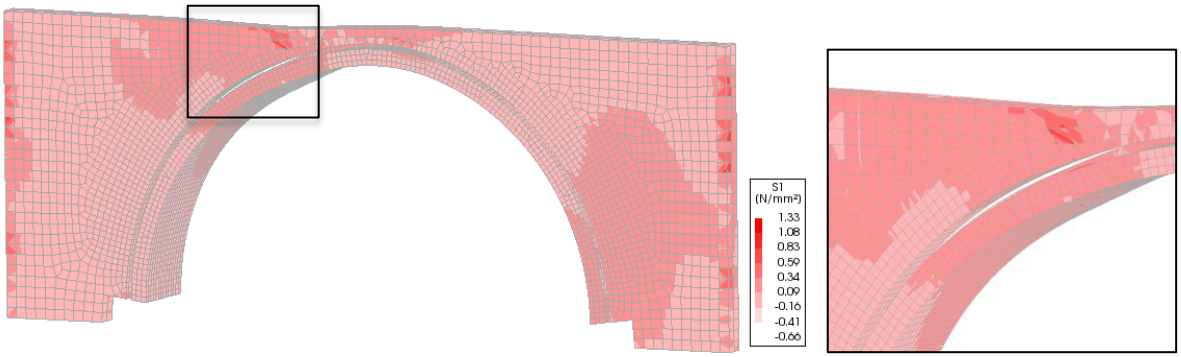

Figure 68 – Principal stresses in the arch and the spandrel wall at a load of 98.4 kN in Model E.

The response of the structure was studied more in detail by analysing and comparing different outputs at different load steps.

When looking at the load-diagram of Model E, we can observe that after the peak value of load is reached, displacements keep increasing, while a process of unloading occurs and a small plateau is reached. Four points of the graph were analysed: the first one is taken at the second load step corresponding to a load of 14.6 kN, the second is taken at a load of 47.8 kN, the third corresponds to the value of ultimate load acting on the structure, equal to 98.4 kN. Finally, the last step is at the end of the plateau, being the last step at which convergence is obtained.

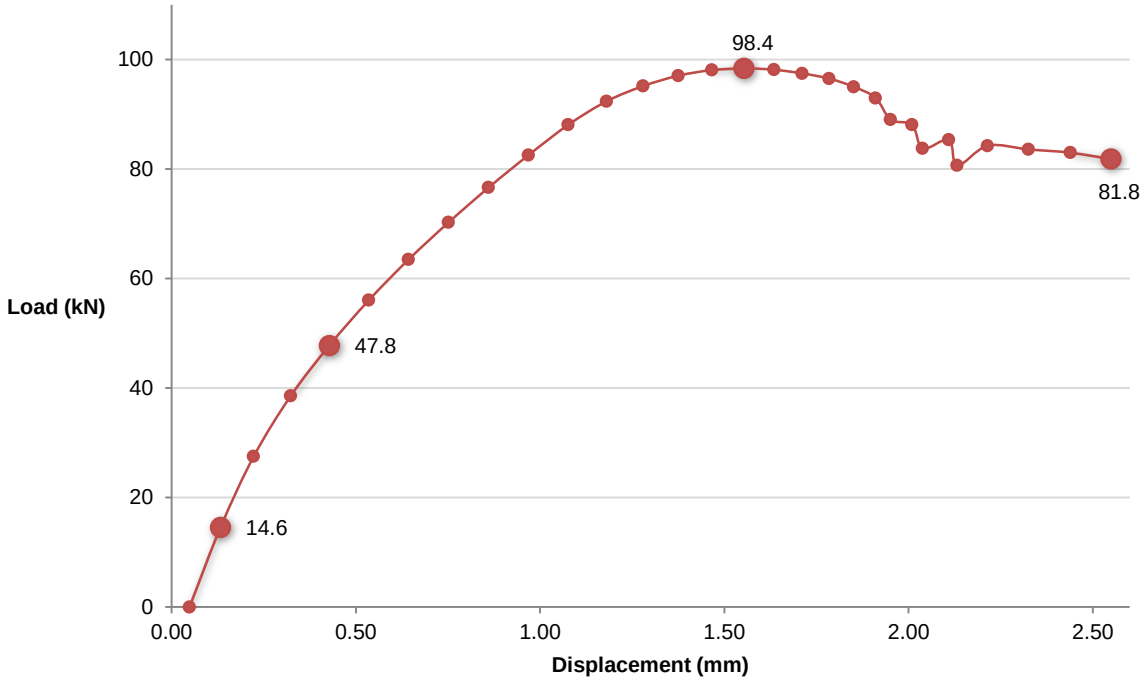

Figure 69 – Load – Displacement curve for Model E at ¼ of the span.

At first, the attention was focused on the evolution of principal stress in the masonry arch. As the following figures show, the distribution of the stress reveals the presence of the spandrel wall and the fact that the gap between arch and wall was not developed at the beginning; this has an effect on the distribution of the stress which appears being not uniform along the whole width of the element.

When the load increases, the stress of the arch increases too. In particular, a concentration of stress can be noticed at ¼ of the span, the area of application of the load.

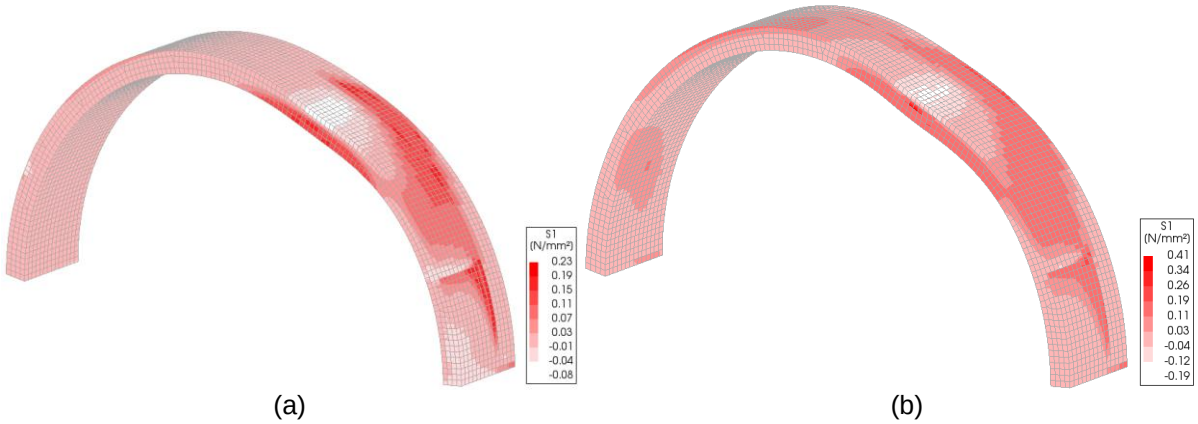

(a) (b)

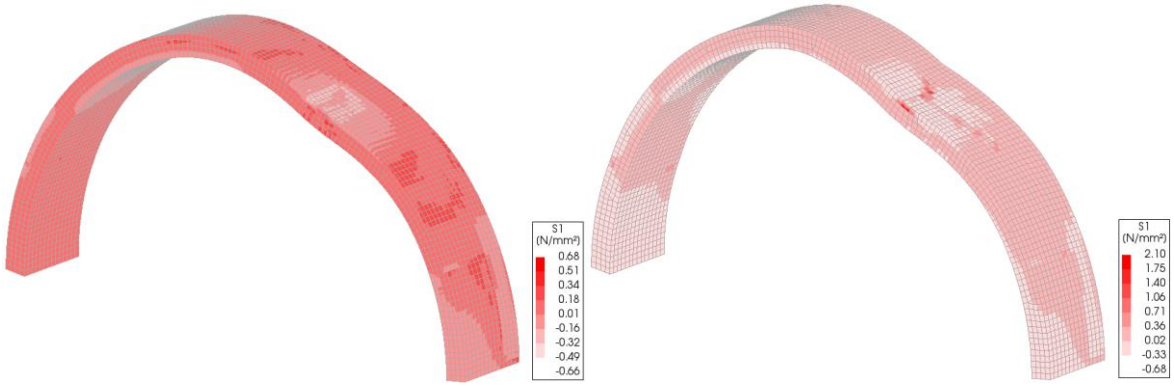

(c) (d)

Figure 70 – Principal stress in the arch at load steps corresponding to 14.6 kN (a), 47.8 kN (b), 98.4 kN (c) and 81.8 kN (d).

Another aspect that was analysed is the development of the gap between spandrel wall and arch. The figures that follow represent the interface. It was observed that, as expected, the gap increased together with the load applied. The gap was noticed in two different areas, as indicated in Figure 71, in which the gap developed at a different pace.

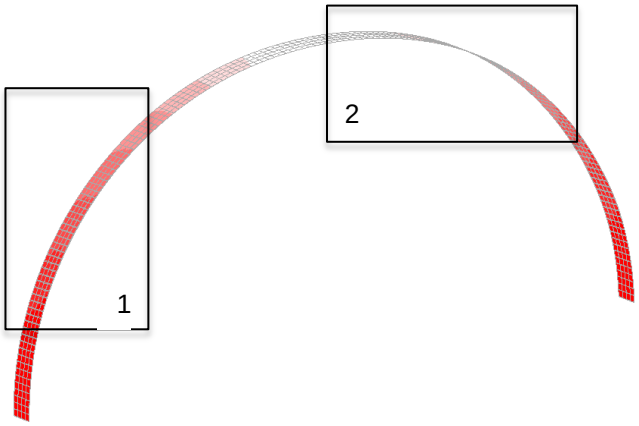

Figure 71 – Interface between arch and spandrel wall showing the areas of formation of the gap.

The images in Figure 72 show the evolution of the gap in area 2, which is already visible at the load step corresponding to 47.8 kN. A larger gap characterises higher values of load. In particular, the gap at lower load steps is visible only in area 2, whereas in area 1 it is visible only at high values of load. At the last load step analysed, the gap in area 1 is equal to 0.89 mm, whereas in area 2 is equal to 2.64 mm.

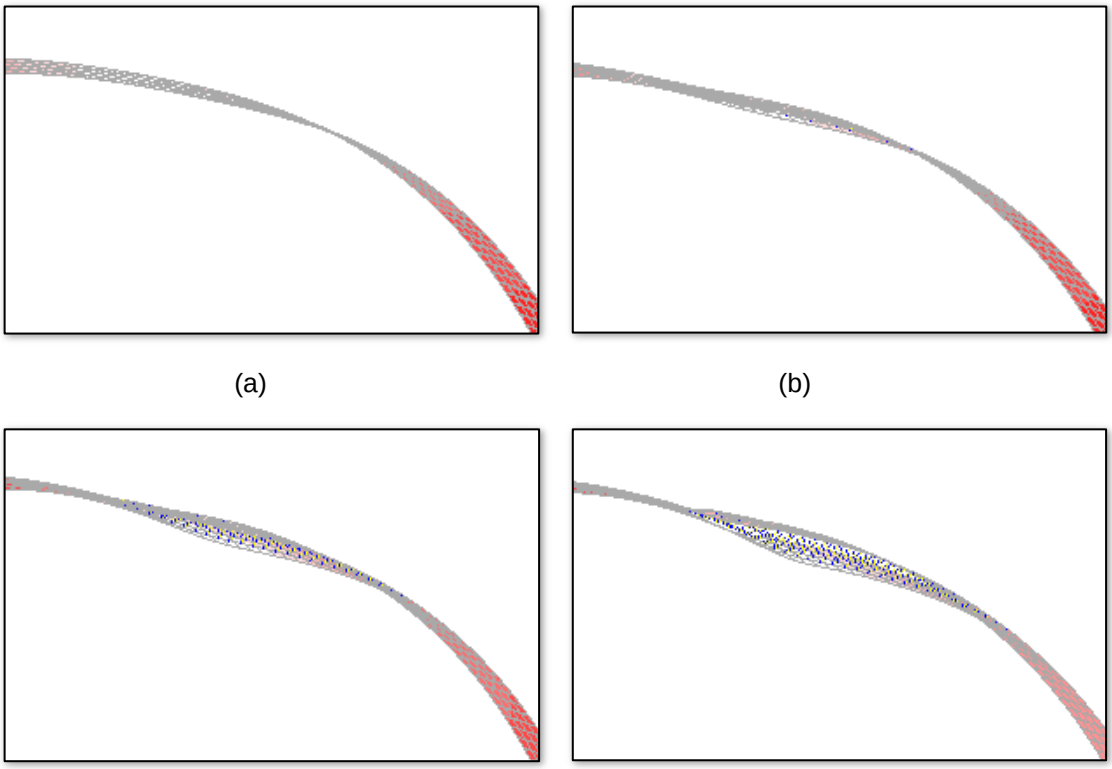

Figure 72 – Evolution of the gap between spandrel wall and arch in area 2 at load steps corresponding to 14.6 kN (a), 47.8 kN (b), 98.4 kN (c) and 81.8 kN (d).

A further aspect that was analysed in detail is the development of crack strains in the arch. Again, the results are shown with reference to the same four load steps. As the following figures show, the crack strains increase with the load. At first, a concentration of crack strains is observed at the intrados of the arch in the area of application of the load (Figure 73); the following step shows an increase of the existing cracks and also the appearance of crack strains at the extrados, at the height of the concrete infill (Figure 74). The load step corresponding to the maximum load, in Figure 75, shows the presence of crack strains concentrated in the area were the formation of hinges is expected, condition that is even more evident in the last load step, shown in Figure 76.

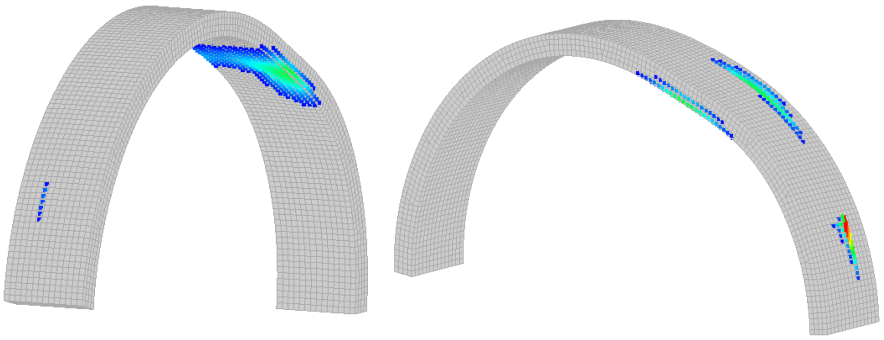

Figure 73 – Crack strains in the masonry arch at 14.6 kN.

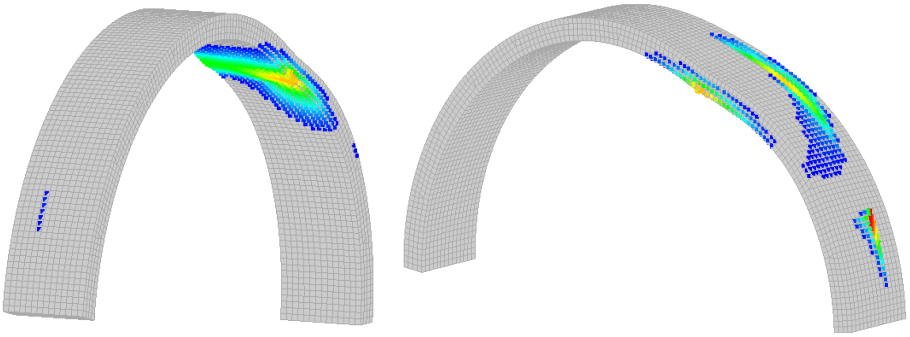

Figure 74 – Crack strains in the masonry arch at 47.8 kN.

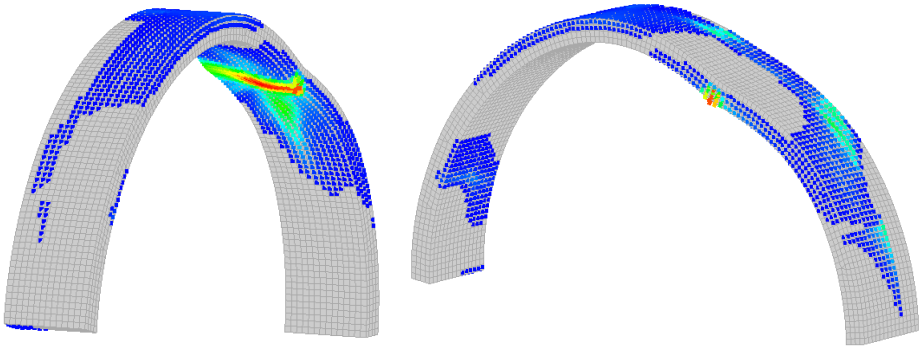

Figure 75 – Crack strains in the masonry arch at 98.4 kN.

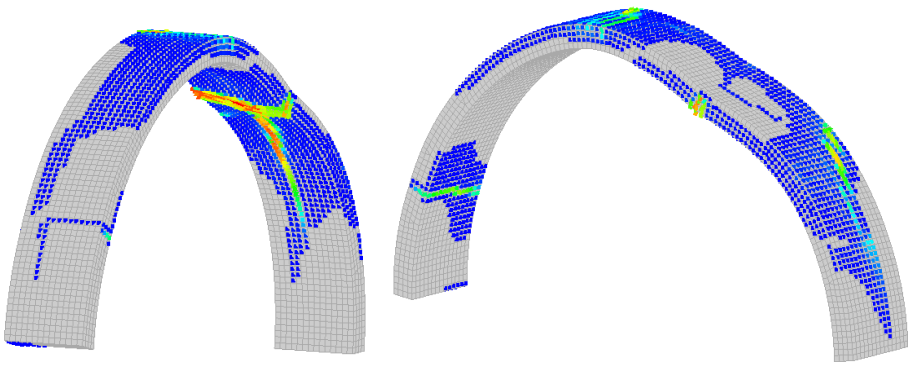

Figure 76 – Crack strains in the masonry arch at 81.8 kN.

Finally, the section of the arch in Figure 77 shows the formation of the cracks and therefore of the hinges responsible for the development of a mechanism of failure in the structure.

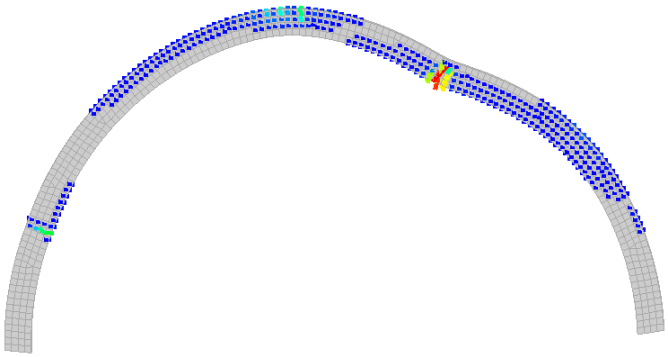

Figure 77 – Section of the masonry arch showing the distribution of the crack strains at 81.8 kN.

This result is also visible in the contour plots of the stress shown in Figure 78 and Figure 79. As it can be observed, a concentration of stress can be noticed in four areas of the arch. In particular, three of them are more visible in the diagram of stress SXX, whereas the fourth can be seen better in the diagram of stress SZZ.

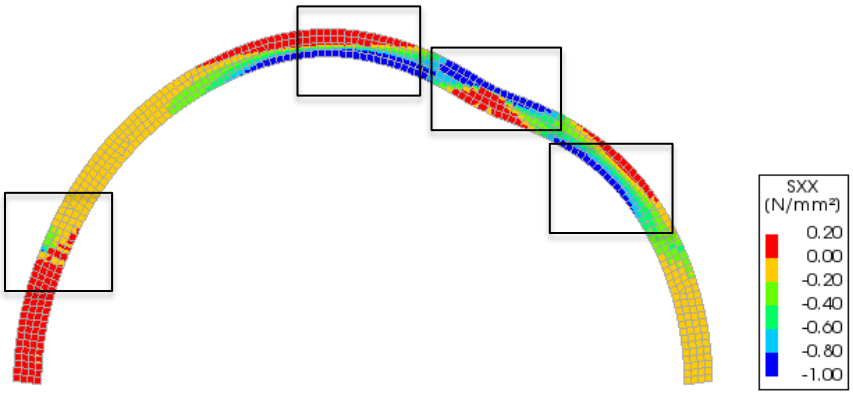

Figure 78 – Contour plot of the stress SXX in a section of the arch.

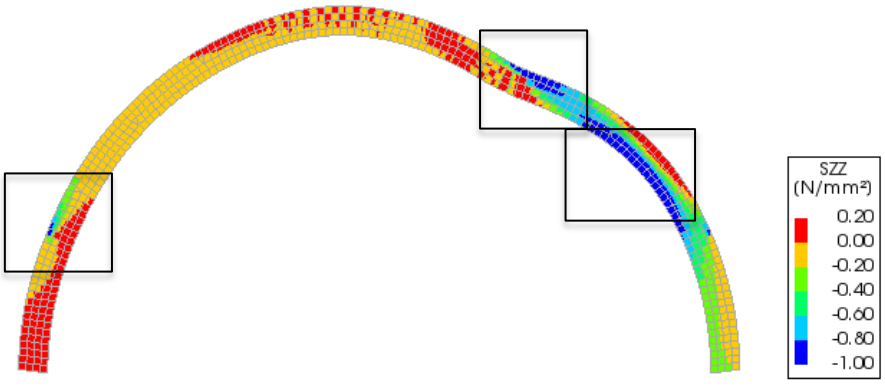

Figure 79 – Contour plot of the stress SZZ in a section of the arch.

The development of crack strains in the spandrel wall was studied too. It can be observed that a concentration of crack strains is present since the first load steps in the area of application of the load. The following steps show a more diffuse presence of cracks. In particular, the last load step, shown in

Figure 80 (d) demonstrates the presence of a large crack at the height of the concrete infill.

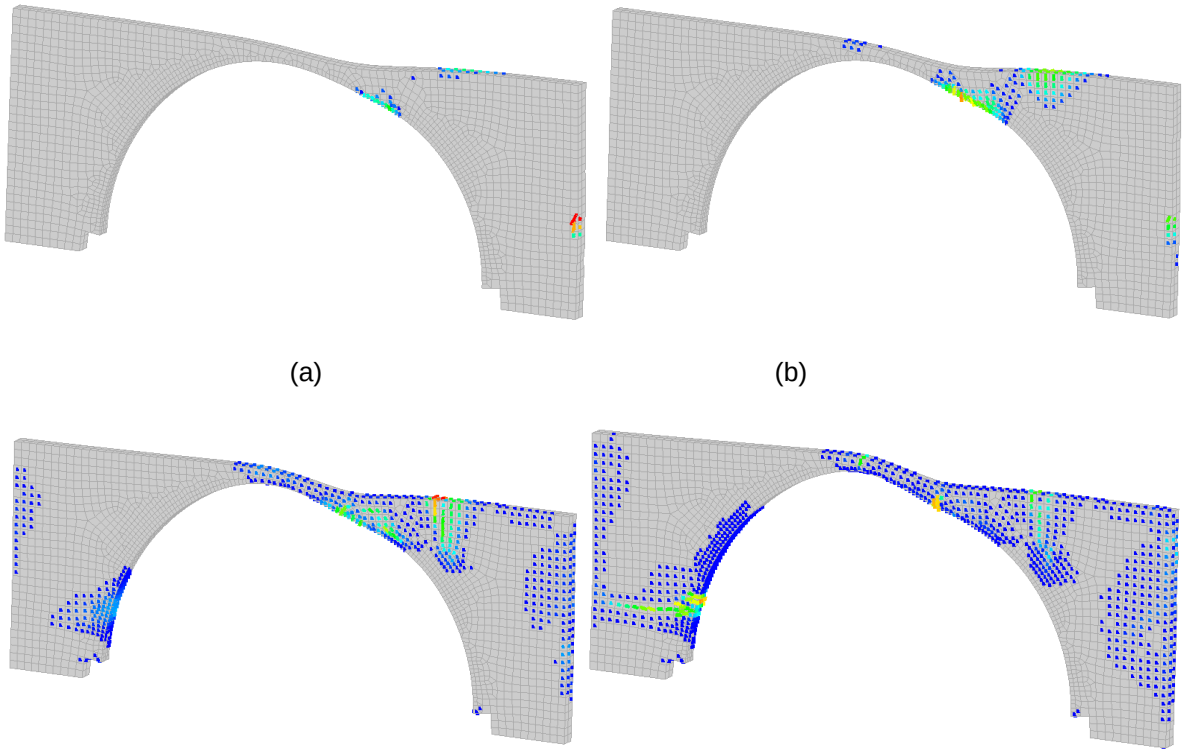

(a) (b)

(c) (d)

Figure 80 – Crack strain in the spandrel wall at load steps corresponding to 14.6 kN (a), 47.8 kN (b), 98.4 kN (c) and 81.8 kN (d).

The last aspect that was evaluated, in order to compare the results of the numerical model with the experimental result, is the lateral thrust produced by the arch, calculated as the sum of the axial forces acting on ties and steel beam. In the case of Model E, a value of 76 kN is obtained when the maximum load is applied in the structure. Unfortunately, the value of lateral thrust developed by the real structure during the experiment was not measured. However, a reference value was estimated by Roca and Molins using an analytical approach and a value of 52.3 kN was obtained. [18]

The results demonstrate that although the overall behaviour of the numerical model is close to the real one, it is still not completely satisfactory, as demonstrated by the load-displacement diagram and the result of the lateral thrust.

7.4 Sensitivity analysis on Model E

A sensitivity analysis was developed on Model E to understand how the change of some parameters affects the response of the structure. The idea when developing a sensitivity analysis is to vary those parameters that present a form of uncertainty.

At first a comparison between different values of Young's Modulus in the soil was developed. Model E1 was analysed applying a value of 25 N/mm^2 and Model E2 with a value of 45 N/mm^2, their results were then compared to those of Model E in which the value of the Young's modulus in the soil was 35 N/mm^2.

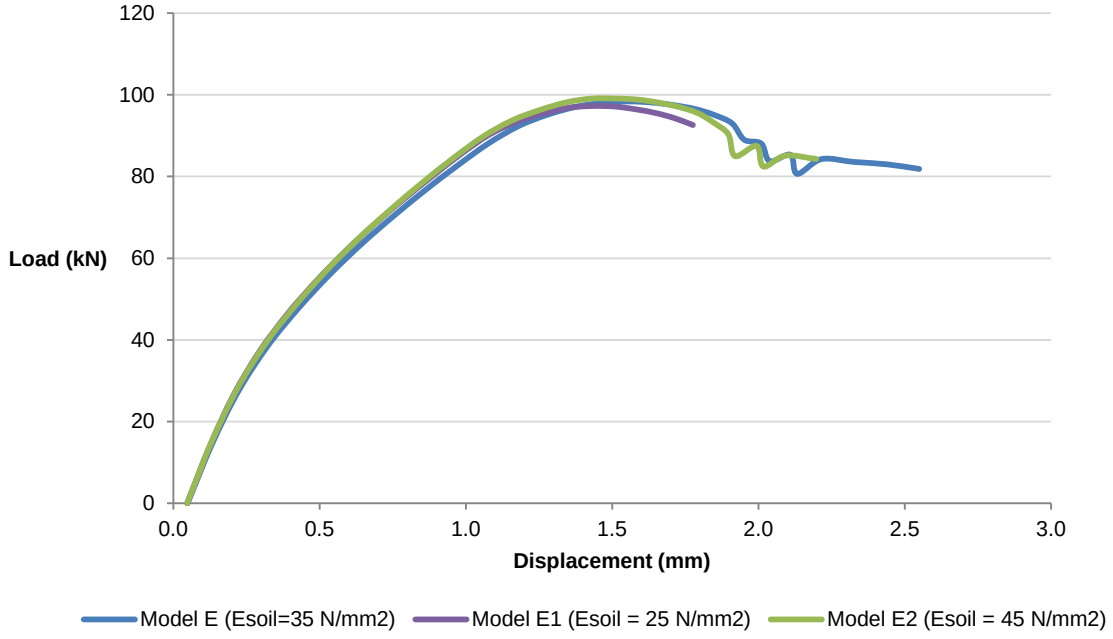

Figure 81 – Load – Displacement diagrams for Model E with different values of Young's Modulus in the soil.

As the load-displacement curves show, no substantial changes are experienced in the model when varying the Young's Modulus if the soil. The curves appear almost perfectly superimposable, except for the fact that Model E1 has a slightly lower ultimate load.

A further analysis was developed by changing the tensile strength of the masonry. In the graph that follows, a comparison between Model E, Model E3 and Model E4 is presented. Model E3 was analysed with a tensile strength of masonry equal to 0.1 N/mm^2 whereas, in Model E4 a value of 0.05 N/mm^2 is applied.

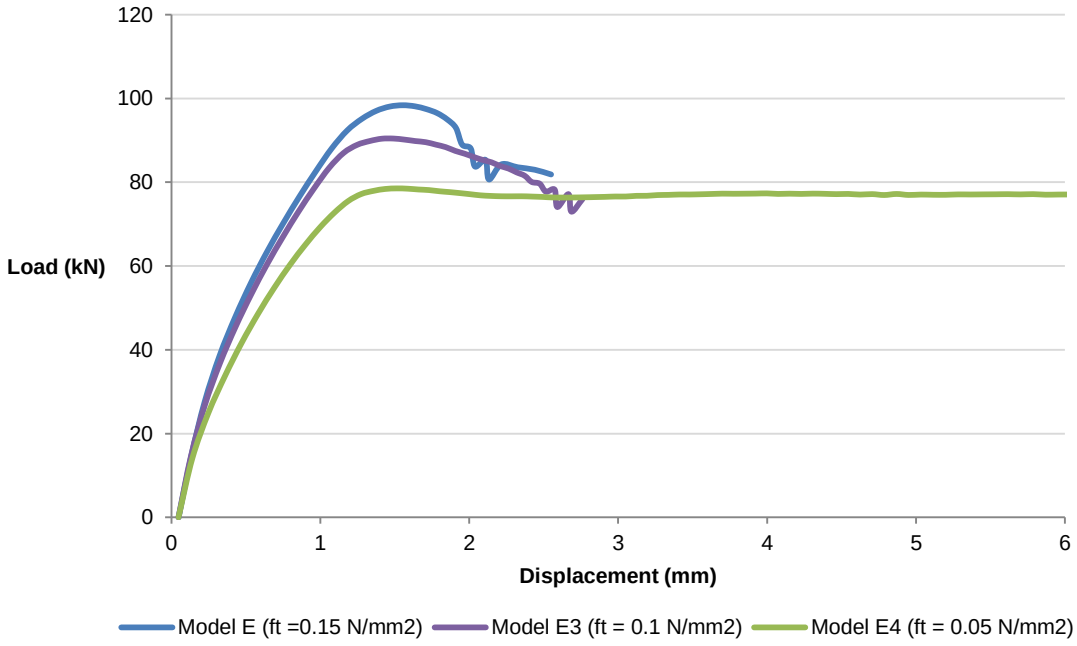

Figure 82 – Load – Displacement diagrams for Model E with different values of tensile strength of the masonry.

As we can see in the load-displacement diagrams of the three models, compared in Figure 82, a reduction of stiffness in the elastic domain characterises the response of the structure when reducing the tensile strength of the masonry. At the same time, a reduction of ultimate load is experienced. Model E reaches a maximum load of 98.4 kN, whereas Model E3 and E4 reach 90.4 kN and 78.5 kN respectively. It can also be noticed that in Model E3 an increase of plastic behaviour compared to model E occurs, whereas the behaviour of Model E4 after the peak is perfectly plastic.

Looking at the results in more detail it appears that the separation between arch and spandrel wall is significantly reduced in Model E4, the reason is due to the fact that, coherently, a reduction of tensile strength and cohesion at the interface should be applied along with a reduction of tensile strength in the masonry.

A further comparison between models was developed in terms of cohesion of the soil. As presented previously, Model E has cohesion in the soil equal to 0.003 N/mm^2, its results were compared with two similar models, Model E5 and E6, in which cohesion equal to 0.001 and 0.005 N/mm^2 respectively was applied. The results, in terms of load-displacement curves, are shown in the following Figure 83.

The results do not show significant differences. In fact, the three models reach a similar value of ultimate load and very similar stiffness in the elastic domain. The only difference, although very little, can be observed in the after-peak phase.

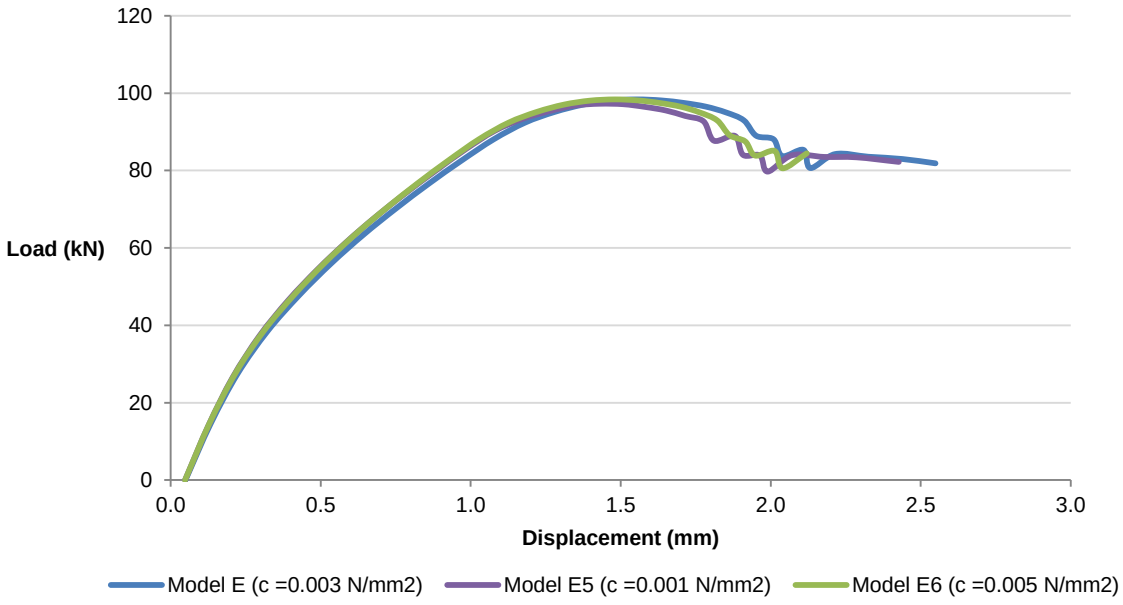

Figure 83 – Load – Displacement diagrams for Model E with different values of cohesion in the soil.

Finally, a comparison between models with different Young's modulus in the masonry was done. As the curves in Figure 84 show, a difference between them can be observed both in terms of stiffness and ultimate load. Both of them face a reduction, although small, when the Young's modulus is reduced.

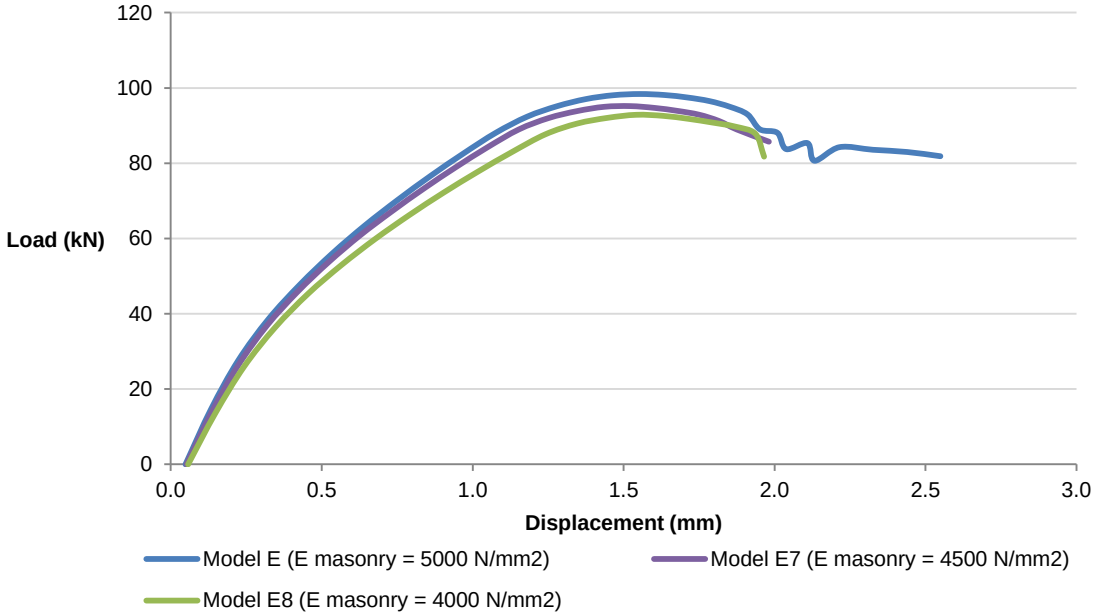

Figure 84 – Load – Displacement diagrams for Model E with different values of Young's modulus in the masonry.

In conclusion, the sensitivity analysis developed on Model E has shown relevant results only when changing the properties of the masonry, namely tensile strength and Young's Modulus, whereas the changes in the soil did not yield significant results.

7.5 Further development of the 3D model

Since the calibration of the parameters in Model E and the following sensitivity analysis did not show a completely satisfactory result, it was decided to analyse Model F shown in Figure 85, in which all the steel elements are present, including the steel profiles located at the sides of the steel plates, acting as stiffening elements. One of the objectives was in this case, to overcome the concentration of stress on the sides of the masonry wall due to the connection of the steel ties.

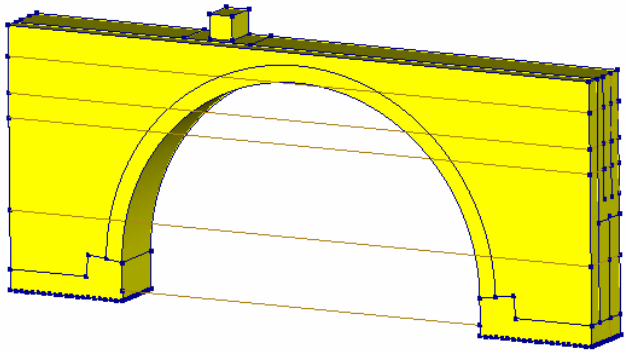

Figure 85 – Model F.

The load-displacement curve shown in Figure 86 together with the curve of Model E shows an important reduction of the ultimate load that is equal to 82.89 kN, along with a reduction of stiffness.

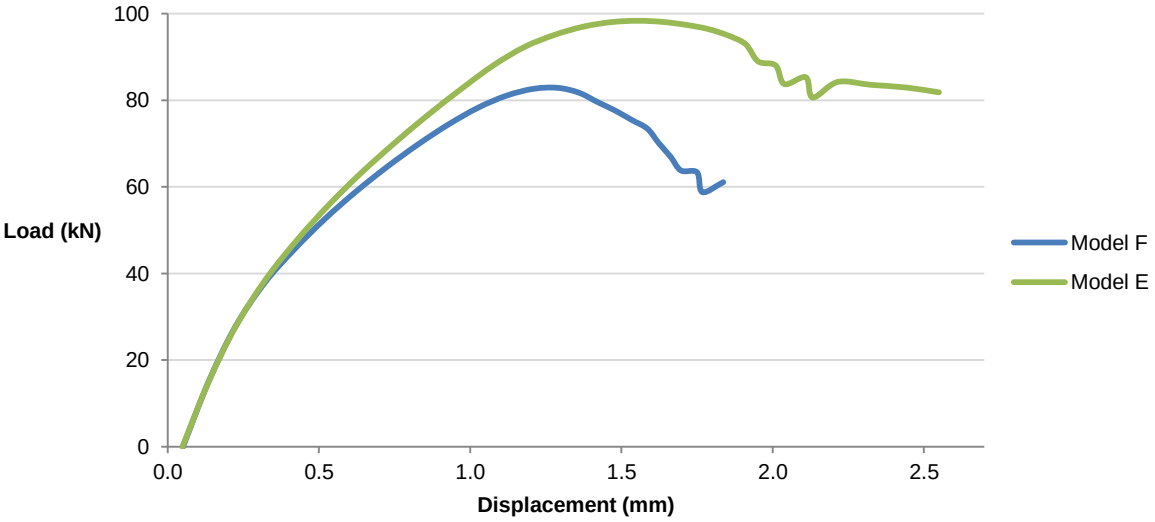

Figure 86 – Load – Displacement diagrams for Model E and Model F.

In order to understand more in detail the behaviour of the structure and the reason why the behaviour differs from Model E, the results were analysed more in detail.

The vertical displacement contour plot at the load step corresponding to the maximum value of load applied, shown in Figure 87, does not differ from the results obtained previously, except for the fact that, as the load-displacement curve showed, the displacements are smaller.

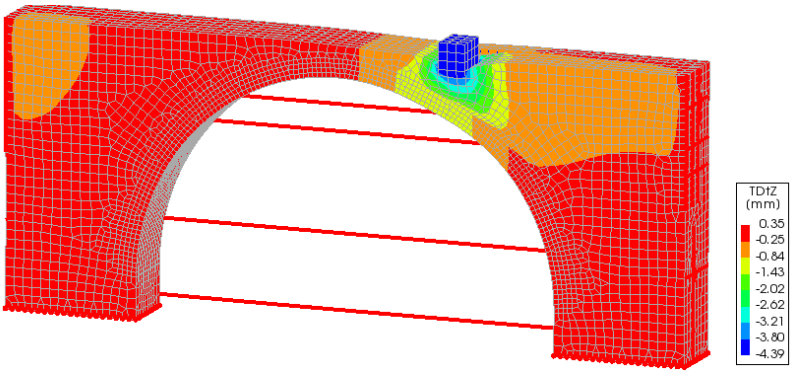

Figure 87– Contour plot of vertical deformations at a load of 82.89 kN in Model F.

Analogously, in terms of behaviour of the masonry, the formation of the gapping between arch and spandrel wall can be observed, as shown in the following Figure 88.

In this case, thanks to the higher level of details in the model, the concentration of stresses in the masonry wall and more specifically in the points of connection of the steel ties was removed.

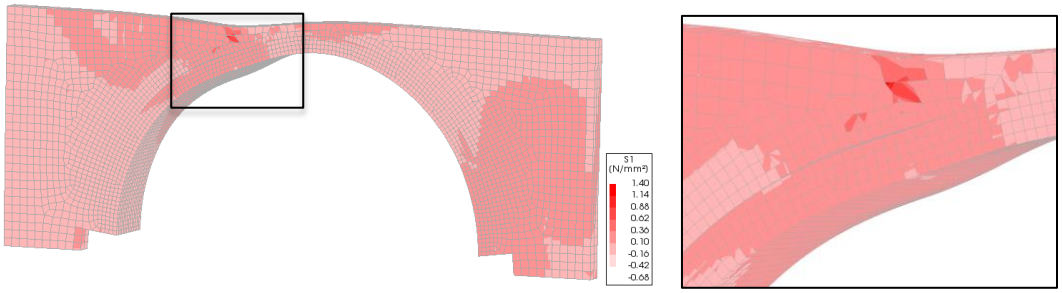

Figure 88 – Principal stresses in the arch and the spandrel wall at a load of 82.89 kN in Model F.

Also, a reduction of plastic strains in the soil at the load step corresponding to the maximum load, similarly to what happened in Model E can be observed.

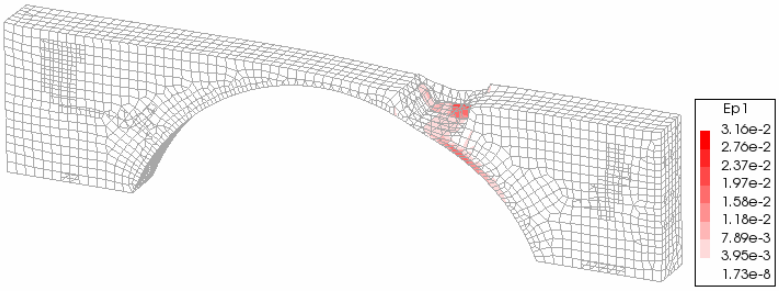

Figure 89 – Plastic strains in the soil at a load of 82.89 kN in Model F.

Looking more in detail at the load-diagram of Model F, we can observe that after the peak value of load is reached, a process of reduction of load occurs, whereas the displacements keep increasing. In this case too, the response of the structure was studied in four points of the graph. The first one is taken at the second load step corresponding to a load of 27.6 kN, the second, at a load of 58.9 kN, the third corresponds to the value of maximum load acting on the structure, 82.9 kN. Finally, the last point is the last step for which convergence is reached before a process of unloading occurred.

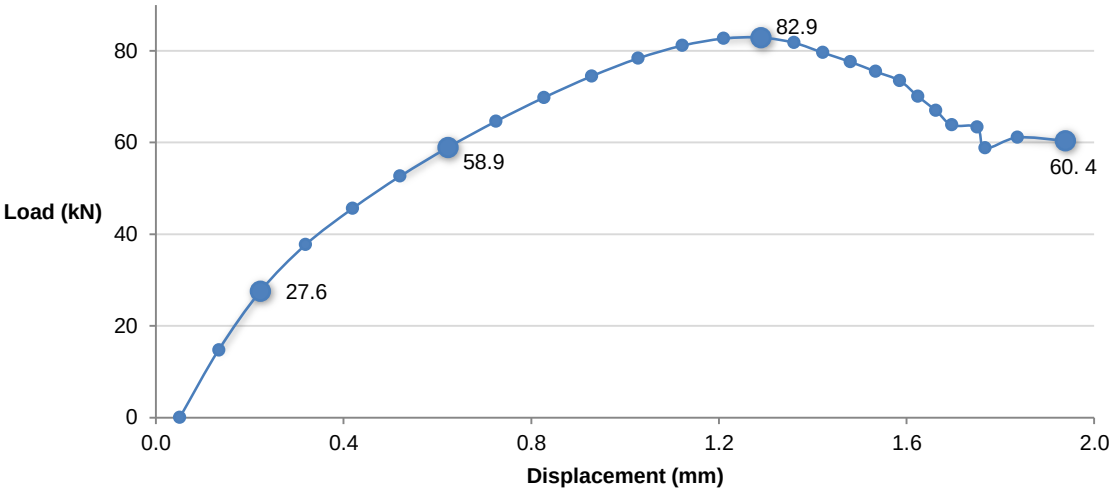

Figure 90 – Load – Displacement curve for Model F at ¼ of the span.

The results evaluated in terms of stress in the arch, do not show large differences with the ones observed in the previous model, except for the fact that the reached values are in this case lower.

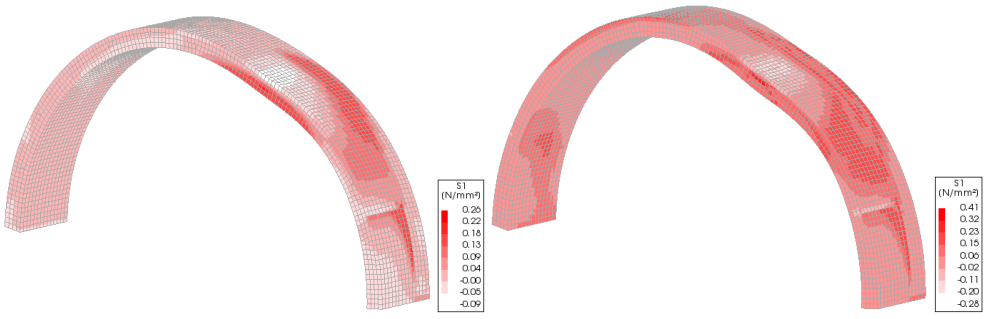

(a) (b)

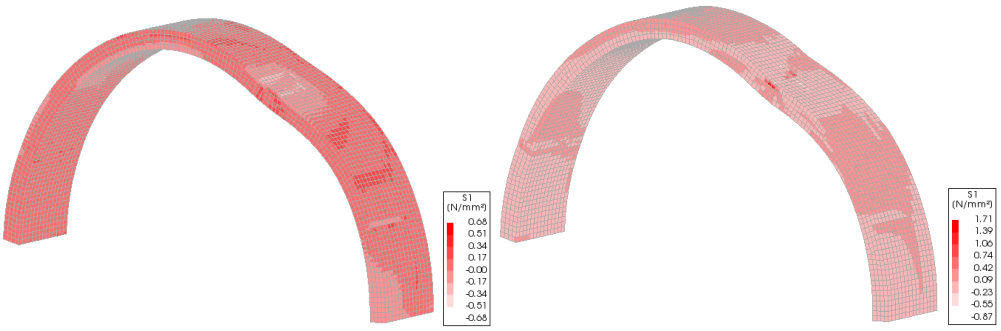

(c) (d)

Figure 91 – Principal stress in the arch at load steps corresponding to 27.6 kN (a), 58.9 kN (b), 82.9 kN (c) and 60.4 kN (d).

Furthermore, Model F, similarly to Model E, experiences the formation of a gap between spandrel wall and arch, in particular in area 2 indicated in Figure 92, as shown in the images that follow.

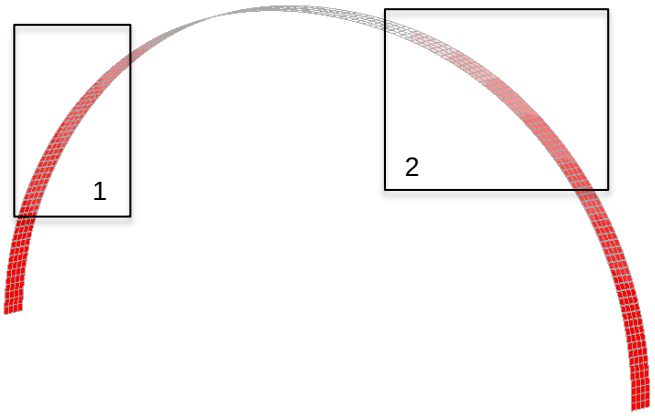

Figure 92 – Interface between arch and spandrel wall showing the areas of formation of the gap.

In this case, the gap formed at the last load step analysed is equal to 2.23 mm, whereas in area 1 is equal to 0.81 mm. The values are very close to those obtained in Model E.

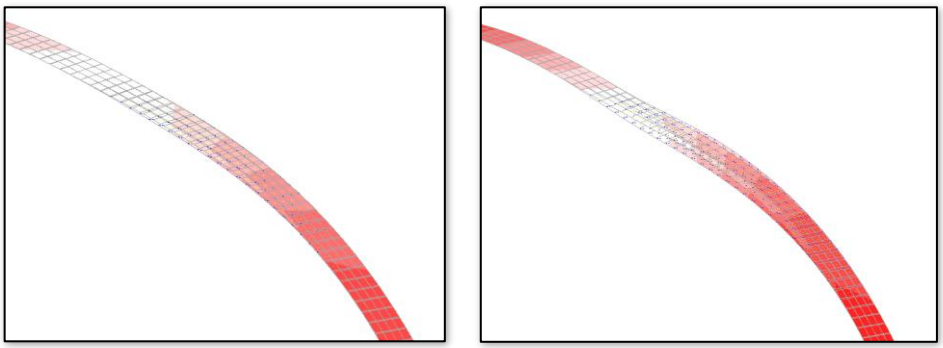

(a) (b)

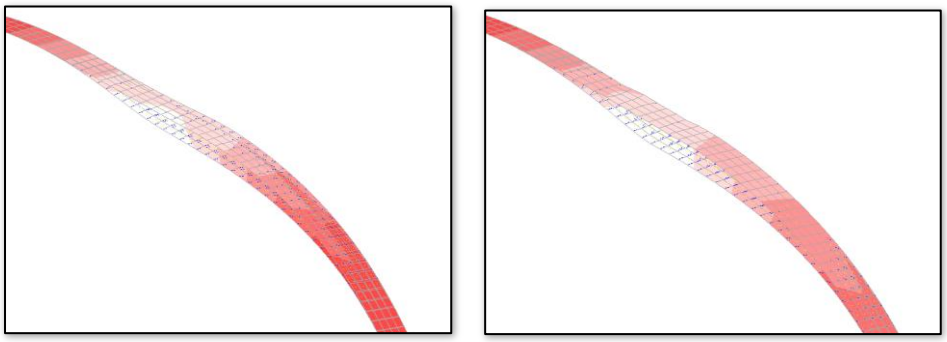

(c) (d)

Figure 93 – Evolution of the gap between spandrel wall and arch in area 1 at load steps corresponding to 27.6 kN (a), 58.9 kN (b), 82.9 kN (c) and 60.4 kN (d).

As for the distribution of the crack strains, the result is pretty similar to the result of Model E. The cracks develop gradually and at the last step, the formation of four hinges and therefore the development of a collapse mechanism of the arch is registered, as visible in Figure 98.

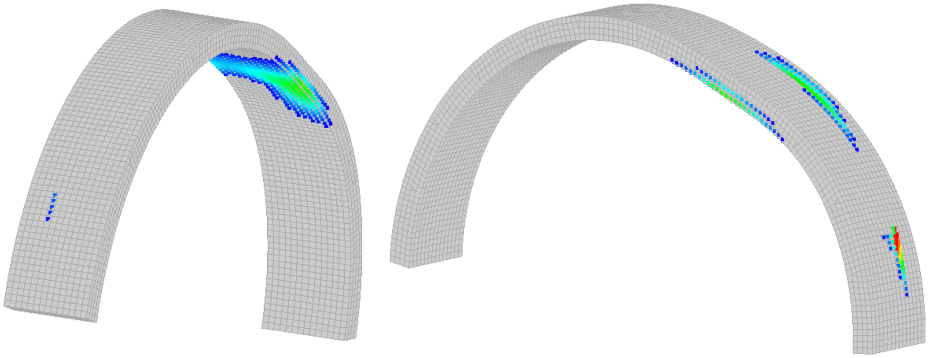

Figure 94 – Crack strains in the masonry arch at 27.6 kN.

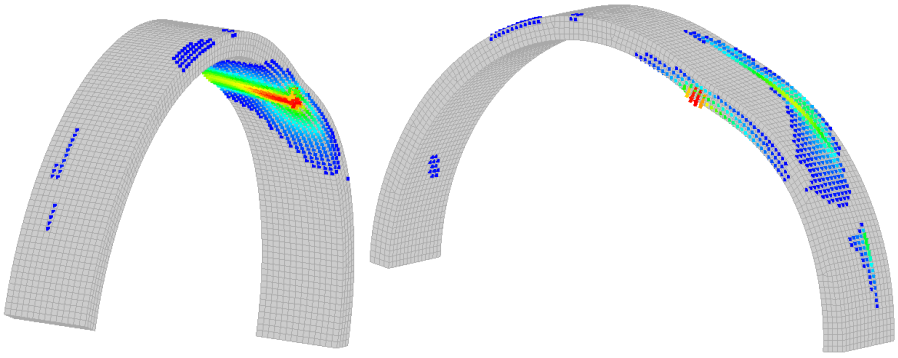

Figure 95 – Crack strains in the masonry arch at 58.9 kN.

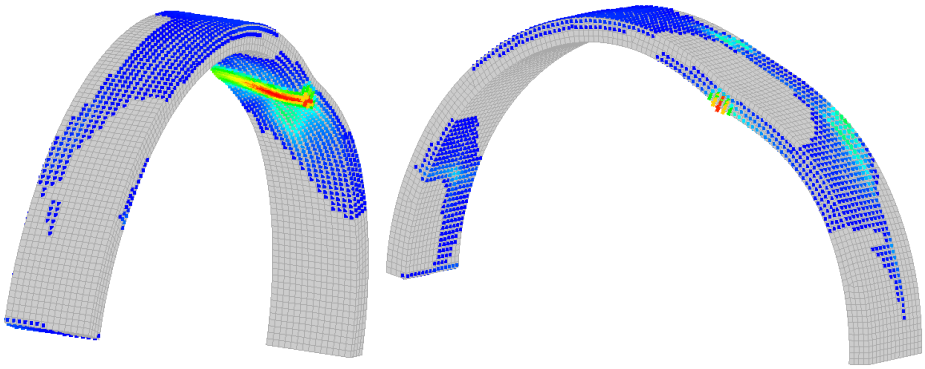

Figure 96 – Crack strains in the masonry arch at 82.9 kN.

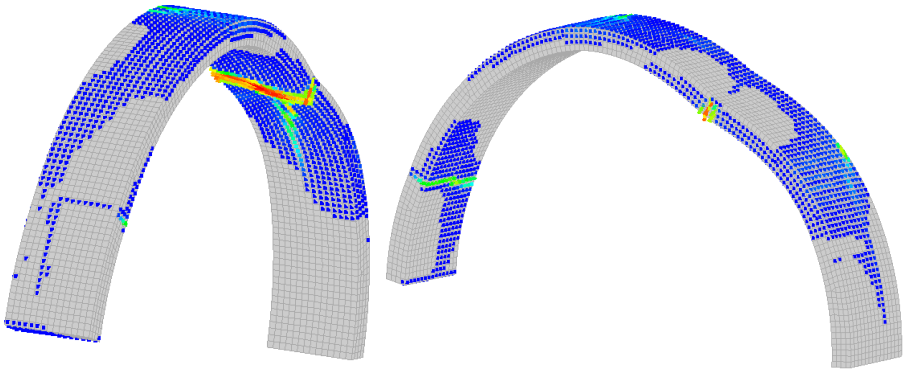

Figure 97 – Crack strains in the masonry arch at 60.4 kN.

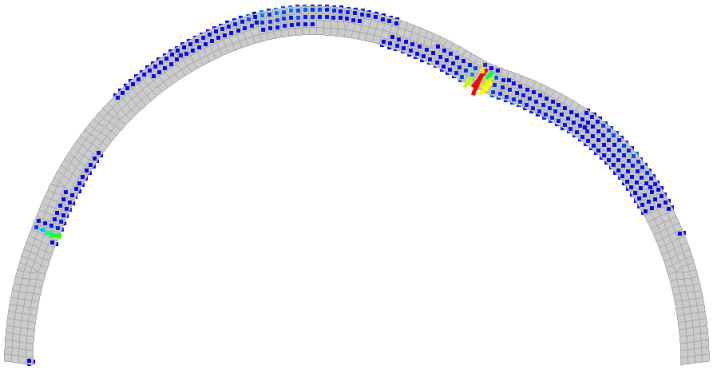

Figure 98 – Section of the masonry arch showing the distribution of the crack strains at 60.4 kN.

As it was observed in Model E, the distribution of the stress along the arch in Model F shows a concentration of stress in four areas, as it can be seen in the following Figure 99 and Figure 100.

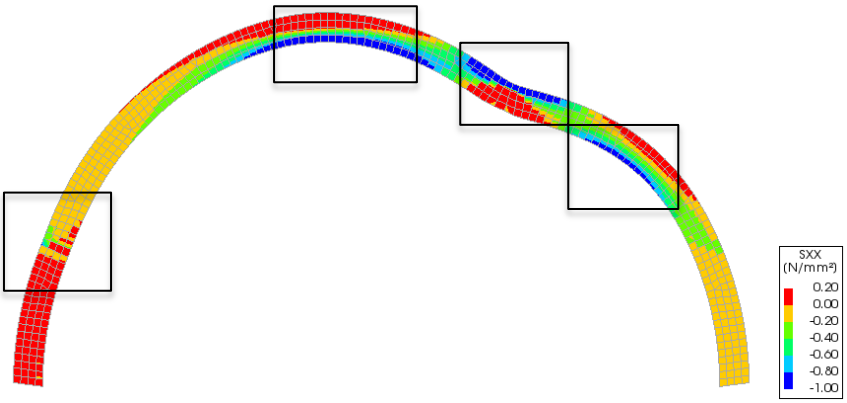

Figure 99 – Contour plot of the stress SXX in a section of the arch.

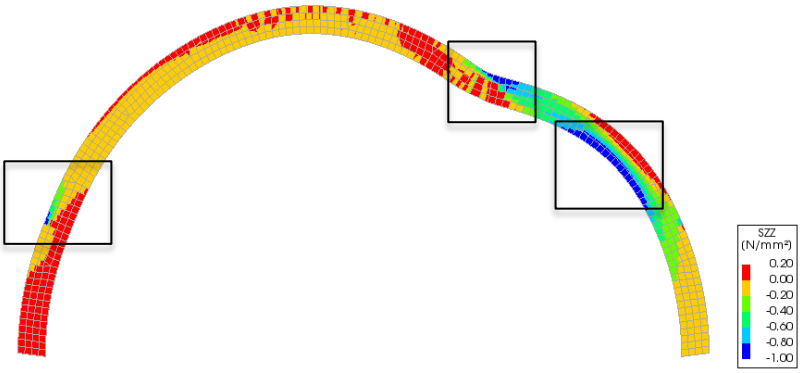

Figure 100 – Contour plot of the stress SZZ in a section of the arch.

Finally, the development of the distribution of the crack strains in the spandrel wall is similar to what was observed previously in Model E.

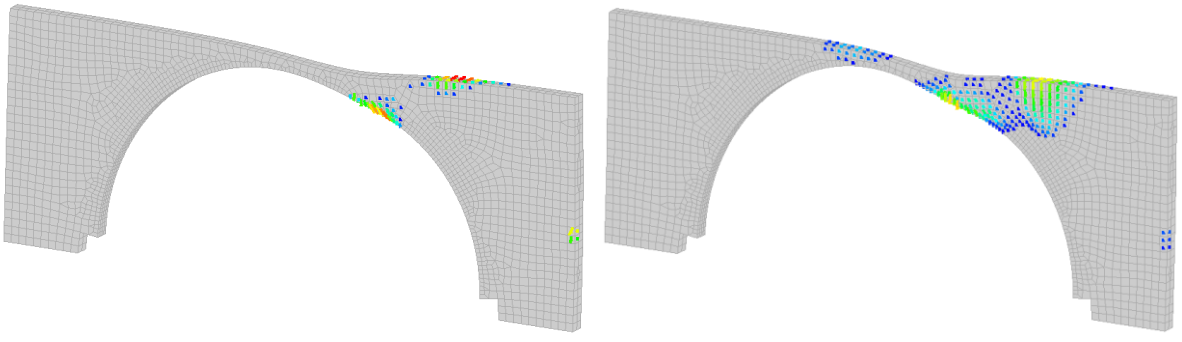

(a) (b)

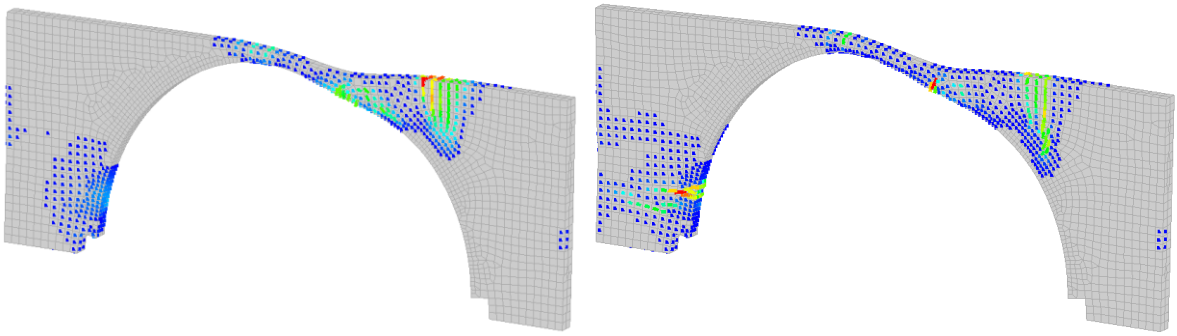

(c) (d)

Figure 101 – Crack strain in the spandrel wall at load steps corresponding to 27.6 kN (a), 58.9 kN (b), 82.9 kN (c) and 60.4 kN (d).

A final remark in terms of comparison between Model E and Model F refers to the result obtained in terms of lateral thrust. In the case of Model E, as it was presented previously, the value obtained was equal to 76 kN. In Model F the lateral thrust obtained is equal to 59 kN.

Understanding which are the mechanisms that affect the results and, therefore, the difference between Model E and Model F is a rather complex task. The results obtained are absolutely unexpected: due to the presence of the steel elements that provide stiffness, Model F was expected to be stiffer than Model E and a higher bearing capacity was predicted. On the opposite, Model F presents a more ductile behaviour and a lower ultimate load.

The presence of the steel elements in Model F provides a higher level of confinement to the soil, this condition changes the way the stresses are distributed between the structural elements, affecting the development of crack strains and therefore the way the whole structure behaves.

This is a clear demonstration of how difficult achieving a result close to reality through numerical models is and how the contribution of every element has an impact on the results.

7.6 Sensitivity analysis on Model F

A sensitivity analysis was developed also on Model F to better understand the behaviour of the model and evaluate the changes due to the variation of different parameters. In particular, the aspects that were analysed referred to soil and masonry: tensile strength and Young's modulus of masonry were studied, along with cohesion and Young's modulus of the soil.

The results showed that the tensile strength of the masonry has an influence on both ultimate load and stiffness of the model. The load-displacement curves in Figure 102 show that the reduction of this parameter determines a reduction of both ultimate load and stiffness, whereas when it is increased, the stiffness increases too but the ultimate load does not face any change.

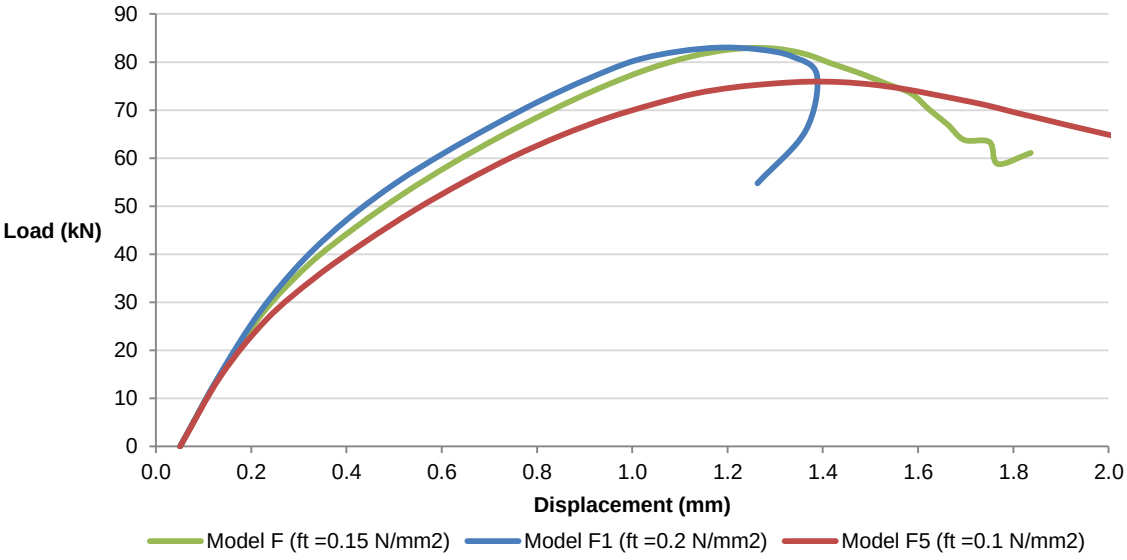

Figure 102 – Load – Displacement diagrams for Model F with different values of tensile strength of the masonry.

The model was also analysing varying the Young's modulus of the masonry; as a consequence of this change, a reduction of ultimate load and the stiffness is observed when reducing E, whereas only the stiffness is affected by its increase, as it can be seen in Figure 103.

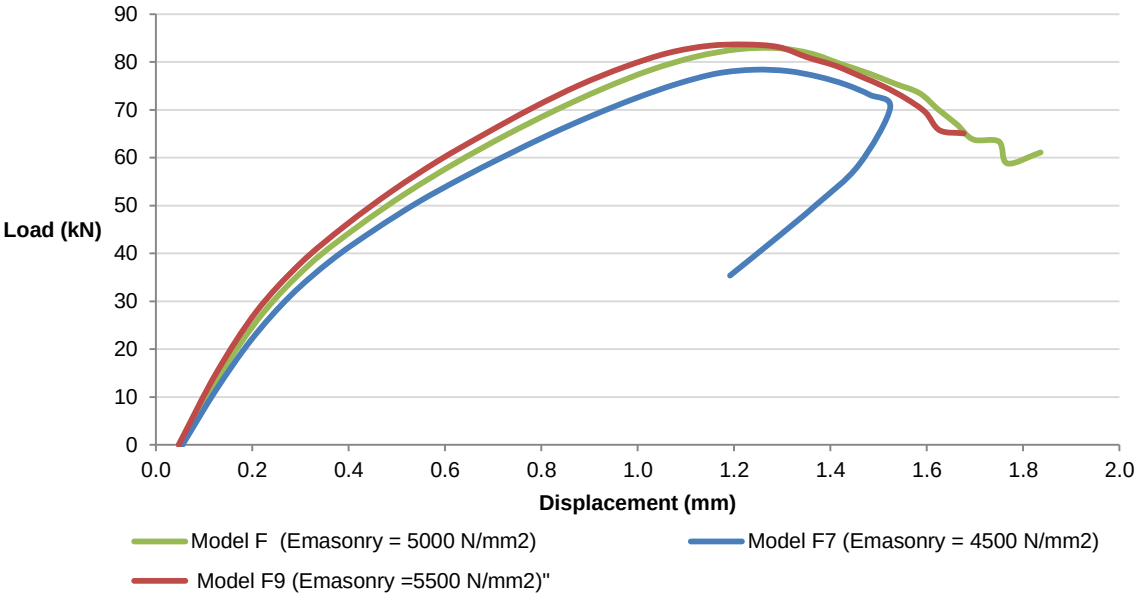

Figure 103 – Load – Displacement diagrams for Model F with different values of Young's modulus in the masonry.

As mentioned, the soil was also analysed, studying the effects of the change of its cohesion and of its Young's modulus. At first, the model was studied with a reduced cohesion of 0.001 N/mm^2, but

surprisingly, no changes compared to the original model were observed. However, when the hardening diagram was removed, a reduction of ultimate load occurred.

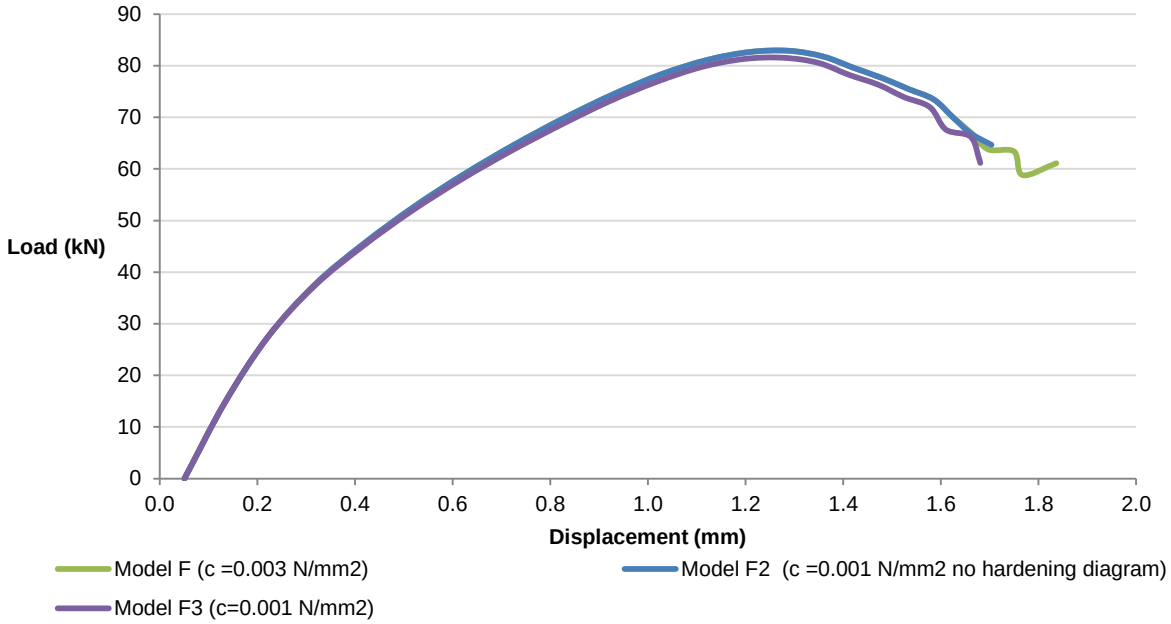

Figure 104 – Load – Displacement diagrams for Model F with different values of cohesion in the soil.

A more visible variation of answer of the structure is linked to the changes in the Young's modulus of the soil. In this case both ultimate load and the stiffness of the model increase or decrease with the parameter.

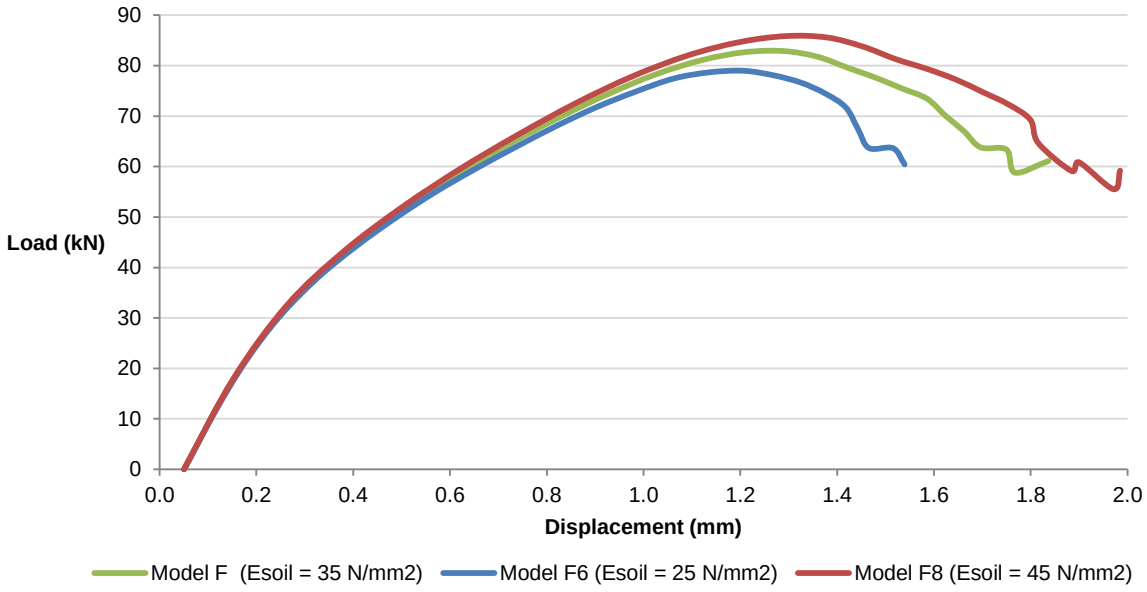

Figure 105 – Load – Displacement diagrams for Model F with different values of Young's modulus in the soil.

8. CONCLUSIONS

The masonry arch bridge object of the study was analysed with a preliminary bi-dimensional approach and more in detail with a tri-dimensional model. The models were defined applying material constitutive models and values of the parameters recommended by literature first and were then improved and calibrated according to the results obtained.

The results obtained with the 2D model showed clearly the need to develop a more complete 3D analysis that, despite its higher complexity and higher requirements in terms of time, allowed obtaining more realistic results.

Throughout the process of development of the model and the analysis of the results obtained step by step, it emerged clearly the importance of considering the contribution of each element. In the 2D models for instance, the presence of the spandrel walls was ignored and as a consequence their high contribution in both the stiffness and the ultimate load of the structure was neglected. However, in this case, it is interesting to notice that despite the fact that the results differed from the experimental evidences in terms of ultimate load, the ductility of the 2D models was similar to the experimental one.

Similarly, the large difference faced when comparing a more simplified 3D model, in which the presence of the steel elements acting as stiffeners for the steel plates was disregarded, and the one in which all the elements were modelled, demonstrated how relevant the presence of every element is, on the results.

The final results of the 3D models showed a good agreement with the experimental data with reference to the development of cracks and hinges, therefore with the real failure mechanism of the structure, along with the phenomenon of opening of a gap between spandrel wall and arch. With a small error, a good estimate of the ultimate load bearing capacity of the structure was obtained too.

Nevertheless, unfortunately, the models analysed did not offer a realistic representation of the ductility of the structure and of its deformations.

As mentioned, the bi-dimensional model offered a good approximation of the experimental results in terms of stiffness, whereas the same cannot be said about the tri-dimensional model. Several can be the reasons for this disagreement. For instance, it might be due to the presence of the spandrel walls that add stiffness to the structure; it is possible that the separation between arch and spandrel wall in the real structure developed differently than in the numerical model. This might have affected the response of the structure. Another possible cause of this discordance might be the way the steel ties are modelled; the numerical model does not take into account the fact that the ties were not pretensioned and were therefore naturally subjected to a deformation due to their self-weight. This condition can be the reason for the additional stiffness experienced in the numerical simulation.

Furthermore, it is important to mention that, as discussed in Chapter 3, while the experiment was being performed, a malfunctioning of the system occurred. This event might have jeopardized the reliability of the data collected, offering a possible explanation of the divergence between numerical and experimental results.

The sensitivity analysis that was developed on the models allowed obtaining some changes in the response of the structure. In particular, it was observed that in Model E, both stiffness and ultimate load were affected by the change in the tensile strength of the masonry, whereas very little changes are seen when changing the Young's modulus of the masonry and no significant results were achieved acting on the values assigned to the properties of the soil. The results of Model F were mainly affected by the tensile strength of the masonry and the Young's moduli of both masonry and soil. These results confirm the importance of selecting the most appropriate constitutive models and assigning correct values to the parameters; and demonstrate how uncertain they may be. In particular, it was observed that the lack of information regarding the properties of the soil makes this material the one whose level of approximation in terms of parameters is higher.

8.1 Suggestions for further researches

The not completely satisfactory results obtained show that it is necessary to develop further the study on the tri-dimensional model in order to achieve results closer to the experimental ones. Many are the aspects that can be investigated, such as for instance:

- Develop a more detailed 3D model taking into account the deformations of the steel ties subjected to their self-weight;
- Analyse the response of the structure and in particular the behaviour of the soil when a different constitutive model is applied or by changing further its properties. For instance, the subdivision of the soil in vertical sections that was applied by Brunet to apply increasing values of Young's Modulus can be investigated.
- Evaluate further the influence of the interfaces, with a focus in particular on the interface between arch and infill and between infill and steel plates.
- Implement a micro-model for the masonry structural elements to obtain a more ductile model able to achieve higher deformations in the numerical analysis.

9. REFERENCES

[1] C. Brookes, “Assessment and strengthening masonry arch bridges,” *Struct. Anal. Hist. Constr. Preserv. Saf. Significance*, pp. 497–505, 2010.

[2] S. Huerta, “Mechanics of masonry vaults: the equilibrium approach,” *Proc. 1st Int. Congr. Struct. Anal. Hist. Constr. Guimaraes*, no. January 2001, pp. 47–70, 2001.

[3] “Ennisnag Bridge.” [Online]. Available: http://www.engineersjournal.ie/2016/11/15/stone-bridges-history-and-heritage-of-masonry-arch-bridges-in-ireland/.

[4] D. V. Oliveira, P. B. Lourenço, and C. Lemos, “Geometric issues and ultimate load capacity of masonry arch bridges from the northwest Iberian Peninsula,” *Eng. Struct.*, vol. 32, no. 12, pp. 3955–3965, 2010.

[5] L. (Mott M. L. McKibbins, C. (University of S. Melburne, N. (Birse R. L. Sawar, and C. (KW L. Sicilia Gaillard, “Masonry arch bridges: condition appraisal and remedial treatment,” *CIRIA C656*. CIRIA, London, 2006.

[6] T. H. Hughes, “The testing, analysis and assessment of masonry arch bridges,” *Struct. Anal. Hist. Constr.*, no. c, 1996.

[7] V. Sarhosis, S. De Santis, and G. de Felice, “A review of experimental investigations and assessment methods for masonry arch bridges,” *Struct. Infrastruct. Eng.*, vol. 12, no. 11, pp. 1439–1464, 2016.

[8] R. Pereira, “Numerical modeling of experimental masonry arch bridge,” UPC, 2015.

[9] L. Nobile and V. Bartolomeo, “Structural analysis of historical masonry arches: State-of-the-art and recent developments,” *Int. J. Math. Model. Methods Appl. Sci.*, vol. 9, pp. 338–344, 2015.

[10] A. De Luca, A. Giordano, and E. Mele, “A simplified procedure for assessing the seismic capacity of masonry arches,” *Eng. Struct.*, vol. 26, no. 13, pp. 1915–1929, 2004.

[11] J. Heyman, *The Stone Skeleton. Structural Engineering of Masonry Architecture.* Cambridge: Cambridge University Press, 1995.

[12] P. B. Lourenço, “Analysis of historical constructions: From thrust-lines to advanced simulations,” *3rd Int. Semin. Hist. Constr. Guimarães, Port.*, no. January 2001, pp. 91–116, 2001.

[13] M. Monaco, A. Gesuado, and G. Frunzio, “3D F.E.M. analysis of a Roman arch bridge,” *Hist. Constr.*, pp. 591–598, 2001.

[14] “Pont Saint Martin.” .

[15] G. Milani and P. B. Lourenço, “3D non-linear behavior of masonry arch bridges,” *Comput. Struct.*, vol. 110–111, no. 1, pp. 133–150, 2012.

[16] A. Cavicchi and L. Gambarotta, “Collapse analysis of masonry bridges taking into account arch-fill interaction,” *Eng. Struct.*, vol. 27, no. 4, pp. 605–615, 2005.

[17] A. S. Gago, J. Alfaiate, and A. Lamas, “The effect of the infill in arched structures: Analytical and numerical modelling,” *Eng. Struct.*, vol. 33, no. 5, pp. 1450–1458, 2011.

[18] P. Roca and C. Molins, “Experiments on arch bridges,” *Arch Bridg. IV-Advances Assessment, Struct. Des. Constr.*, pp. 365–374, 2004.

[19] J. A. Charry Ablanque and P. Roca Fabregat, “Estudio experimental del comportamiento de paredes de obra de fábrica de ladrillo ante la acción de cargas laterales,” 2010.

[20] P. R. Fabregat, “Análisis experimental de la capacidad portante de un puente arco de obra de fábrica de ladrillo,” 2003.

[21] I. C. Brunet, “3D numerical simulation of experiments on masonry arch bridges,” 2016.

[22] DIANA FEA, “Diana Documentation - Release 10.3.” .

[23] M. Angelillo and P. B. Lourenço, “Masonry behaviour and modelling,” vol. 551, no. April 2016, 2014.

[24] P. B. Lourenço, “Structural masonry analysis: recent developments and prospects,” *Proc. 14th Int. brick block Mason. Conf.*, no. 2004, pp. 1341–1356, 2008.

[25] M. Tomazevic, “Earthquake-Resistant Design of Masonry Buildings,” *World Sci. Publ. Co.*, p. 268 pp., 1998.

[26] S. Arash, “MECHANICAL PROPERTIES OF MASONRY SAMPLES FOR,” no. 1, 2012.

[27] D. Vitorino and D. C. Oliveira, “experimental and numerical analysis of blocky masonry structures under cyclic loading análise experimental e numérica de estruturas de alvenaria de blocos sob acções cíclicas,” 2003.

[28] Plaxis, “Material Models Manual - Plaxis,” 2014.

[29] R. Sandhya Rani., K. Nagendra Prasad., and T. Sai Krishna., “Applicability of Mohr-Coulomb & Drucker- Prager models for assessment of undrained shear behaviour of clayey soils,” *Int. J. Civ. Eng. Technol.*, vol. 5, no. 10, pp. 104–123, 2014.

[30] N. Subramanian, “Appendix C - Properties of Soil,” in *Design of Steel Structures*, Oxford University Press, 2016, p. 5.

[31] G. Giardina, M. J. Dejong, and R. J. Mair, “Interaction between surface structures and tunnelling in sand : Centrifuge and computational modelling,” *Tunn. Undergr. Sp. Technol.*, vol. 50, pp. 465–478, 2015.

[32] R. F. Obrzud and A. Truty, “The Hardening Soil model - A practical guidebook,” vol. 05, p. 205, 2018.

[33] M. A. Hicks, R. B. J. Brinkgreve, and A. Rohe, *Numerical Methods in Geotechnical Engineering*. CRC Press, 2014.

[34] T. D. BV., “DIANA-9.6 User’s Manual - Geotechnical Analysis.” 2015.

[35] M. Saberi, C. D. Annan, and J. M. Konrad, “Implementation of a soil-structure interface constitutive model for application in geo-structures,” *Soil Dyn. Earthq. Eng.*, vol. 116, no. May 2018, pp. 714–731, 2019.

[36] R. Renzi, “Centrifuge cone penetration tests in sand,” no. 1999, pp. 543–552, 1980.

[37] A. Gupta, “Relationship between the Mean Particle Size, the Size Factor, Optimum Moisture Content, and Permeability of Sandy Soils,” *12th Int. Conf. Int. Assoc. Comput. Methods Adv.*

Geomarks, pp. 1–6, 2008.

[38] DIANA FEA, “DIANA frequently asked questions.” [Online]. Available: https://dianafea.com/diana-faq.

[39] P. B. B. Lourenço, “A user/programmer guide for the micro-modelling of masonry structures,” *Report*, vol. 3, no. 1.31, p. 35, 1996.

[40] T. D. F. BV., “DIANA-10.2 User’s Manual - Material Library.” 2017.

[41] P. B. Lourenço and J. G. Rots, “Multisurface Interface Model for Analysis of Masonry Structures,” *J. Eng. Mech.*, vol. 123, no. 7, pp. 660–668, 2002.

[42] K. Palacio, “Practical Recommendations for Nonlinear Structural Analysis in DIANA,” *TNO DIANA BV, Netherlands*, no. July, 2013.